UNIVERSITY OF CALIFORNIA

SANTA CRUZ

REGULATION OF CORTICAL ACTIN DYNAMICS DURING CENTROSOME SEPARATION AND CYTOKINESIS IN THE DROSOPHILA EMBRYO

A dissertation submitted in partial satisfaction
of the requirements for the degree of

DOCTOR OF PHILOSOPHY

in

MOLECULAR, CELL AND DEVELOPMENTAL BIOLOGY

by

Justin Crest

June 2012

The Dissertation of Justin Crest
is approved:

_____
Professor William Sullivan, Chair

_____
Professor Douglas Kellogg

_____
Professor William Saxton

_____
Tyrus Miller
Vice Provost and Dean of Graduate Studies

List of Figures and Tables

Abstract

REGULATION OF CORTICAL ACTIN DYNAMICS DURING CENTROSOME SEPARATION AND CYTOKINESIS IN THE *DROSOPHILA* EMBRYO

Justin Crest

The cytoskeleton plays a variety of roles during the cell cycle, none more dramatic than the formation of a bipolar mitotic spindle and the subsequent cleavage of one cell into two. Proper centrosome separation is a prerequisite for positioning the bipolar spindle. Although studies demonstrate that microtubules and their associated motors drive centrosome separation, the role of actin in centrosome separation remains less clear. Studies in tissue culture cells indicate that actin- and myosin-based cortical flow is primarily responsible for driving late centrosome separation, whereas other studies suggest that actin plays a more passive role by serving as an attachment site for astral microtubules to pull centrosomes apart. Here we demonstrate that prior to nuclear envelope breakdown (NEB) in *Drosophila* embryos; proper centrosome separation does not require myosin II but requires dynamic actin rearrangements at the growing edge of the interphase cap. Both Arp2/3- and Formin-mediated actin remodeling are required for separating the centrosome pairs before NEB. The Apc2-Armadillo complex appears to link cap expansion to centrosome separation. In contrast, the mechanisms driving centrosome separation after NEB are dependent of the actin cytoskeleton and compensate for earlier separation defects. Our studies show that the dynamics of actin polymerization drive centrosome separation and this has

important implications for centrosome positioning during processes such as cell migration, cell polarity maintenance, and asymmetric cell division.

Another vital role for spindle formation is in positioning the site of cleavage following anaphase separation of DNA. Rappaport's experiments with sand dollar embryos showed that cleavage furrow positioning is determined by the relationship between the spindle and the actin cortex. In his embryos, astral microtubules, which extend out to the cortex were primarily responsible for initiating a furrow, however, smaller somatic cells seem to position the furrow through the overlapping antiparallel central spindle. This balance between astral and central spindle influences is not well understood however. In the early *Drosophila* embryo, nuclei divide within a syncytium yet invaginate cortical actin and membrane, encompassing them, in order to complete mitosis in close proximity to neighboring nuclei. These furrows are considered natural Rappaport furrows since they form at astral microtubule overlap. Upon cellularization, the furrow positioning seems to shift from astral microtubule-based to central spindle-based. Our findings show that during the syncytial divisions, key conserved central spindle components Centralspindlin complex, Polo, and Fascetto (Prc1) all localize to regions of overlap astral microtubules during furrow formation. Given that the central spindle does not induce formation of conventional cytokinesis, finding that all of these components, plus the chromosomal passenger complex (Aurora B and INCENP), also localize to the central spindle was unexpected. The lack of furrow formation at the central spindle then is explained by the fact that the syncytial divisions rely on a maternally supplied form of RhoGEF,

RhoGEF2, lacking the specific domains that localize zygotically expressed RhoGEF (Pebble) to the central spindle. RhoGEF2 instead localizes to the overlap astral microtubules of the syncytial divisions. Thus, in spite of proper localization of many key furrowing components to the central spindle in syncytial embryos, the failure of RhoGEF to localize to the central spindle may preclude formation of conventional cleavage furrows bisecting the spindle. In support of this idea, we bypass the need for RhoGEF by injecting constitutively active Rho into the syncytial embryos. This generates ectopic furrows strikingly similar to conventional cleavage furrows that form perpendicular to the central spindle during the syncytial divisions. While metaphase furrow formation is myosin independent these Rho-induced ectopic furrows, like conventional furrows, require myosin in addition to microtubules. These studies demonstrate that the early *Drosophila* embryo is primed to form furrows at either the overlapping astral microtubules or central spindle with the shift to the latter being driven in large part by a corresponding shift from maternal-to-zygotic forms of RhoGEF.

My studies predict that the delivery of RhoGEF2 to the metaphase furrows must be different than the mechanism that localizes Pebble to the central spindle (the Centralspindlin complex). Recently, it has been shown that RhoGEF2 localization to the metaphase furrows requires vesicle trafficking from the recycling endosome (RE). This vesicle trafficking is regulated by the Rab11-GTPase in the RE and its associated effector, Nuclear Fallout (Nuf). Previous observations of Nuf in the early embryo show that it accumulates at the RE from interphase to prophase during the

time when furrows are being made. At prophase, Nuf is phosphorylated, which coincides with its diffusion away from the RE. I will present evidence that Nuf localization is regulated by its phosphorylation state and that the mitotic kinase, Polo directly phosphorylates Nuf, inhibiting its localization at the RE, decreasing vesicle trafficking to the furrow. I propose that this mechanism serves as a major component in timing the formation of a furrow and may provide valuable insight into timing cytokinesis in general.

Finally, the regulation of actin dynamics in cytokinesis has been well studied in terms of actin-interacting proteins such as Cofilin and Profilin. However, the direct modifications of actin and microtubules are similarly important for stable furrow ingression and abscission. Here I will present a newly characterized gene *push po*p that potentially indicates methylation of actin or tubulin as a previously unappreciated mechanism of regulating the cytoskeleton as well as other potential mitotic proteins in the events of cytokinesis.

The thesis work presented here promotes a broader understanding of cytokinetic furrow timing and positioning. On one hand, both centrosome separation and central spindle signaling are vital for proper furrow positioning. On the other hand, vesicle trafficking and folate metabolism are required for the proper timing and maintenance of a furrow during the cell cycle. A deeper understanding of both these processes of cytokinesis will provide valuable insight into the mechanisms of cell division and potentially how they are perturbed in tumorigenesis.

Acknowledgements

I would like to thank my advisor, William Sullivan, for endless ideas, unbridled enthusiasm, and financial as well as moral support. I am also grateful to my current and former fellow lab mates in the Sullivan lab: Shaila, Catharina, Frederic, Jian, Laura, Anne, Kate and Travis. They are full of helpful advice and provide an excellent scientific atmosphere.

I would like to specifically thank Jian Cao and Barbara Fasulo for collaboration on the studies described in chapter 2; Kirsten Concha-Moore for collaboration on the studies described in chapter 3 and the Harvard FlyTRiP Project for providing fly stocks; Jian Cao, Ellen Homola, Anne Royou and the UCSF Mass Spectrometry Facility for collaboration on the studies in chapter 4; and Jian Cao, Andrew Guzman, and Helen Francis Lang for collaboration on the studies in chapter 5.

Chapter 1: Introduction

Mitosis and cell division

Cell division is a complex orchestration of events essential for every organism from single-cell to metazoans. Faithful transmission of DNA, organelles and determinants are critical for cell function and development. In its simplest form, it is the separation of chromosomes by microtubule arrays to either side of the cell and the subsequent cleavage of the cell. Mitosis was first described during the second half of the 19th century by simple light microscopy (Flemming, 1965). The importance of maintaining a healthy karyotype of chromosomes by proper division was also described at this time in studies with asymmetrically dividing malignant tumors (Boveri, 2008). Since then, technology has allowed the study of the smallest of subcellular structures giving us insight into the many events of a dividing cell. None of these events are more visually dramatic or defining as cytokinesis when the single cell constricts, dividing the cell into two daughter cells. Here I will present the relevant history of cytokinesis and my own data that furthers our knowledge of the complex regulation of this morphogenetic event.

Microtubule-based models of furrow positioning during cytokinesis

Cytokinesis is the event that immediately follows anaphase separation of DNA. In eukaryotic animal cells, the position of the cytokinetic furrow, composed of filamentous actin (F-actin) myosin-II and several other proteins is always down the

midzone and perpendicular to the mitotic spindle, formerly the metaphase plate (Balasubramanian et al., 1992; Bi et al., 1998; Fujiwara and Pollard, 1976; Mabuchi and Okuno, 1977; Schroeder, 1968). For over 100 years, the signal that positioned the furrow has been hypothesized to be the mitotic spindle apparatus (Gurwitch, 1904). However, this hypothesis was unsatisfactory due to the correlative nature of timing and spatial relation of these two events. The furrow forms at the cortex during telophase while the spindle forms during anapahase in the center of the cell. It wasn't until the 1960's that Rappaport, who like many at the time studying cell division used marine invertebrate embryos, performed the critical experiments with sand dollar embryos that gave new insight into the mechanism of furrow positioning. By artificially creating a binucleate embryo, he observed that during the following cell division, two furrows formed down the metaphase plate as expected, however a third ectopic furrow was formed between neighboring centrosomes, where there was never a nucleus or a central spindle (Rappaport, 1961). Rappaport proposed that the overlapping astral microtubules must be the signal that initiates the ectopic furrow. This Astral-stimulation model was sufficient for the cleavage during these large embryonic divisions and mathematical modeling has confirmed this (Devore et al., 1989).

Work with smaller cells, which generally have smaller asters than large embryos and the cortex is closer to the spindle, have indicated that signals emanating from the central spindle are the driving force behind furrow positioning (Bringmann and Hyman, 2005; Wheatley and Wang, 1996). The central spindle is a region of

overlapping antiparallel microtubules which shows a strong accumulation of a variety of proteins required for cytokinesis. Studies in grasshopper neuroblasts showed that continuous signaling from the central spindle was required for furrowing (Kawamura, 1977). Furthermore, in cells that do not have asters and self assemble a spindle, cleavage furrows still form adjacent to the central spindle (Szollosi et al., 1972). Even by simply flattening Rappaport's sand dollar embryos so that the central spindle can interact with the cortex, it can indeed induce a furrow (Rappaport, 1971; Ris, 1949). Taken together, these studies suggested a model in which cell size determines which population of microtubules induces furrow formation.

Molecular furrow positioning cues and the mitotic spindle

Since this work defining the spindle as the activating component of cleavage, a lot has been found in terms of the key molecular signals associated with the spindle that induce this activation. First, furrow formation is primarily driven by the narrow activation of a Rho-GTPase in a stripe at the cell cortex (Bement et al., 2005). Activation of Rho is required for the polymerization of F-actin and the activation of myosin-II (Amano et al., 1996; Watanabe et al., 1997). The overlapping regions of the microtubules are thought to concentrate Rho regulating proteins (GEFs) to the cortex (Oliferenko et al., 2009). The accumulation of RhoGEF/Ect2 to the plus-ends of the microtubules depends on other central spindle proteins that co localize to the central spindle during anaphase and telophase. Recent cytological methods identified that Aurora B, Borealin, Survivin and INCENP, which form the chromosomal

passenger complex and is required for furrow formation, localize to a region of overlap of interpolar microtubules. Furthermore, this complex is required for the localization of the centralspindlin complex (mKLP1 and Cyk-4), which is responsible for binding the RhoGEF/Ect2 and localizing it to the microtubule ends (Severson et al., 2000; Somers and Saint, 2003). Plk1 and Prc1 have also been shown to localize and interact with these central spindle components as well as being required for RhoGEF/Ect2 localization (Neef et al., 2007; Petronczki et al., 2007). This model predicts that RhoGEF/centralspindlin complexes move along the interpolar microtubules and stably accumulate at the overlapping plus-ends. The difficulty with this model is in explaining how this central spindle accumulation of RhoGEF/Ect2 is transmitted to the cortex, which can be as much as ten microns away. However, this may be explained by the inability to resolve fine localizations of these components and the microtubules at the cell periphery.

Another model for spindle-based positioning of a furrow is the Polar-relaxation model. In this model, astral microtubules that interact with the poles of the cell send negative signals that inhibit cortical contraction. This model is built primarily on mathematical modeling and mictotubule density observations. Microtubule density is lower at the cortex near the furrow induction site while density is highest at the poles of the cell (Asnes and Schroeder, 1979; Dechant and Glotzer, 2003; White and Borisy, 1983; Yoshigaki, 2003). While at the cell equator, overlapping interpolar microtubules of the central spindle contact the cortex and send positive signals to specify cleavage sites. Thus, distinct groups of spindles cooperate

together to signal the furrowing site (Bringmann and Hyman, 2005; Glotzer, 2009). This model attempts to bring together observations from a variety of cell types into a more unifying theory.

Cytokinesis and Membrane Trafficking

For years it was thought that a fundamental difference between plant and animal cytokinesis was that plants require membrane trafficking and animals do not. In truth, plants rely on membrane trafficking to a greater extent than animals, in order to build a cell plate formed of fused vesicles at the cleavage site (Jurgens, 2005). In comparison, animal cells rely primarily on an acto-myosin contractile ring, which for the better part of a century is where the comparison stops. However, recent evidence in a variety of cell types and organisms has shown that membrane trafficking is essential for animal cytokines (Albertson et al., 2008; Otegui et al., 2005; Strickland and Burgess, 2004). For example, several studies have implicated trafficking of internal stores of membrane (golgi and recycling endosome) are required for cytokinesis (Lecuit and Wieschaus, 2000; Sisson et al., 2000). Further evidence comes from the observation that proteins involved in vesicle transport are localized to the furrow and are required for abscission, as well as a significant number of membrane trafficking genes that have been identified from cytokinesis screens in both *Drosophila* and *C. elegans* (Echard et al., 2004; Eggert et al., 2006; Finger and White, 2002; Schweitzer and D'Souza-Schorey, 2004). The delivery of vesicles seems to play important roles at every step of cytokinesis and is clearly that it is not solely

required for membrane addition, but also trafficking of necessary actin remodelers and other furrow components (Albertson et al., 2008; Cao et al., 2008).

Drosophila early embryo

The early *Drosophila* embryo is an excellent system to study these components of cytokinesis. Upon fertilization, the embryo divides 13 times within a common cytoplasm also known as a syncytium (Zalokar, 1976). These divisions are rapid and synchronous, consisting of only an S- and M-phase and rely only on the presence of Cyclin B to enter mitosis and its degradation to exit (Edgar et al., 1986). The syncytial divisions are entirely maternally controlled, which allows for easy genetic manipulation in the mother. The first 9 divisions occur in the middle of the embryo, away from the cortex. Nuclei are widely spaced from one another yet a dense network of astral microtubules develops and is necessary to drive nuclei out to the cortex during cycle 10 (Baker et al., 1993). Upon reaching the cortex, nuclei and their associated centrosomes and microtubules interact with the actin cortex resulting in the concentration of polymerized F-actin into apical caps above each nucleus (Karr and Alberts, 1986). These syncytial blastoderm divisions, as they are known, continue synchronously until the surface of the embryo is composed of a 6,000 nuclei monolayer.

The close proximity of these dividing nuclei at the surface requires some degree of separation in order to properly form a mitotic spindle and separate each nucleus during mitosis. Starting in interphase, apically positioned centrosomes

migrate around the nuclear envelope until they are 180° apposed from one another, roughly the equator of the nucleus and approximately 3 µm below the cortical actin. During this time of centrosome separation, the actin cap is uniformly expanding until neighboring cap edges collide. During mid-interphase to metaphase, the primary components of actin, membrane and myosin ingress from the surface to 5-7µm, encapsulating each nucleus laterally. These structures have been shown to be compositionally analogous to cytokinetic furrows and are termed metaphase furrows (Miller and Kiehart, 1995; Stevenson et al., 2002). In addition, mutations that affect cytokinesis in a variety of cell types have similar affects on metaphase furrow formation (Glotzer, 2005; Miller and Kiehart, 1995; Stevenson et al., 2002; Strickland and Burgess, 2004). However, metaphase furrows seem to rely more on vesicle trafficking than on acto-myosin contraction since inhibition of myosin has little effect on their formation (Royou et al., 2004). Regardless, the early *Drosophila* embryo has shown to be a remarkable system for exploring the regulation of furrow formation and was the primary system used in the following work.

Overview

Here I present a comprehensive study of cortical actin dynamics is they relate to mitotic spindle positioning, furrow positioning and the timing of furrow formation. I will show that in *Drosophila* embryos, centrosome separation prior to nuclear envelope breakdown, requires Rho1 and Diaphanous-dependent actin polymerization.

I will also show that furrow positioning in the syncytial divisions exists in two competing states (astral versus central spindle positioned) and until cellularization astral positioning is chosen do to the use of a maternal RhoGEF2. After cellularization, a zygotic RhoGEF localizes to the central spindle, making this the dominant furrow positioning signal. Lastly I will describe two mechanisms of regulating furrow formation. The first will show how Polo kinase directly regulates the activity of Nuf, which activates or inhibits vesicle trafficking to the cleavage furrow. Second, I will show a phenotypic description of a newly characterized gene Pops that indicates a novel role for folic acid metabolism and potentially methylation of the cytoskeleton in furrow formation and cellularization in the *Drosophila* embryo.

Chapter 2: Cortical actin dynamics contribute to the early stage of centrosome separation

Introduction

Centrosomes play important roles during both dividing and non-dividing cells. The primary role of centrosome pairs during mitosis is to organize microtubules into a functional bipolar spindle. Not only is a spindle essential for dividing chromosomes into the appropriate compartment of the dividing cell, but proper positioning and orientation of the spindle is essential for cleaving the dividing cell properly during cytokinesis. The primary way a bipolar spindle is positioned is through the regulated movement of centrosome pairs to apposing sides of the cell.

Conventional models of centrosome separation describe pushing and pulling forces derived from motors on the overlapping microtubules emanating from the centrosomes (Cytrynbaum et al., 2005; Robinson et al., 1999; Sharp et al., 2000). A more complete model of centrosome separation has shown it to include both nuclear envelope-dependent and -independent mechanisms (Rosenblatt, 2005). Current evidence has shown that the mechanisms on either side of NEB to separate centrosomes are very different. Prior to NEB, the minus-end directed motor Dynein is primarily responsible for moving centrosomes by anchoring to the nuclear envelope and to the actin cortex while moving along microtubules (Uzbekov et al., 2002; Vaisberg et al., 1993; Whitehead et al., 1996). After NEB, however, centrosomes are driven apart primarily by myosin-II driven cortical flow (Rosenblatt et al., 2004).

Additionally, *in vivo* studies suggest actin plays a passive role by serving as merely an attachment site of astral MTs to pull centrosomes apart (Buttrick et al., 2008; Cytrynbaum et al., 2005; Robinson et al., 1999; Stevenson et al., 2001). The role of actin and the interaction with dynein prior to NEB is less clear, however.

Here I will present studies using the early *Drosophila* embryo to demonstrate an active role for actin dynamics in positioning the centrosomes prior to NEB. The first 13 divisions of the *Drosophila* embryo occur rapidly, synchronously, and within a syncytium (Zalokar, 1976). From interphase of cycle 10 until cellularization at cycle 14, nuclei divide near the cortex of the embryo and these divisions a termed "Cortical blastoderm divisions". The close proximity of the nuclei to neighboring nuclei and spindles creates a need for physical barriers during mitosis. Dramatically, these nuclei reorganize the cortical actin into structures that surround each nuclei and spindle until metaphase when these structures are deconstructed. These structures are termed "Metaphase furrows" (Sullivan and Theurkauf, 1995). This system is ideal to study cellular events of mitosis since structures are clearly visible at the superficial depth. Furthermore, the synchrony of the divisions and the ease of genetic and pharmacologic manipulations provide huge amounts of information from a relatively small amount of embryos. In these embryos, centrosomes can be seen attached during telophase and early interphase and are apically localized to a cap of actin. We found that centrosomes separation correlates with the actin cap expansion that occurs prior to metaphase furrow formation. Furthermore, we show that proper centrosome separation during interphase does not require myosin II, but requires dynamic actin

rearrangements at the growing edge of this interphase cap. Both Arp2/3- and Formin-mediated actin remodeling are required for separating the centrosome pairs before NEB. The Apc2-Armadillo complex appears to link cap expansion to centrosome separation. In contrast, the mechanisms driving centrosome separation after NEB are independent of the actin cytoskeleton and can compensate for earlier separation defects. These studies show that the dynamics of actin polymerization drive centrosome separation and this has important implications for centrosome positioning during processes such as cell migration, cell polarity maintenance and asymmetric cell division.

Materials and Methods

Fly Strains and Genetics

Germline clones of *diaphanous*^{5} or *Arpc1*^{R337st} were generated using the FLP-DFS technique (Afshar et al., 2000; Chou and Perrimon, 1996; Stevenson et al., 2002). These two mutants and *Apc2*$^{\Delta S}$ were acquired from Bloomington *Drosophila* stock center. *sponge*^{335} was a gift from Eric Wieschaus. For live embryo imaging, we used the following stocks: GFP-alpha-Tubulin (a gift from Thomas Kaufman, (Grieder et al., 2000), GFP-Moesin (a gift from Daniel Kiehart, (Edwards et al., 1997) and GFP-Dlg (Discs Large) (FlyTrap Project, (Quinones-Coello et al., 2007). All stocks were raised at 25˚C on standard corn meal/molasses media.

Live Embryo Analysis

Embryos were prepared for microinjection and time-lapse scanning confocal microscopy as previously described (Tram et al., 2001). All the reagents were injected at 50% egg length and were diluted approximately 100 fold in the embryos (Foe and Alberts, 1983). For *sponge*, *diaphanous* and *Arpc1* mutant embryos, Rhodamine-conjugated tubulin (10mg/ml, Cytoskeleton) or Rhodamine-conjugated actin (10mg/ml, Cytoskeleton) was injected into the embryos at late cycle 10 or early cycle 11. The following drugs were injected at cycle 11 anaphase: DMSO alone (Sigma-Aldrich), LatA (10mM in DMSO, Sigma-Aldrich), Y-27632 (50mM and 2mM, Tocris), Jasp (1mM in DMSO, Calbiochem), C3 exotransferase (1mg/ml,

Cytoskeleton) and colchicine (0.5mM, Sigma-Aldrich). GFP-Dlg was used to mark the furrow membrane (Cao et al., 2008).

Confocal Microscopy and FRAP analysis

Confocal microscope images were captured on an inverted photoscope (DMIRB; Leitz) equipped with a laser confocal imaging system (TCS SP2; Leica) using an HCX PL APO 1.4 NA 63X oil objective (Leica). ImageJ software (National Institutes of Health, Bethesda, MD) was used to quantify the confocal images.

FRAP analysis were performed as previously described (Cao et al., 2008). Imaging was controlled by the Leica Confocal Software Microlab. After five prebleach scans of an entire image, 10 bleaching scans (0.7s each) with 100% intensity of 488 nm and 543 nm over the region of interest in the actin caps (10μm x 10μm) were performed. After photobleaching, fluorescence recovery was monitored 10 times every 0.7s and 60 times every 2s, and 10 times every 5s. The recovery of fluorescence intensities was measured with Microlab. The intensity of the bleached cap area was normalized to the background nonbleached area. Recovery percentage was calculated as the final plateau intensity (I_F) minus the first intensity after photobleaching (I_0) all divided by the difference between prebleach (I_I) and postbleach (I_0) intensities ($[I_F - I_0]/[I_I - I_0]$). The fluorescence intensity of each time-point (I_t) was transformed into a 0-1 scale calculated by $[I_t - I_0]/[I_I - I_0]$). The values of relative intensities versus time were plotted using Excel (2007; Microsoft), and the recovery $t_{1/2}$ was measured from the plots.

Image Quantifications and Statistics

Centrosome pair distances were quantified in the optical section with the strongest centrosome signal (GFP-Tubulin or injected Rhodamine-Tubulin). Centrosome pair angles were measured using the angle tool in ImageJ by placing the vertex at the approximate center of each nucleus. In Jasp-injected embryos, although centrosomes can separate further during subsequent prometaphase and metaphase, spindles tend to fuse with each other. To avoid secondary defects due to spindle fusion, we analyzed centrosomes only prior to NEB in Jasp-treated embryos.

For cap expansion analysis, time-lapse confocal images were taken of either GFP-Moesin or Rhodamine-actin injected embryos from NEF to NEB of cycle 12. A z-series was taken every 30 seconds during this time period with z-steps of 0.75μm starting at the very surface of the embryo. Cap expansion was measured using ImageJ. Confocal sections representing just the actin cap were used in all experiments. The freehand tool in ImageJ was used to encircle each cap, which allowed an area measurement. Four individual caps were measured in each embryo from the beginning of cycle 12. These four were followed every minute until the boundaries of each cap could no longer be differentiated from that of neighboring caps. In C3 treated embryos, caps were tracked only until 4 minutes after NEF when the cap boundaries became indiscernible. 3-4 caps per embryo were measured by this method with at least 3 embryos analyzed per genotype/drug treatment.

Student's t-tests (two-tailed, equal variance) were performed to analyze the data. For each embryo, multiple mitotic apparati were quantified and averaged. These averaged values were then used for statistics to estimate the variance between embryos under the same treatment. Error bars represent the standard error of the mean (SEM) from at least three independent experiments. For videos, image series collected over time were cropped in ImageReady (v9.0; Adobe) and converted to QuickTime (Apple) videos using PNG lossless compression.

Results

Centrosome separation is concomitant with actin cap expansion

To define the role of the actin cytoskeleton in centrosome separation, we examined centrosome separation in early *Drosophila* embryos. During the rapid synchronous divisions in the syncytial *Drosophila* embryo, the nuclei divide on a plane just beneath the plasma membrane, providing a means to simultaneously follow centrosomes, MTs and actin dynamics (Fig. 2.1A). During these divisions, centrosomes duplicate during telophase when actin caps form directly above each centrosome pair. Centrosome pairs migrate along the nuclear envelope at nuclear envelope formation (NEF) and move to the opposite poles (close to 180 degrees) before nuclear envelope breakdown (NEB) (Fig. 2.1A arrows, Fig. 2.2A-E). During this time, lateral expansion of the actin caps occurs (Fig. 2.1A-B). Centrosome separation is concomitant with actin cap expansion (Fig. 2.1A).

Disruption of F-actin cytoskeleton prevents centrosome separation before, but not after, NEB

To investigate the roles of the cortical actin cytoskeleton in centrosome separation and spindle assembly, embryos expressing GFP-Tubulin were injected with Latrunculin A (LatA) just prior to NEF. Since F-actin is constantly turning over in the furrows (Cao et al., 2008) and caps (Fig. 2.8C), LatA injection resulted in a rapid loss of F-actin from both these structures and prevented furrow invagination in

the following cell cycle (Fig. 2.6). In wild-type uninjected cycle-12 embryos, the distance between centrosome pairs at cycle 12 NEB is about 8μm (Fig. 2.4A and 2.5A). DMSO injection had very little effect on centrosome separation (Fig. 2.4B and Fig. 2.5A-C). In LatA injected embryos, approximately a quarter of the nuclei clustered during early interphase, which resulted in failed centrosome separation and multipolar spindles (Fig 2.3). To avoid secondary effects on centrosome separation due to LatA-induced clustering of nuclei, we only quantified centrosome separation in nuclei that did not cluster (the same criteria also applies to the other genetic or drug manipulations). For the unclustered nuclei, LatA did not appear to affect centrosome splitting, as the centrosome pairs were clearly distinguishable and detached from each other after NEF (Fig. 2.4C). However, during the interval between centrosome splitting and NEB, centrosomes failed to separate normally (Fig. 2.4C, 2.5BA-C). The distance between centrosomes (4.0±0.5μm) was significantly shorter and the separation angle (65±11°) was also significantly smaller at NEB of cycle-12 than in control embryos injected with DMSO (7.4±0.5μm and 158±5°), indicating a role for actin in early separation of centrosomes (Fig. 2.4C). Defects in early centrosome separation were also observed in embryos derived from females homozygous for the *sponge* (*spg*) maternal-effect mutation (Fig. 2.4D and 2.5A-C), which lack both actin caps and furrows (Postner et al., 1992). However, following NEB in LatA treated embryos and embryos laid by *sponge* mutant females, sister centrosomes separated fully to ultimately establish a bi-polar spindle during prometaphase-metaphase (Fig.

2.4C-D, 2.5C), indicating that a nuclear envelope and actin independent pathway compensates for the earlier actin-based separation defects.

Actin turnover is required for centrosome separation before NEB

To determine whether actin dynamics are required for centrosome separation, the actin-stabilizing drug, Jasplakinolide (Jasp), was injected into embryos immediately prior to NEF. Similar to LatA-mediated inhibition of actin polymerization, Jasp-mediated actin stabilization strongly inhibited centrosome migration before NEB (Fig. 2.4E, 2.5A-C). The respective pole-pole distance and separation angle were 5.5±0.4μm and 98±25° in Jasp-treated embryos, compared to 7.4±0.5μm and 158±5° in DMSO treated control embryos. Since both disruption and stabilization of F-actin inhibit early centrosome separation, these data suggest that actin turnover is important for proper centrosome separation before NEB.

Inhibition of actin turnover during interphase prevents actin cap expansion

Injecting Jasp before NEF resulted in strong actin accumulation at the cap (Fig. 2.6). In control embryos, actin caps expanded laterally from NEF through early interphase and eventually made contact with one another (Fig. 2.7A-B). In contrast, actin caps failed to expand and actually shrunk over time after Jasp treatment (Fig. 2.7A-B). FRAP analysis indicated the Jasp-induced defects in actin cap expansion could be due to failed actin turnover at the cap. Actin turnover rates ($t_{1/2}$) at the interphase caps in untreated (N=10 embryos) or DMSO (N=10 embryos) injected

embryos were 18.9±1.7s and 17.9±2.2%, with most of the actin (87.3±2.4% and 85.0±4.3%, respectively) recovered in the photobleached region after 80s (Fig. 2.8C-D). However, in Jasp-treated embryos, only 25.5±3.0% of the total actin recovered after 80s (N=10 embryos), with a very slow turnover halftime of 50.5±5.3s (Fig. 2.8C-D).

Thus inhibition of actin turnover results in failed actin cap expansion and failed centrosome separation. Previous studies have demonstrated that centrosome separation is not required for actin cap expansion: centrosome separation fails in colchicine-treated embryo but there is very little effect on actin cap expansion (Stevenson et al., 2001). Our experiments confirm this finding (Fig. 2.4F and 2.7A).

Disruption of Arp2/3, an actin branching complex, strongly inhibits actin cap expansion and centrosome separation

To test the converse relationship, whether actin-cap expansion is required for centrosome separation, we analyzed mutants in Arpc1, a key component of the Arp2/3 complex. The Arp2/3 complex has been shown to localize to the margins of the actin caps and promote cap expansion, presumably through its actin branching activity (Stevenson et al., 2002). In control embryos, actin caps expanded to their maximum size (117.4±4.1μm^2) 5 min after NEF. However, the cap size in *Arpc1* embryos (the progeny of *Arpc1* mutant maternal germline clones) had only increased slightly 5 min after NEF and from then on maintained an almost constant size until NEB (63.7±7.8μm^2, Fig. 2.3A-B). This is about half of the maximum cap size

observed in wild-type controls. These data are consistent with the published *Arpc1* phenotype (Stevenson et al., 2002). Concomitantly, *Arpc1* mutant embryos displayed a significant reduction in the distance and angle of separation between centrosome pairs at NEB (6.1±0.2μm and 136±7°, compared to 8.0±0.2μm and 169±1° in wild-type controls, Fig. 2.4G and 2.5A-C).

Blocking Formin/Diaphanous and RhoA activities also interferes with cap expansion and centrosome separation before NEB

Cap expansion driven by Formin-mediated actin bundling is also required for centrosome separation before NEB. Diaphanous (Dia), the *Drosophila* Formin homolog, is required for actin bundling and metaphase furrow formation (Afshar et al., 2000). Initial cap size was normal in *dia* embryos (the progeny of *dia* mutant maternal germlines) but cap expansion was strongly inhibited, with the cap size at NEB (76.6±4.4μm^2) reaching only 65% of the normal cap size (Fig. 2.7-8). Inhibition of RhoA, the upstream regulator of Diaphanous (Padash Barmchi et al., 2005), through C3 exotransferase (C3), resulted in stronger defects in cap expansion (Fig. 2.7-8). Corresponding decreases in centrosome separation before NEB were observed in *dia* and C3 treated embryos (Fig.2.4H-I and 2.5A-C). Together these studies demonstrate that cap expansion is required for centrosome separation.

***Apc2* mutant embryos exhibit relatively normal cap expansion**

The Apc2-Armadillo complex in the fly early embryo has been shown to regulate centrosome separation (Buttrick et al., 2008). Based on its localization to cortical sites where actin and MTs interact (McCartney et al., 2001), it was proposed that the Apc2-Armadillo complex facilitates centrosome separation through stabilizing the interaction between the actin cortex and astral MTs (Buttrick et al., 2008). Alternatively, since we have shown actin cap expansion is required for centrosome separation before NEB, it is possible that the Apc2-Armadillo complex facilitates centrosome separation by directly promoting actin cap expansion. To differentiate these two possibilities, cap expansion was examined in *Apc2* mutant embryos. The initial cap size and the cap expansion rate in *Apc2* embryos are very similar to that observed in uninjected control embryos (Fig.2.7-8). To confirm that these *Apc2* embryos were defective in centrosome separation, Rhodamine-labeled tubulin was injected into these embryos to follow centrosome movements. Our data showed very similar centrosome separation defects before NEB (159±2° compared to 169±1° in wild-type controls, Fig. 2.4J and 2.5B) as previously published results (Buttrick et al., 2008). Because *Apc2* embryos do not disrupt actin cap organization (McCartney et al., 2001; Webb et al., 2009), the effects on centrosome separation were not as dramatic as those observed for the actin inhibitors and thus we did not observe significant differences in distance in which the centrosomes separated (Fig. 2.5A). In addition, after NEB, the incomplete separated centrosome pairs were able to correct the earlier defects and achieve full separation by metaphase (Fig. 2.4C).Taken

together, these suggest that Apc2-Armadillo complex functions downstream of actin cap expansion to regulate centrosome separation before NEB.

Myosin II-driven cortical flow is not required for centrosome separation before NEB

Actin-myosin II driven cortical flow has been proposed to separate centrosomes after NEB in mammalian cultured cells (Rosenblatt et al., 2004). To determine whether myosin II, similar to actin, facilitates centrosome separation during the cortical divisions in *Drosophila* embryos, we relied on the small molecule inhibitor Y-27632, a drug that inhibits Rho kinase, which in turn blocks myosin II light chain kinase and thus myosin II activity. We used a drug concentration (50mM) that has been proven to effectively block myosin II activity in our system (Royou et al., 2004). Significant delay into mitosis was often observed after Y-27632 injection (from cycle 12 NEF to NEB, 1455 ± 296 s versus 588 ± 15 s in control embryos). Unlike LatA injection, myosin II inhibition by Y-27632 had only a very mild effect on centrosome separation before NEB and the metaphase spindle length was about the same as that in control embryos (Fig. 2.9A-C). The relatively normal centrosome separation and spindle formation after inhibiting myosin II is consistent with previously published results (Royou et al., 2004). Thus, it appears that centrosome separation during the cortical divisions in the *Drosophila* embryo does not rely on myosin II activity.

Discussion

Centrosome migration around the nuclear envelope relies on actin dynamics

In the early *Drosophila* embryo, centrosomes migrate to opposite poles prior to NEB. Microtubules and the motor protein dynein are required for this period of separation (Cytrynbaum et al., 2005; Robinson et al., 1999; Sharp et al., 2000). Another minus-end directed motor, Ncd, slides anti-parallel microtubules as a brake against dynein (Cytrynbaum et al., 2005; Sharp et al., 2000). However, these motors alone are not sufficient for separation of centrosomes prior to NEB since cytochalasin treatment produces defects and mathmatical models also support dynein/actin-dependent separation (Cytrynbaum et al., 2005; Stevenson et al., 2001). Our data plus another study also suggests that aster microtubules a linked to the actin cortex by the Armadillo-APC2 complex prior to NEB (Buttrick et al., 2008).

Our results show that cortical actin is actively involved in centrosome separation prior to NEB. Similar to dynein mutants, centrosomes fail to migrate completely when treated with the actin disrupting drugs, Latrunculin A and Jasplakinolide (Robinson et al., 1999; Sharp et al., 2000). In dissecting the specific role of the expanding actin cap, we genetically disrupted the formation of caps or limited their expansion resulting in reduced centrosome distances. Finally we demonstrated that the actin regulators RhoA and Diaphanous are required for centrosome separation before NEB. Therefore, we propose that the growing edge of the actin cap and the following invagination drive centrosomes apart by the cortical interaction with dynein and this expanding cap is dependent upon Rho1 and

Diaphanous. Furthermore, we propose one potential connection between the astral microtubules and the growing edge is the Apc2-Armadillo complex of proteins.

Mammalian tissue culture cells offer another role for actin prior to NEB. Cortactin, an F-actin binding protein was shown to be required for separation prior to NEB (Wang et al., 2008). This model proposes that phosphorylated Cortactin localizes to the centrosome and serves as an attachment point between centrosomes and F-actin. This provides direst force to separate the centrosomes.

Nuclear envelope independent centrosome separation serves as a backup when centrosome migration fails before NEB

Despite the lack of separation in our treatments, once a bipolar spindle forms after NEB, the centrosomes rapidly move to a proper orientation. Actin appears to be dispensable for separation after NEB. Since the actin cortex is abolished, microtubule motors that crosslink the newly formed spindle are most likely generating the force for this correction. Moreover, since the effect is not seen prior to NEB, the most likely candidates would be active during prometaphase. One possibility is the kinesin KLP61F, which is released from the nucleus at NEB. It has been proposed that it can counter the inward forces generated by Ncd by sliding antiparallel microtubules apart (Sharp et al., 2000; Sharp et al., 1999). Nonetheless, our data proposes that the spindle can both elongate and correct orientation of the spindles in a nuclear envelope and actin independent mechanism.

Figures

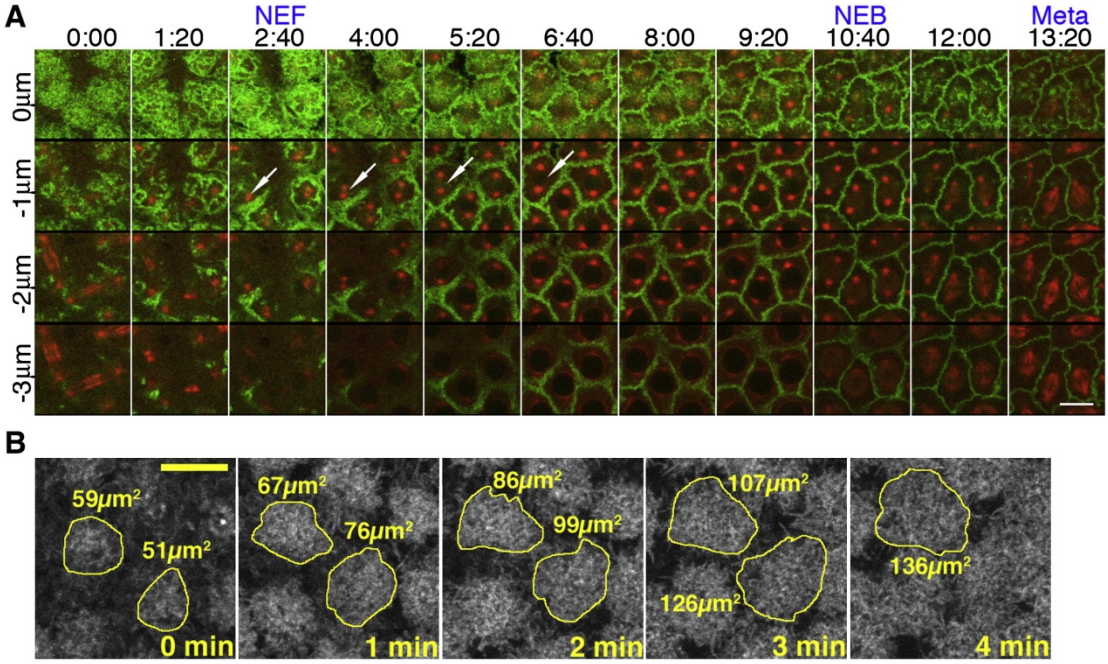

Figure 2.1. **Centrosome separation is concomitant with actin cap expansion. (**A) Cycle 12 syncytial blastoderm. Green depicts GFP-moesin; red depicts Rhodamine-tubulin; x axis represents time; y axis represents depth. Z series are shown, starting from the cortical surface (z = 0) to 3 µm below the surface (z = −3 µm) at 1 µm increments. At telophase, actin caps form at the cortical surface and initiate lateral expansion. This cap expansion is shown in the top panel, where gaps between caps are seen initially from time 0:00 to 6:40, after which GFP-moesin-marked actin has filled the entire frame. Concurrently, centrosome pairs separate from each other (arrows). See also Figure S1. (B) Panels depict the method of measuring actin cap area in wild-type embryos expressing GFP-moesin. The freehand tool in ImageJ was used to outline individual caps at the beginning of cycle 12. Each cap is measured every minute until it can no longer be distinguished from its neighbors. Scale bars represent 10 µm.

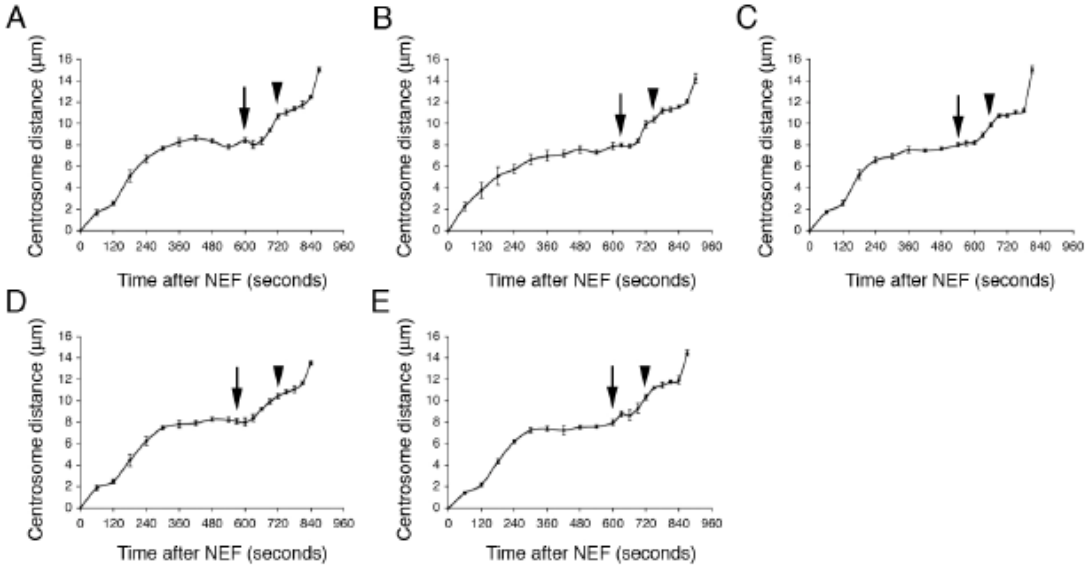

Figure 2.2. **Centrosome separation during nuclear cycle 12.** Centrosome pair distances were measured during nuclear cycle 12 in five uninjected GFP-Tubulin embryos, represented by different colors. Filled arrows indicate the time of nuclear envelope breakdown (NEB). Open arrows indicate the time point before initiation of anaphase A. Standard errors are calculated from the variance of nuclei within each embryo.

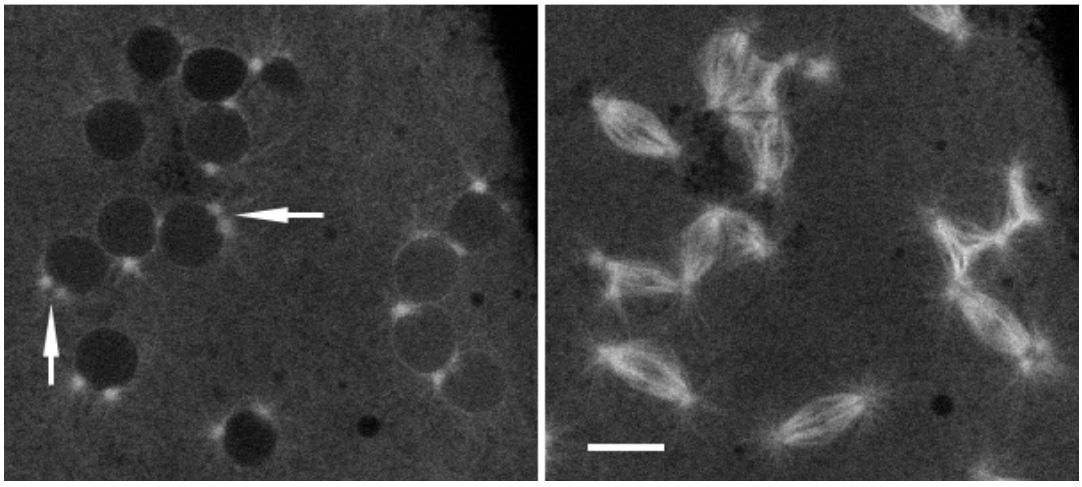

Figure 2.3. **Clustering of nuclei in LatA injected embryos produces secondary centrosome phenotypes.** GFP-Tubulin embryos injected with 10mM LatA during late anaphase of cycle 11. Arrows indicate centrosomes that prematurely stop migrating after nuclear collisions. Note the multipolar spindle formed between these nuclei. Arrows indicate prematurely halted centrosomes due to clustering of nuclei. Scale bar: 10 microns.

Figure 2.4. **Cortical actin reorganization is required for centrosome separation before nuclear envelope breakdown.** Time-lapse images of: (A) Uninjected GFP-Tub embryo. See Movie S1. (B) Dimethyl sulfoxide (DMSO)-injected GFP-Tub embryo. (C) 10 mM latrunculin A (LatA)-injected GFP-Tub embryo. (D) Rhodamine-tubulin-injected spg embryo. (E) 1 mM Jasp-injected GFP-Tub embryo. (F) 0.5 mM colchicine-injected GFP-Tub embryo. (G) Rhodamine-tubulin-injected Arpc1 embryo. (H) Rhodamine-tubulin-injected dia embryo. Centrosomes in dia and Arpc1 embryos were imaged more apically than controls, indicating a slowed migration toward the midline of the nucleus. (I) 1 mg/mL C3 exotransferase-injected GFP-Tub embryo. (J) Rhodamine-tubulin-injected Apc2 embryo. Schematic drawings on the right side of each image series (A–J) illustrate the degree of centrosome separation from nuclear envelope formation (NEF) to nuclear envelope breakdown (NEB).

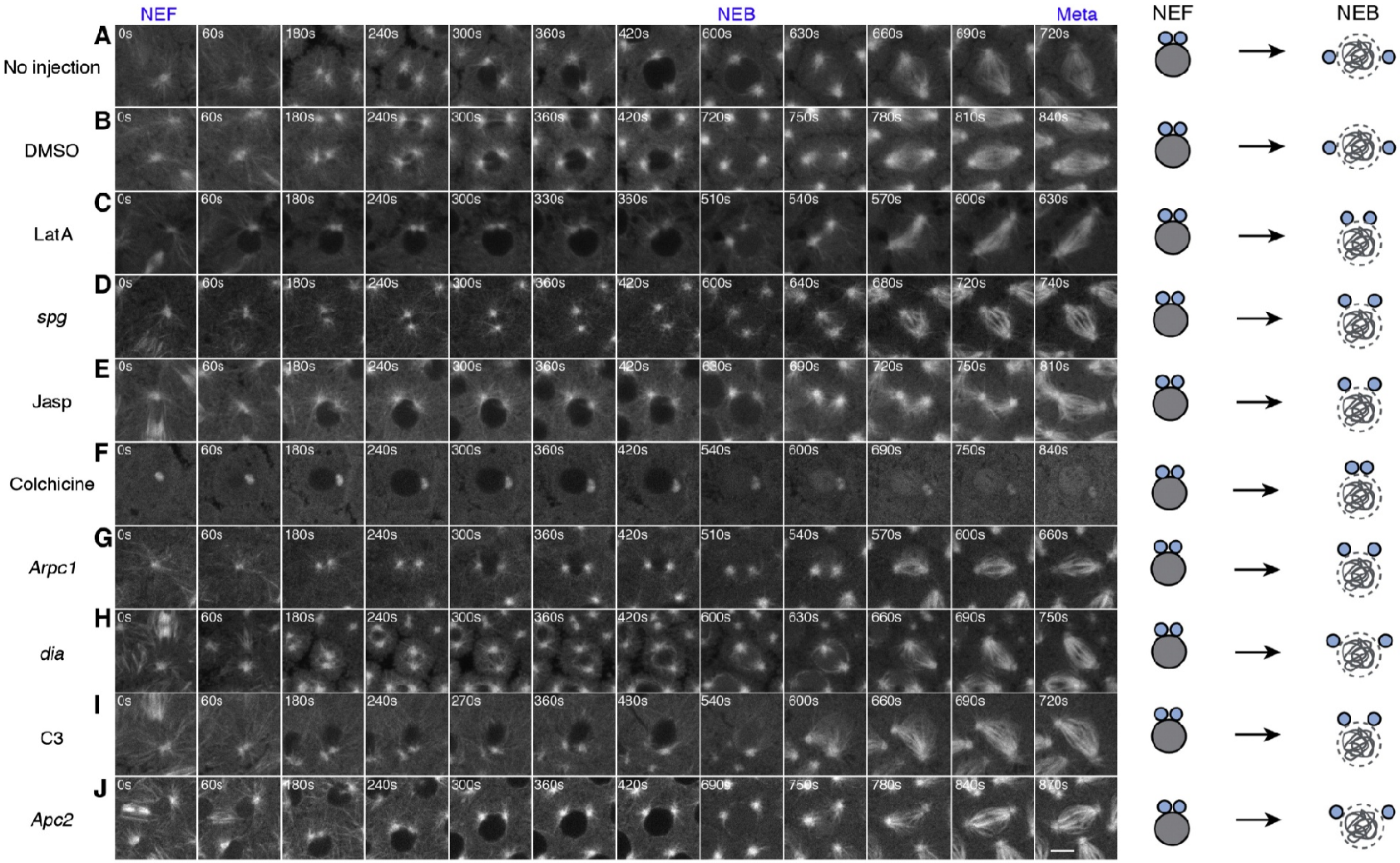
NEF
NEB
Meta
A
No injection
0s 60s 180s 240s 300s 360s 420s 600s 630s 660s 690s 720s
B
DMSO
0s 60s 180s 240s 300s 360s 420s 720s 750s 780s 810s 840s
C
LatA
0s 60s 180s 240s 300s 330s 330s 510s 540s 570s 600s 630s
D
spg
0s 60s 180s 240s 300s 360s 420s 600s 640s 680s 720s 740s
E
Jasp
0s 60s 180s 240s 300s 360s 420s 630s 690s 720s 750s 810s
F
Colchicine
0s 60s 180s 240s 300s 360s 420s 540s 600s 690s 750s 840s
G
Arpc1
0s 60s 180s 240s 300s 360s 420s 510s 540s 570s 600s 660s
H
dia
0s 60s 180s 240s 300s 360s 420s 600s 630s 660s 690s 750s
I
C3
0s 60s 180s 240s 270s 360s 430s 540s 600s 660s 690s 720s
J
Apc2
0s 60s 180s 240s 300s 360s 420s 690s 750s 780s 840s 870s
NEF
NEB

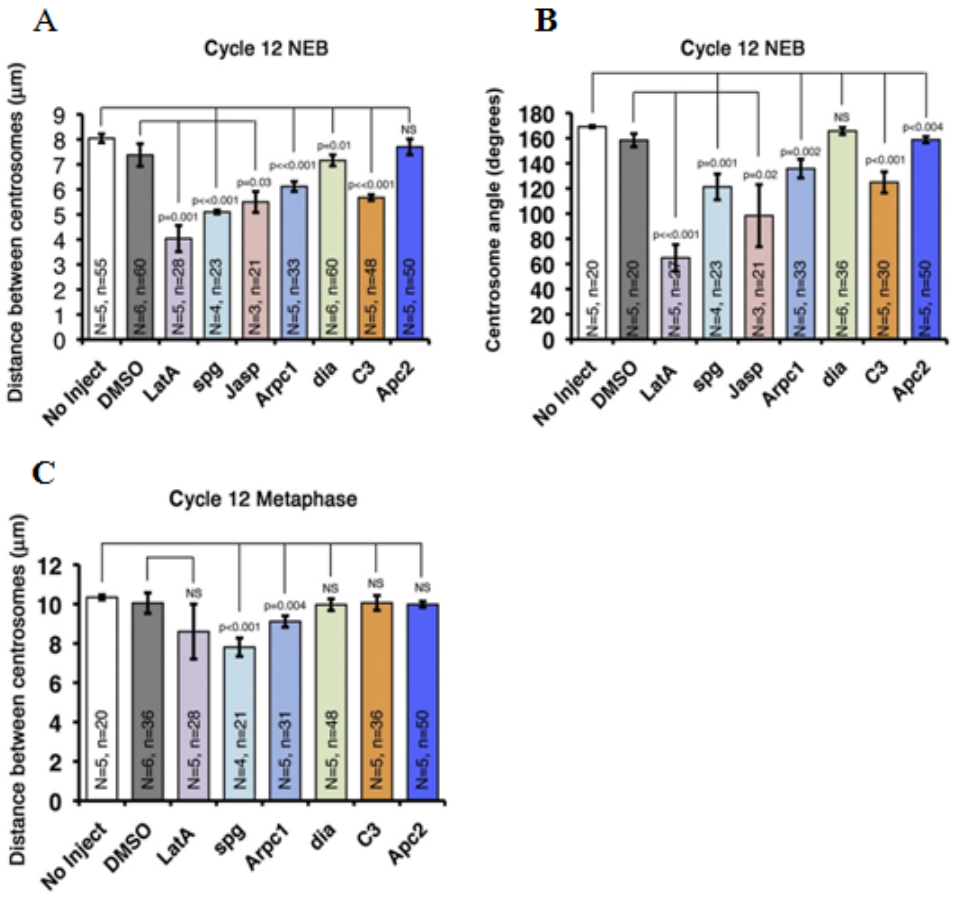

Quantification of centrosome separation prior to nuclear envelope breakdown. (A) Mean distance between centrosome pairs at NEB. (B) Mean angle between centrosome pairs at NEB with respect to the nuclear center. The centrosome pairs of dia embryos failed to migrate basally but were able to separate from each other normally at a focal plane above the equator of each nucleus. (C) Mean centrosome pair distances at metaphase. The following abbreviations are used: N, total number of embryos counted; n, total number of nuclei counted; NS, not statistically significant. Error bars represent the standard error of the mean (SEM) from at least three different embryos.

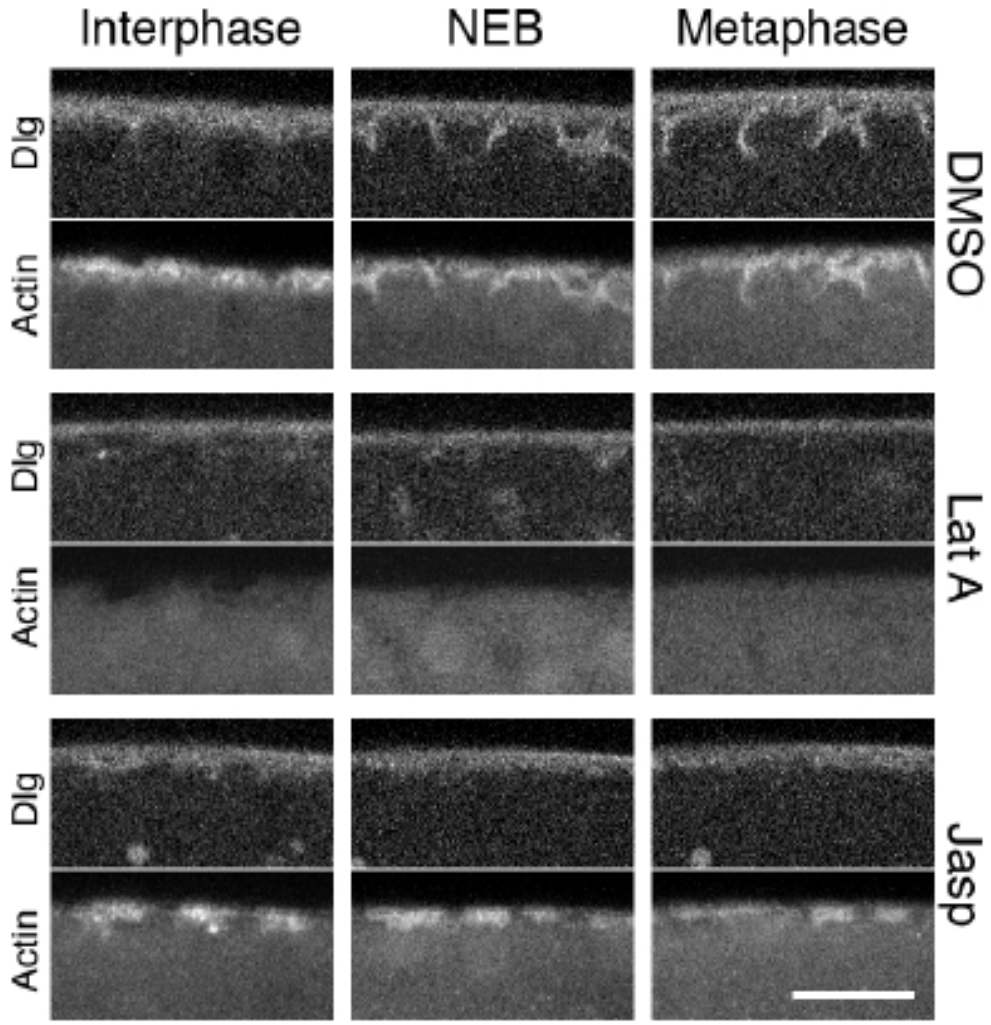

Figure 2.6. **The effects of LatA and Jasp on actin Cap expansion and furrow invagination.** 1mM Jasp, 10mM LatA, or DMSO control were injected into GFP-Dlg embryos, which have been previously injected with Rhodamine-actin, at anaphase of cycle 11. Furrow invagination and actin distribution were imaged during cycle 12. Scale bar: 20 microns.

Figure 2.7. **Actin cap expansion Is driven by Arp2/3- and RhoA-Diaphanous-mediated actin remodeling.** (A) Actin-based cap expansion was imaged after NEF in wild-type untreated, DMSO-treated, Jasp-treated, colchicine-treated, C3-treated, Arpc1, dia, and Apc2 embryos. In each row, cap expansion is illustrated by dotted lines. Schematic drawings on the right side of each image series illustrate actin cap expansion (actin is in red) relative to centrosome separation from NEF to NEB.

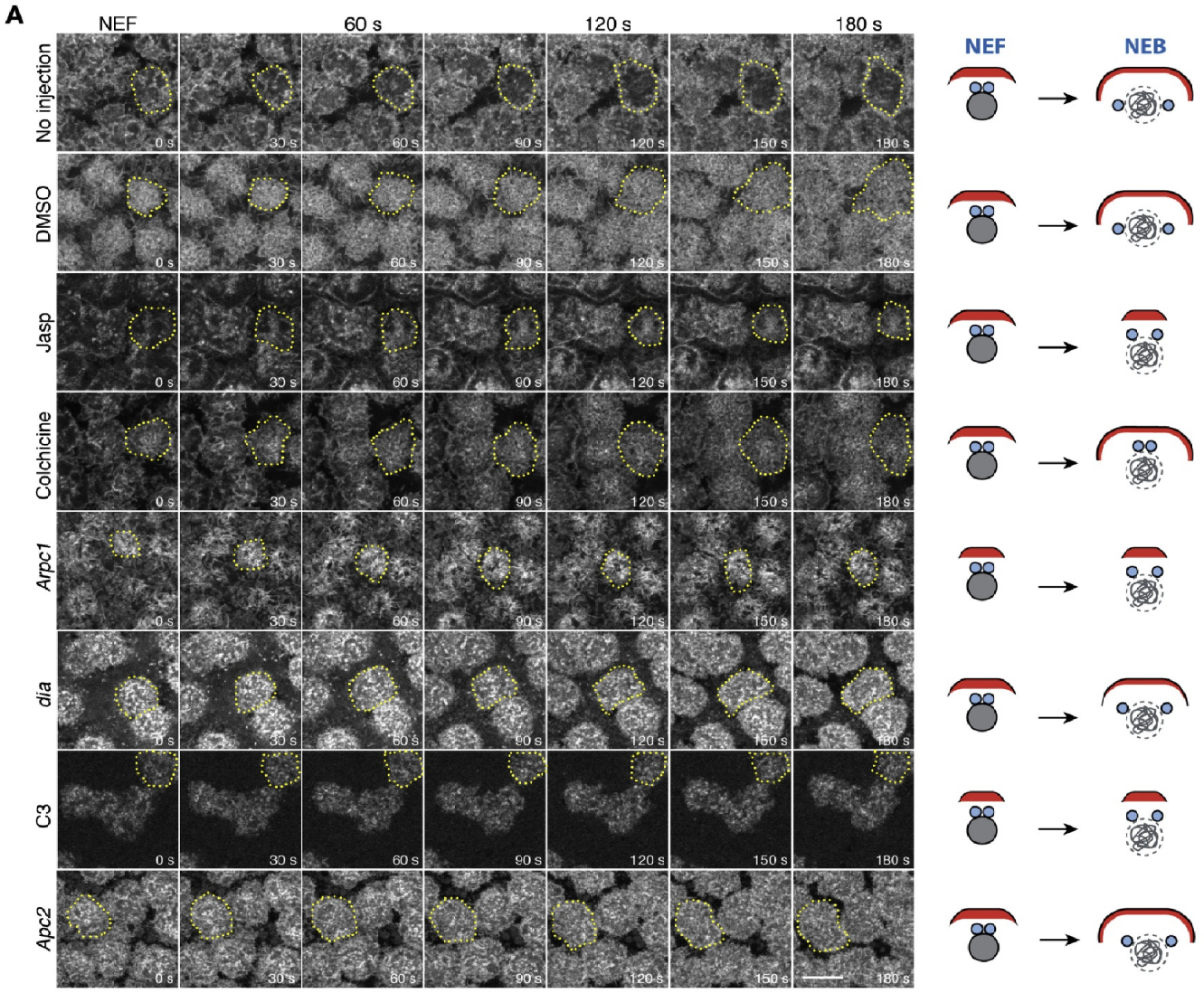
A
NEF
60 s
120 s
180 s
No injection
DMSO
Jasp
Colchicine
Arpc1
dia
C3
Apc2
0 s
30 s
60 s
90 s
120 s
150 s
180 s
NEF
NEB

Figure 2.8. **Quantification of actin cap expansion and inhibition of actin turnover by Jasplakinolide.** (A) The rate of actin cap area expansion after NEF in the drug-treated and mutant embryos imaged in Figure 2.7. The following abbreviations are used: N, total number of embryos; n, total number of caps counted.(B and C) Fluorescence recovery after photobleaching analysis of actin turnover at the interphase cap in untreated and Jasp-treated embryos, showing relative fluorescence intensities of Rhodamine-actin at the caps after photobleaching. The prebleach intensities were arbitrarily set to 1. Scale bars represent 10 μm. Error bars represent the SEM from at least three different embryos.

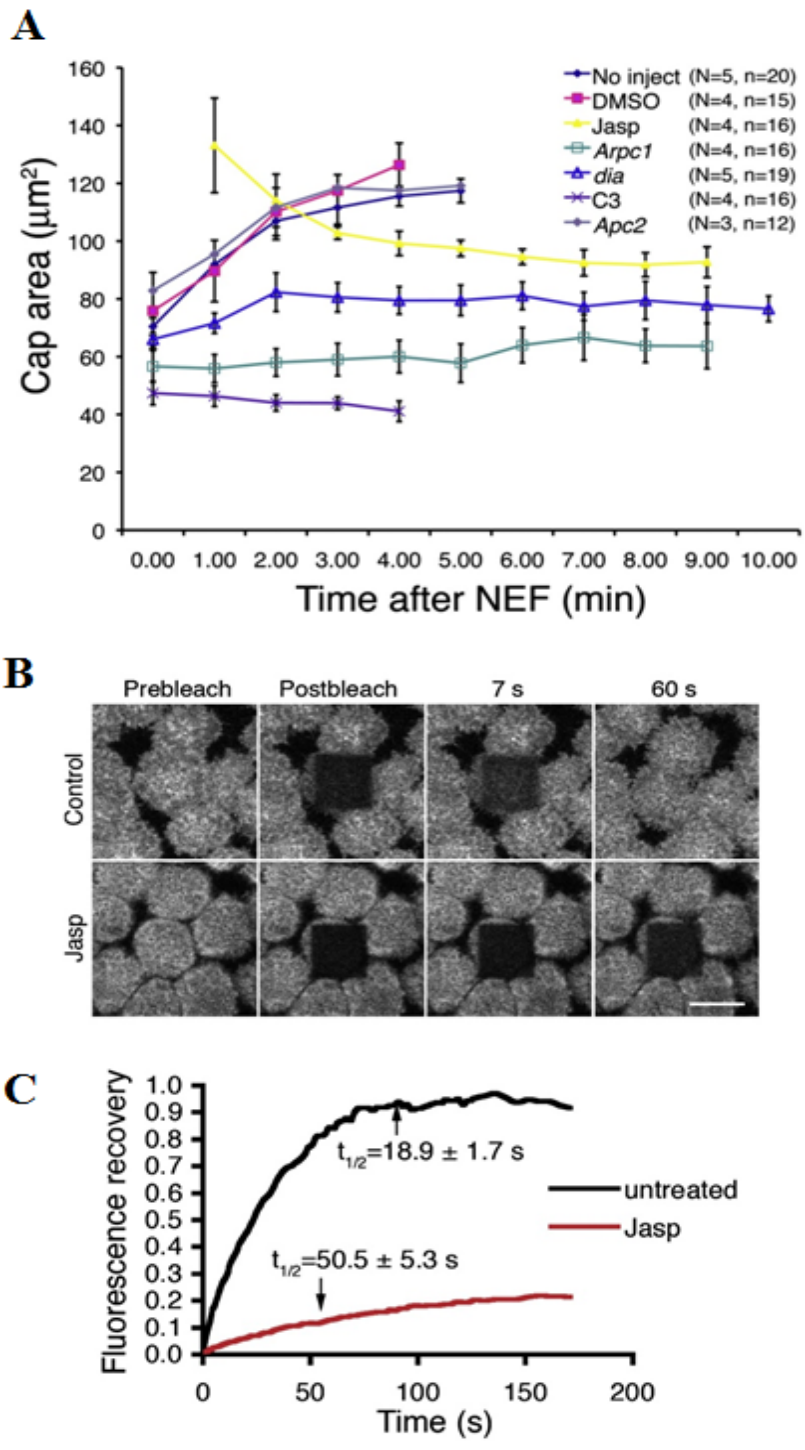
A
Cap area (µm²)
Time after NEF (min)
No inject (N=5, n=20)
DMSO (N=4, n=15)
Jasp (N=4, n=16)
Arpc1 (N=4, n=16)
dia (N=5, n=19)
C3 (N=4, n=16)
Apc2 (N=3, n=12)
B
Prebleach
Postbleach
7 s
60 s
Control
Jasp
C
Fluorescence recovery
Time (s)
t1/2=18.9 ± 1.7 s
t1/2=50.5 ± 5.3 s
untreated
Jasp

Figure 2.9. **Disruption of myosin II by Y-27632 has a very mild effect on centrosome separation before NEB.** (A) 50 mM Y-27632 was injected into GFP-tubulin embryos. Prolonged interphase, nuclear swelling, and centrosome detachment from the nuclear envelope were observed. A lower drug concentration (2 mM) failed to produce any of these phenotypes (data not shown). Scale bar represents 10 μm. (B) Mean angle of centrosome pairs at NEB of uninjected embryos and Y-27632-treated embryos. Because the 50 mM Y-27632 injection induced prolonged interphase, the centrosome angle of Y-27632-treated embryos was also measured at 600 s after NEF, the equivalent timing of NEB in control embryos.(C) Centrosome distance at NEB and metaphase of uninjected embryos and Y-27632-treated embryos. The increase in centrosome distance in Y-27632-treated embryos at NEB was due to the nuclear swelling phenotype induced by this drug injected at 50 mM. The following abbreviations are used: N, total number of embryos; n, total number of nuclei counted. Error bars represent the SEM from at least three different embryos.

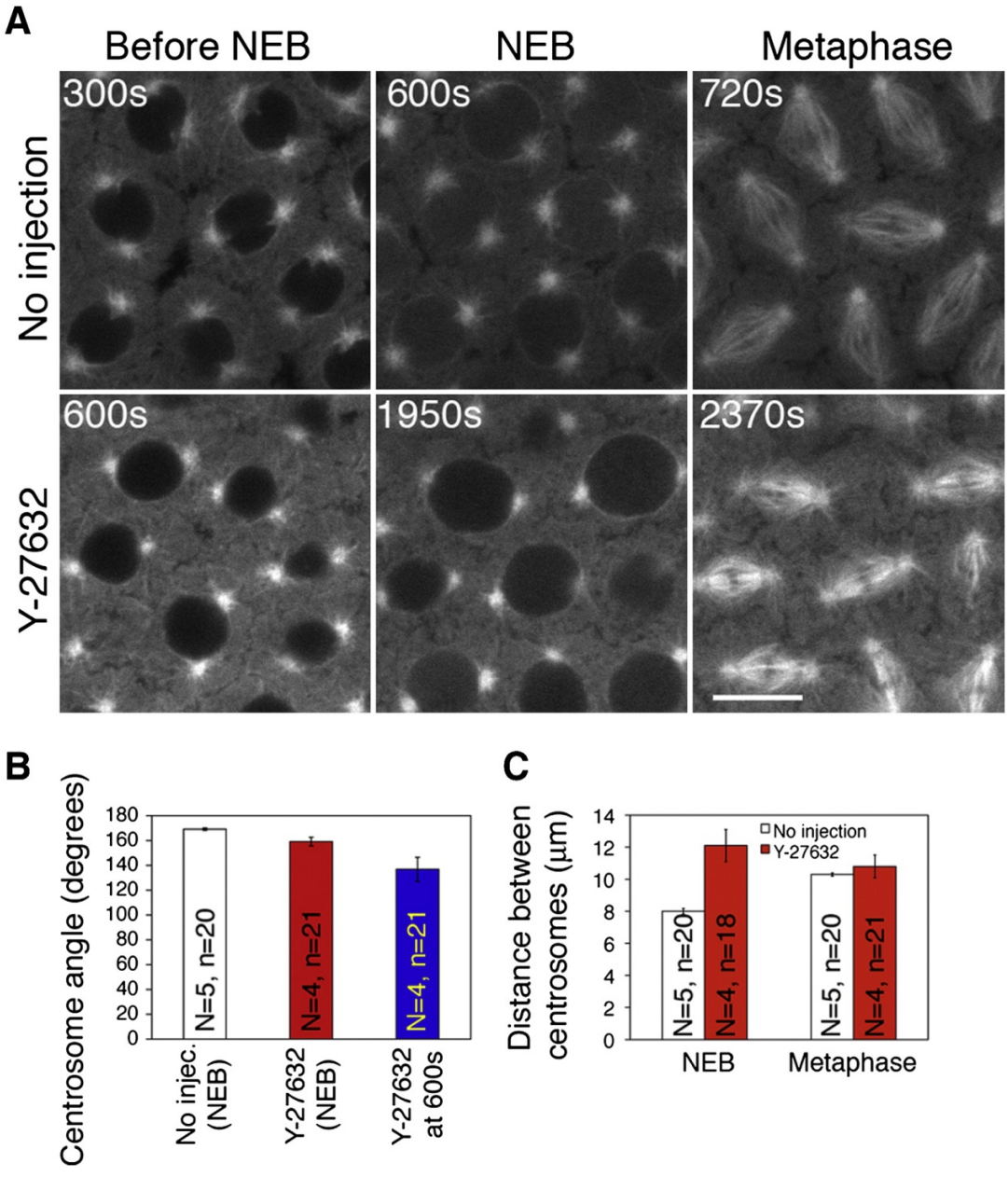
A
Before NEB
NEB
Metaphase
No injection
Y-27632
300s
600s
720s
600s
1950s
2370s
B
Centrosome angle (degrees)
180
160
140
120
100
80
60
40
20
0
N=5, n=20
N=4, n=21
N=4, n=21
No injec. (NEB)
Y-27632 (NEB)
Y-27632 at 600s
C
Distance between centrosomes (µm)
14
12
10
8
6
4
2
0
No injection
Y-27632
N=5, n=20
N=4, n=18
N=5, n=20
N=4, n=21
NEB
Metaphase

Chapter 3: RhoGEF, ectopic furrow induction and positioning Rappaport-like furrows in the early *Drosophila* embryo

Introduction

Cytokinesis, the final event of the cell cycle, produces two distinct daughter cells through the formation of an acto-myosin based contractile ring. This ring forms perpendicular and midway to the spindle apparatus during anaphase and telophase (Barr and Gruneberg, 2007). An outstanding issue in the field is understanding the mechanisms that position the contractile ring. Classic work by Rappaport in sand dollar embryos demonstrated that overlapping astral microtubules are essential for establishing furrow position (Rappaport, 1961). Subsequent to this, studies in *C. elegans* and mammalian tissue culture cells determined that the overlapping microtubules of the central spindle also play a key role in inducing furrow formation (Bringmann and Hyman, 2005; Wheatley and Wang, 1996). Current models suggest that, in fact, both of these microtubule populations are acting in concert to position the cleavage furrow, however it has been shown that, in specific cell types, one population may play a more prominent role than the other (reviewed in(von Dassow, 2009) .

Recent studies have made significant progress regarding the mechanisms by which the central spindle establishes furrow position (reviewed in (D'Avino et al., 2005; Gatti et al., 2000). The central spindle is composed of overlapping anti-parallel microtubules that form during anaphase/telophase and loss of the central spindle

results in a failure to initiate furrow formation. Identification of protein complexes associated with the central spindle, centralspindlin and the chromosomal passenger complex, provide molecular insight into how the central spindle might position the furrow (reviewed in (Oegema and Mitchison, 1997). During anaphase, bundling of overlap microtubules at the central spindle provides an essential scaffold to recruit and position components that drive the formation of the contractile ring. An early step in this process is driven by Prc1 (*Drosophila* Fascetto), which promotes the bundling and crosslinking of microtubules to form the central spindle (Mollinari et al., 2002). Once formed, the chromosome passenger complex (CPC), consisting of Aurora-B kinase, INCENP, Survivin, and Borealin/Dasra, recruits a second complex, called centralspindlin, to the central spindle (Carmena, 2008). Centralspindlin consists of the plus-end motor protein kinesin-MKLP (*Drosophila* Pavarotti) and the RacGAP50C protein (*Drosophila* Tumbleweed). Localization of the centralspindlin complex at the central spindle is required for furrow ingression (Mishima et al., 2002). Polo kinase binds or phosphorylates several of these central spindle proteins, including Prc1 and RacGAP50C and is required for furrow formation (Ebrahimi et al., 2010; Rape, 2007).

Taken together these proteins are thought to set the stage for positioning and formation of the contractile ring. The current model is that RhoGEF binds Centralspindlin, which accumulates RhoGEF to the plus-ends of the microtubules (the midpoint of the central spindle) near the equatorial cortex (D'Avino and Glover, 2009; Somers and Saint, 2003). The most peripheral microtubules of the central

spindle are in fact close to the cell cortex. Once recruited and cortically positioned, RhoGEF binds and locally activates cortically localized RhoA, a GTPase responsible for actin polymerization and myosin activation via the Rho pathway (Gregory et al., 2010). While this model is satisfying, several studies indicate that in some cell types the central spindle is completely dispensable for furrow initiation. For example, in sea urchin embryos, both the central spindle and the astral microtubule arrays can independently induce normal cytokinetic furrows (von Dassow, 2009). Further support comes from the ectopic furrows formed in sand dollar embryos, which are induced solely by astral microtubules (Rappaport, 1961). In addition experiments in which cells with monopolar spindles enter anaphase form ectopic cleavage furrows at sites where astral microtubules interact with cortex (Canman et al., 2003; Hu et al., 2008).

Given these studies, it is of interest to determine the relative roles of the central spindle and astral microtubules in situations of unconventional positioning of the cleavage furrow. For example, during the cortical syncytial division of insect embryos, cytokinesis furrows, known as metaphase furrows, encompass rather than bisect the spindle. Also in contrast to conventional cytokinesis, these furrows form during prophase/metaphase in order to isolate each spindle and prevent it from inappropriately interacting with neighboring spindles. In addition, unlike conventional cleavage furrows, metaphase furrow ingression is myosin independent, relying exclusively on vesicle mediated membrane addition (Rothwell et al., 1999; Royou et al., 2004). During anaphase/telophase these furrows are dismantled and new

metaphase furrows form in the next cell cycle. Despite the spatio/temporal differences between conventional furrows and metaphase furrows, they are structurally and compositionally identical and the formation of both requires microtubules (Miller, 1995; Stevenson et al., 2002).

The mechanisms positioning metaphase furrows are unclear. They are analogous to Rappaport furrows and overlapping astral microtubules between neighboring spindles may induce furrow formation. Supporting evidence comes from the observation that metaphase furrows form only after the nuclei are at a sufficient density such that overlap of astral microtubules occurs. In addition, disrupting microtubules prevents metaphase furrow formation (Riggs et al., 2007). RhoGEF2, the maternally-supplied RhoGEF, relies on microtubule based vesicle trafficking from the recycling endosomes (Cao et al., 2008). The roles, if any, of the other central spindle proteins in forming these furrows have yet to be determined. Furthermore, it is unclear whether other critical furrow components localize to the central spindle during anaphase/telophase as observed in conventional furrows. Failure to localize one or more of these key components would explain the lack of furrow formation at the central spindle.

To further understand the mechanisms by which metaphase furrows are positioned, we analyzed the localization of the central spindle proteins during the *Drosophila* embryonic cortical divisions. We find that Fascetto, Polo, and Centralspindlin all localize to the metaphase furrows from interphase to metaphase. Our findings also show that despite the lack of cytokinetic furrow formation at the

central spindle, embryos properly localize all of these central spindle proteins, with the significant exception of RhoGEF. Based on this finding, we bypassed the requirement for RhoGEF by treating embryos with a constitutively active form of RhoA. Strikingly, this resulted in ectopic furrows that are positioned over the prophase nuclei. Additional experiments suggest a model in which the transition from unconventional metaphase furrows to conventional cytokinetic furrows during *Drosophila* embryogenesis, is driven primarily by the transition from a specialized maternal form of RhoGEF (RhoGEF2) to zygotically expressed RhoGEF (Pebble).

Materials and Methods

Fly strains and genetics

All *Drosophila* strains were maintained on standard cornmeal-molasses food at 25°C. Wild-type Oregon-R strains were used as controls unless otherwise noted. Live imaging of Rho1 and Polo relied on w, GFP-Rho1 (Bloomington) and w;;P{w+, GFP-Polo} transgenic lines. Sqh-GFP (Royou et al., 2004) and Dlg-GFP (FlyTrap Project; (Quinones-Coello et al., 2007) transgenic lines were used to follow myosin and membrane dynamics. His2Av-RFP flies (Pandey et al., 2005)and GFP-Moesin (D. Kiehart, Duke University, NC; (Edwards et al., 1997) transgenic lines were used to follow chromosome and actin dynamics. The UAS RNAi stock, sqhHMS00437, was obtained through the FlyTRiP center at Harvard University and expressed using a Gal4 under the alpha-tubulin promoter VP16[V37] (Bloomington).

Immunohistochemistry

Embryo collection and preparation for immunofluorescent analysis was performed as described in (Cao et al., 2008). Alexa488-conjugated phalloidin (Invitrogen) was used to stain F-actin, and Propidium Iodide was used to stain DNA. Primary antibodies used included: Rb anti-RhoGEF2 used at 1:500 (S. Rogers, UNC-Chapel Hill, NC; (Rogers et al., 2004), Rb anti-Fascetto was used at 1:100 (M. Gatti, University of Rome, Italy; (Verni et al., 2004), Rb anti-INCENP and Rb anti-Aurora B antibodies were used at 1:500 (W. Earnshaw, University of Edinbugh, UK; (Adams

et al., 2001), Rat anti-Tumbleweed at 1:300 (M. Murray, University of Melbourne, Australia; (Somers and Saint, 2003). Goat anti-rabbit Cy5 and Goat anti-rat Cy5 (Invitrogen) secondary antibodies were used at 1:300.

Live analysis

Embryos for microinjection and time-lapse confocal imaging were prepared as previously described (Tram et al., 2001). All embryos were injected at 50% egg length. Rhodamin-labelled actin or tubulin (Cytoskeleton, Inc.) was injected (both at 10mg/mL) between cycles 10 and 11 in order to allow for even incorporation. Constitutively active RhoA (Cytoskeleton, Inc.), previously described in (Cao et al., 2008), was injected at 1mg/mL (2 mM Tris pH 7.6, 0.5 mM MgCl2, 0.5% sucrose and 0.1% dextran) immediately following telophase of cycle 12. Colchicine (Sigma) was injected during interphase of cycle 13 at 0.5mM (dH2O). Cy5-labelled histones H2A/B (gift from E. Homola, University of Alberta, Canada) were injected at least one cycle prior to cycle 12. All buffer injections used 2 mM Tris pH 7.6, 0.5 mM MgCl2, 0.5% sucrose and 0.1% dextran.

Constitutively active-RhoA injections

RhoA* was injected at the beginning of cycle 12 in embryos also injected with Cy5-Histones and Rhodamine Actin. Alternatively embryos derived from stocks bearing the Moesin-GFP transgene were used to label actin. A digital zoom was used to capture a 13000μm^2 area including and surrounding the injection site. After

injection of either RhoA* or buffer, images from the surface to a depth of 6 microns at 1 micron intervals were taken every 30 seconds. In order to focus on the areas with the highest concentration of RhoA*, we quantified the ectopic furrows in a 5000μm^2 area centered on the injection site. Ectopic furrows were counted in each embryo and then divided by the number of nuclei in the 5000μm^2 area to obtain an ectopic furrow percentage.

Confocal microscopy, image quantifications, and statistics

Confocal images were acquired using an inverted photoscope (DMIRB; Leitz) with a TCS SP2 (Leica) laser confocal system. For all images, a HCX PL APO 1.4 NA 63× oil objective (Leica) was used. Images were processed using ImageJ (National Institutes of Health). Figures were made using Photoshop and Illustrator (Adobe).

Student's t-test (two-tailed, equal variance) was performed on ectopic furrow data and significance was set at $P < .005$. Videos were converted to QuickTime (Apple) videos using PNG lossless compression.

Results

Normal and ectopic localization of central spindle proteins in the early *Drosophila* embryo

Given the current model of furrow positioning by the centralspindlin complex, we determined the localization of these and other core furrow components during metaphase furrow formation in the *Drosophila* embryo. Using both live and fixed fluorescent analysis of cycle 12 embryos, conserved central spindle components were localized during interphase, prophase, metaphase and telophase (Fig. 3.1A-B). We found that Fascetto (Feo, Prc1 homolog), Tumbleweed (Tum, RacGAP50C homolog), and Polo (Plk1 homolog) all localize to the site of metaphase furrow formation (Fig. 3.1A). Of these components, Feo is the first to co-localize with the actin-rich metaphase furrows during interphase. By metaphase, Feo becomes punctate in the furrow. Tum has no specific localization to the furrows during interphase, but becomes localized to the furrows at metaphase. The other member of the Centralspindlin complex, Pavarotti (Pav, mKLP1 homolog) was previously shown to localize to the metaphase furrows from interphase to metaphase as well as decorating the spindle from prophase to anaphase (Minestrini et al., 2003). Polo is weakly associated with the furrows during interphase, and strongly localized to the furrows during prophase and metaphase. The components of the Chromosomal Passenger Complex (CPC), Aurora B (AurB) and INCENP, have little to no significant localization to the furrows at any time of the cell cycle.

We next examined whether these proteins localize to the central spindle during the cortical syncytial divisions as they do during conventional cytokinesis. We found all of these proteins (Feo, Tum, AurB, Polo, AurB, and INCENP) show nearly identical localization to a small region between recently divided nuclei where the central spindle is formed (Fig. 3.1B). This result indicates that despite the lack of conventionally positioned cleavage furrows, the central spindle proteins are still regulated and localized properly as in somatic cells. These findings were unexpected and left unresolved the explanation for the lack of a cleavage furrow at the central spindle. Therefore, we examined the localization of components downstream of the centralspindlin complex.

Central spindle proteins are thought to position the furrow through localized activation of Rho1 at the cortex (Piekny et al., 2005). It has been shown previously that Rho1 is tightly localized to the metaphase furrows (Padash Barmchi et al., 2005) (Cao et al., 2008), therefore we tested whether it was also present at the cortex immediately apical to the central spindle as found in mammalian and C. *elegans* cells (Yonemura et al., 2004; Yuce et al., 2005). Fig. 3.2B shows a cortical stripe of Rho1 forming during mid-interphase. By prophase, we observed a band of RhoA 0.5-1µm below the cortex, directly above the nucleus. At metaphase, this subcortical band of Rho1 is more clearly defined and is positioned perpendicular to the plane of division. However, by telophase no localization to the equatorial cortex is observed. Thus, the position of this cortical stripe of Rho1 is equivalent to that found in cells undergoing conventional cytokinesis, however the timing is altered. During cycle14, after

cellularization, when conventional furrows are first formed, Rho1 is concentrated at the equatorial cortex during late anaphase and telophase (Albertson et al., 2008). In contrast, here we observe this stripe from interphase to metaphase in the syncytial embryo.

Given these results, we conclude that all of the necessary central spindle proteins localize to the central spindle of syncytial embryos properly and are therefore potentially competent to accumulate RhoGEF to the central spindle. However, the lack of cortical Rho1 localization may indicate the crucial missing component for inducing a furrow down the midzone. Furthermore, the metaphase furrow localization may indicate potentially novel roles for these proteins outside of the central spindle. We also examined the localization of RhoGEF which targets and activates Rho1. *Drosophila* expresses both zygotic and maternal forms of RhoGEF, known as pebble and RhoGEF2, respectively (Hime and Saint, 1992; Padash Barmchi et al., 2005). During the zygotically controlled post-cellularization divisions, Pebble is responsible for activating Rho1 at the site of furrow formation and is located at the plus-ends of the central spindle near the equatorial cortex (O'Keefe et al., 2001). The role of Pebble in the maternally controlled pre-cellularization divisions is less clear as loss of Pebble does not disrupt metaphase furrow formation (Lehner, 1992). These divisions appear largely driven by RhoGEF2. In contrast to Pbl, maternal RhoGEF2 localizes to the site of metaphase furrows and loss of RhoGEF2 produces profound disruptions in their formation (Padash Barmchi et al., 2005). In accordance with previous studies, we observe a clear concentration of RhoGEF2 at the site of metaphase furrow

formation from interphase and until metaphase (Fig. 3.2A). However, we find RhoGEF2 does not localize to the central spindle or equatorial cortex during anaphase and telophase. This lack of RhoGEF localization to the central spindle may also explain the lack of a conventionally positioned cleavage furrow during the cortical syncytial divisions.

Sequence analysis provides insight into the failure of RhoGEF2 to localize at the central spindle. Two protein domains (RADECL and BRCT1) in the N-terminal region of Pbl are required for RacGAP50C binding (Somers and Saint, 2003). While Pbl and RhoGEF2 both possess functional GEF domains (DH and PH) in their C-terminus, RhoGEF2 does not contain the RacGAP binding domains in its N-terminus (Fig. 3.3). This readily explains the lack of RhoGEF2 localization at the central spindle and with previous work demonstrating that RhoGEF2 relies on an alternative vesicle –based mechanism for localization at the metaphase furrows (Cao et al., 2008). RhoGEF2 mutants do not have post-cellularization cytokinesis phenotypes indicating its primary role is in metaphase furrow formation (Padash Barmchi et al., 2005). The conventional RhoGEF, Pbl, is zygotically required immediately in the conventional divisions following cellularization (Lehner, 1992).

Ectopic RhoA activation induces furrows down the central spindle

Our findings identified RhoGEF2 as the only component absent from the central spindle in syncytial embryos. Therefore, we were interested in the consequences of bypassing the requirement for RhoGEF. We accomplished this

through injecting an *in vitro* purified form of mammalian RhoA that is constitutively active due to a point mutation in the GTP binding region of the protein (Cao et al., 2008). Embryos bearing the Moesin-GFP (actin binding protein) transgene, were injected at the beginning of interphase of cycle 12 with Cy5-labeled Histones followed by a RhoA (1mg/ml) injection. Within a 5000μm^2 area around the injection site (30-35 nuclei), 20%±1.3 of the nuclei (N=8 embryos) of RhoA injected embryos ectopic furrows form at the same position as conventional furrows: in the center and perpendicular to the central spindle (Fig. 3.4A). Buffer injected embryos produced ectopic furrows in 1.6% ±0.7 (N=11 embryos) of the dividing nuclei. Unlike conventional furrows, these ectopic furrows form during prophase and metaphase. These furrows ingress to depths of 3-4µm and nuclei below these furrows are displaced basally.

To determine the orientation of these ectopic furrows in relation to the mitotic spindle, Moesin-GFP embryos were injected during cycle 11 with rhodamine-conjugated tubulin. This was followed by an injection of active RhoA at the beginning of cycle 12 interphase. All ectopic furrows formed perpendicular to the spindle and bisected the region between the centrosome pairs (Fig. 3.4B). Furthermore, these furrows contain actin, myosin and membrane, all core components of conventional cytokinetic furrows (Fig. 3.4C).

Both ectopic and conventional cleavage furrows require overlapping microtubules

Anti-parallel overlapping microtubules play a key role in positioning and initiation of the cleavage furrow in many cell types (Glotzer, 2009). Therefore we addressed the role of microtubules in the formation of these ectopic furrows. Embryos were injected with RhoA at the beginning of interphase of cycle 12 then immediately injected with Colchicine (a microtubule depolymerizer). In accordance with previous studies which demonstrated that microtubules from interphase through metaphase are not required for metaphase furrows formation (Riggs et al., 2007). However, ectopic furrows formed at a rate of 2.2%±0.9 compared to 20%±1.3 when RhoA* is injected alone (Fig. 3.5). Thus, unlike metaphase furrows, ectopic furrows are sensitive to microtubule depolymerization during interphase and prophase. Given the position of ectopic furrows, it is likely that like conventional furrows overlap spindle microtubules play an important role in positioning the furrows. Thus, although RhoA-induced ectopic furrows form earlier in the cell cycle (prophase/metaphase) than conventional cleavage furrows (anaphase/telophase), both appear to depend on overlap anti-parallel microtubules for furrow establishment and position.

Despite the incorporation of Myosin in metaphase furrows, its role in furrow formation is not clear since metaphase furrows form properly in the absence of myosin (Royou et al., 2004). Therefore, we tested whether formation of RhoA-induced ectopic furrows require Myosin. We expressed *UAS-sqh*^{rnai} during oogenesis using VP16 alpha-tubulin Gal4 driver and observed no effect on metaphase furrow formation in buffer-injected embryos, nor did it result in a significant amount of ectopic furrows (1.8%±1.2 of nuclei in 5 embryos; Fig. 3.5). Upon injection of these

embryos with RhoA we found no significant increase in ectopic furrow formation (0.6%±0.6 of nuclei in 5 embryos). This indicates that Myosin is a structural component of these ectopic furrows and like conventional furrows is required for furrow formation. These results indicate ectopic furrows are functionally equivalent to conventional furrows and distinct from metaphase furrows.

Discussion

These results show that in the *Drosophila* embryo, prior to cellularization, almost all of the central spindle proteins required to make a furrow are at the astral overlap and incorporated into the metaphase furrows. Additionally, all of these same components are at the central spindle as well, however, the inhibition of furrowing here is due to the lack of RhoGEF localization to the central spindle and the lack of a cortical band of Rho1 (Fig. 3.6). After cellularization, RhoGEF/Pebble, which can bind to the central spindling complex, localizes to the plus-ends of the central spindle and activates cortical Rho1(Albertson et al., 2008). Our model predicts a simple yet elegant mechanism of rapidly changing furrow position in the developing embryo by use of structurally different RhoGEFs.

Localization of central spindle proteins to astral microtubules

Our observation that all of the components were localized to the astral microtubule overlap was unexpected. With the exception of the chromosomal passenger complex, which has been shown to be transported by its association with the chromosomes, therefore we would not have expected this complex to associate with astral microtubules. Some evidence centralspindlin has been shown to localize to the tips of astral microtubules in mammalian cells, although only in asters that contact the equatorial cortex of the cell (Nishimura and Yonemura, 2006). It is likely that localization of the centralspindlin complex to the sites of metaphase and conventional

furrow formation rely on distinct mechanisms. Potentially, vesicle trafficking may play a role in their localization as it does for RhoGEF2 (Cao et al., 2008). Interestingly, the localization of RhoGEF2 to the metaphase furrows compared to the cellularization furrows may in fact be mediated by two different mechanisms. The cellularization localization is dependent on the binding of the zygotically expressed Slam protein through RhoGEF2's PDZ domain (Wenzl et al., 2010). Further evidence for this is that ectopic localization of Slam induces a similar ectopic localization of RhoGEF2. Although the mechanism is unclear, Slam is thought to recruit RhoGEF2 to the site of the furrow canals by way of binding to its PDZ domain, leading to a stable accumulation of RhoGEF2. However, Slam is not present in the metaphase furrows during the pre-cellularized divisions (Lecuit et al., 2002; Stein et al., 2002). Therefore, an alternative mechanism of positioning RhoGEF2 during these divisions might involve the Pav (mKLP1) motor protein to drive localization of RhoGEF2 containing vesicles to the metaphase furrows. The early embryo may in fact be a perfect system to study localization mechanisms of other components as well.

Temporal regulation of furrow formation

The experiments described here were able to elucidate the spatial differences between syncytial and cellularized epithelium as they relate to the furrow components; however, they call attention the unknown nature of the timing differences. Although, ectopic activation of Rho1 was able to induce midzone furrowing, it did so during pro-metaphase rather than telophase. The fact that this

coincides with the timing of robust furrow formation seems more than just a coincidence. To account for this, of the components we looked at, the only one that we can say is temporally shifted is the cortical stripe of Rho1. This stripe appears throughout interphase and until metaphase. It would be interesting to look at whether all of the cortical components are behaving similarly, which may indicate that upstream components that interact with Rho1 or anillin, for example, are differently regulated during the syncytial cycles. Based on evidence from other cell types, Tumbleweed may be the most likely protein to affect these cortical components since it appears to have central spindle independent roles related to anillin and Rho1(Yuce et al., 2005) . How this timing regulation is shifted after cellularization is another big question. Some indication may come from experiments where the mid-blastula transition (MBT) is delayed. The MBT is a series of events that occurs during cellularization resulting in an elongated interphase due to the inclusion of gap phases, degradation of maternally supplied transcripts and proteins, and the initiation of zygotic transcription (Edgar et al., 1986; Edgar and O'Farrell, 1989). Delaying these events with transcriptional inhibitors or genetic tools results in extra divisions (cycles 14 and 15) that continue to make metaphase furrows and delay cellularization (Edgar et al., 1986). This lends support to the idea that zygotic transcription is key to shifting the timing of and positioning of the furrow to the midzone at telophase.

Developmental switches between astral and central spindle dominance

Rappaport's classic experiments in large invertebrate embryos and more recent studies on experimentally induced monopolar spindles demonstrate that even in cells in which furrow position is dictated by the central spindle, astral microtubules have the potential to induce furrows (Canman et al., 2003; Hu et al., 2008; Rappaport, 1961) . In many respects, metaphase furrows which form between neighboring asters of the *Drosophila* syncytial cortical divisions are natural versions of these experimentally induced ectopic furrows. As with ectopic furrows formed upon monopolar spindle induction, during metaphase key furrowing components which normally associate with the central spindle, localize at the astral microtubule plus-ends. We suspect these components are likely to be localized at astral microtubule plus-ends in Rappoport furrows. The mechanisms guiding this ectopic localization are not known. In syncytial *Drosophila* embryos, studies demonstrated that RhoGEF2 transported to the metaphase furrows via recycling endosome derived vesicles (Cao et al., 2008; Rothwell et al., 1999). Whether other furrow components rely on similar vesicle-based transport mechanisms is not known.

The lack of furrows at the central spindle during the *Drosophila* cortical divisions is surprising because key furrow components are localized both at the central spindle as well as overlapping astral microtubules. This is explained by the fact that the maternally supplied RhoGEF, RhoGEF2 lacks the RacGAP binding domain, and thus does not localize at the central spindle and activation of Rho-GTPase fails. Simply by providing activated Rho-GTPase, we induce conventional central-spindle based furrows. Normally, however, the switch from astral-based to

central spindle-based furrow formation is likely driven by expression of the zygotic form of RhoGEF (Pebble), which localizes at the central spindle and promotes central spindle based contractile ring formation. Taken together, these results indicate that the early *Drosophila* embryo is poised to form either astral-based or central-spindle based furrows. With key furrowing components localized at both the astral microtubules and central spindle, localization of RhoGEF and activation of Rho-GTPase are the rate limiting factors driving furrow position. This strategy is advantageous given that a dramatic shift from astral-based to central spindle based furrow position must occur in a very short period of time at the mid blastula transition.

Figures

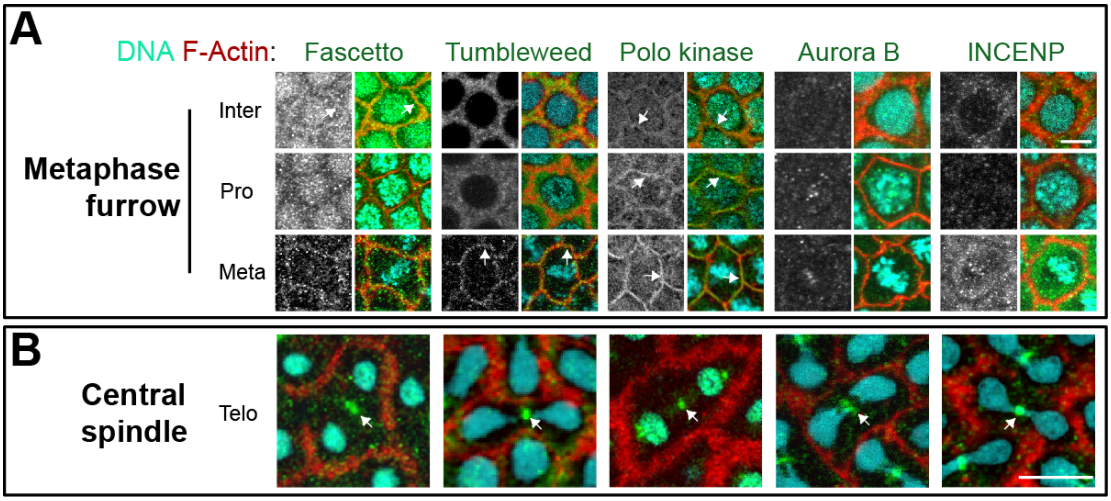

Figure 3.1. **Central spindle proteins localize to the metaphase furrows and the spindle midzone.** (A) Localization of central spindle proteins (grayscale and green) during metaphase furrow formation in both live and fixed cycle 12 embryos. Arrows indicate colocalization with actin furrows. DNA is cyan and F-actin is red in all panels. Scale bar equals 5 µm. (B) Telophase localization of central spindle proteins. Arrows indicate accumulations of these proteins at the spindle midzone between two recently divided nuclei. Scale bar equals 10 µm.

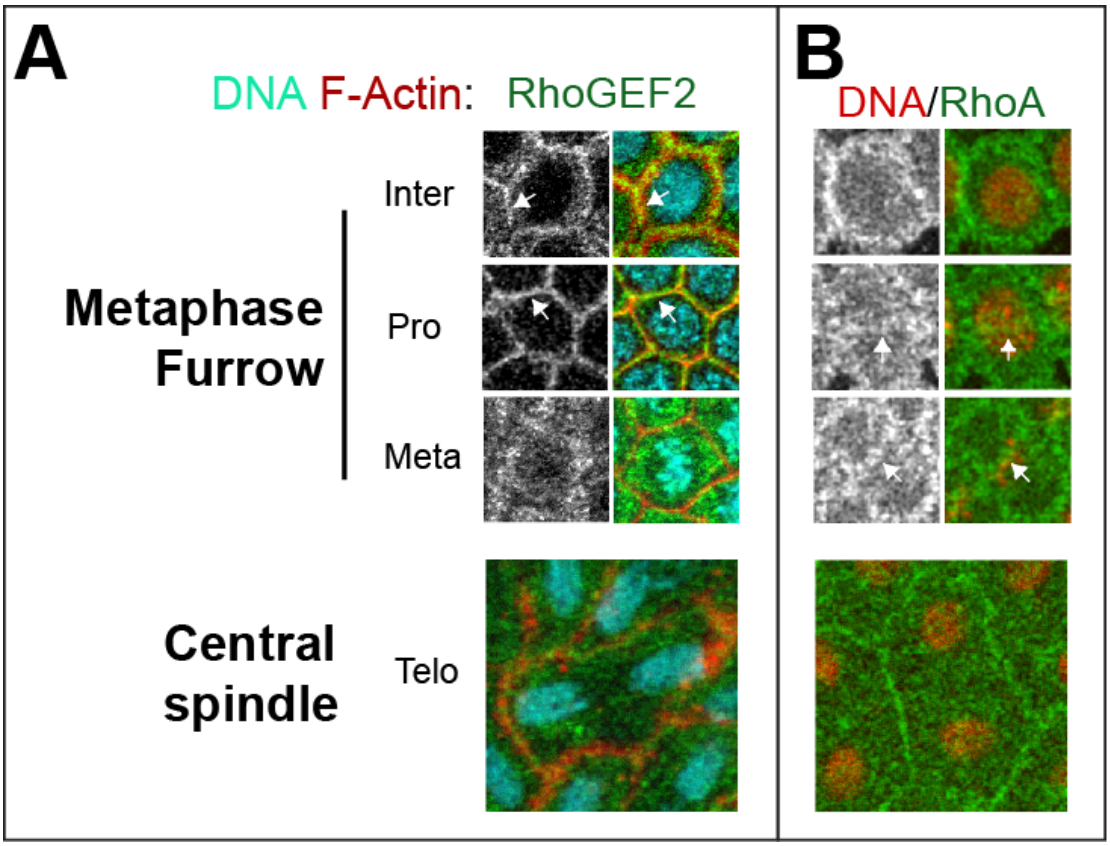

Figure 3.2. **Spindle and cortical localization of Rho pathway components.** (A) RhoGEF2 (grayscale and green) localization during metaphase furrow formation and midzone formation at telophase. Arrows indicate colocalization of RhoGEF2 and actin furrows. (B) RhoA-GFP (grayscale and green) localization 0.5-1µm below embryo cortex. Arrows in left and right panels highlight a concentrated stripe of RhoA forming directly above each nucleus (red). Nuclei in right panels have been superimposed from a lower z-plane in order to highlight nuclear morphology and orientation with respect to the RhoA stripe. Actin is not labeled in these images.

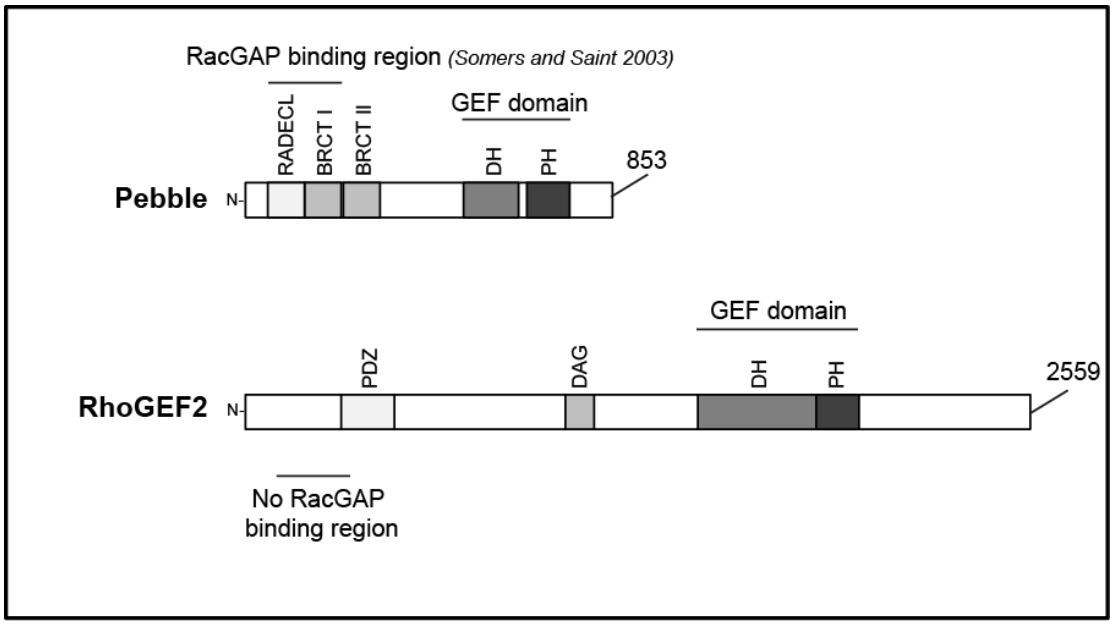

Figure 3.3. **Schematic representations of conserved protein domains in RhoGEF/Pebble and RhoGEF2**. RacGAP binding regions are comprised of RADECL and BRCTI domains of Pebble (Somers and Saint, 2003). RhoGEF2 does not have the equivalent domains and instead has a PDZ domain, which is required for its binding of Slam.

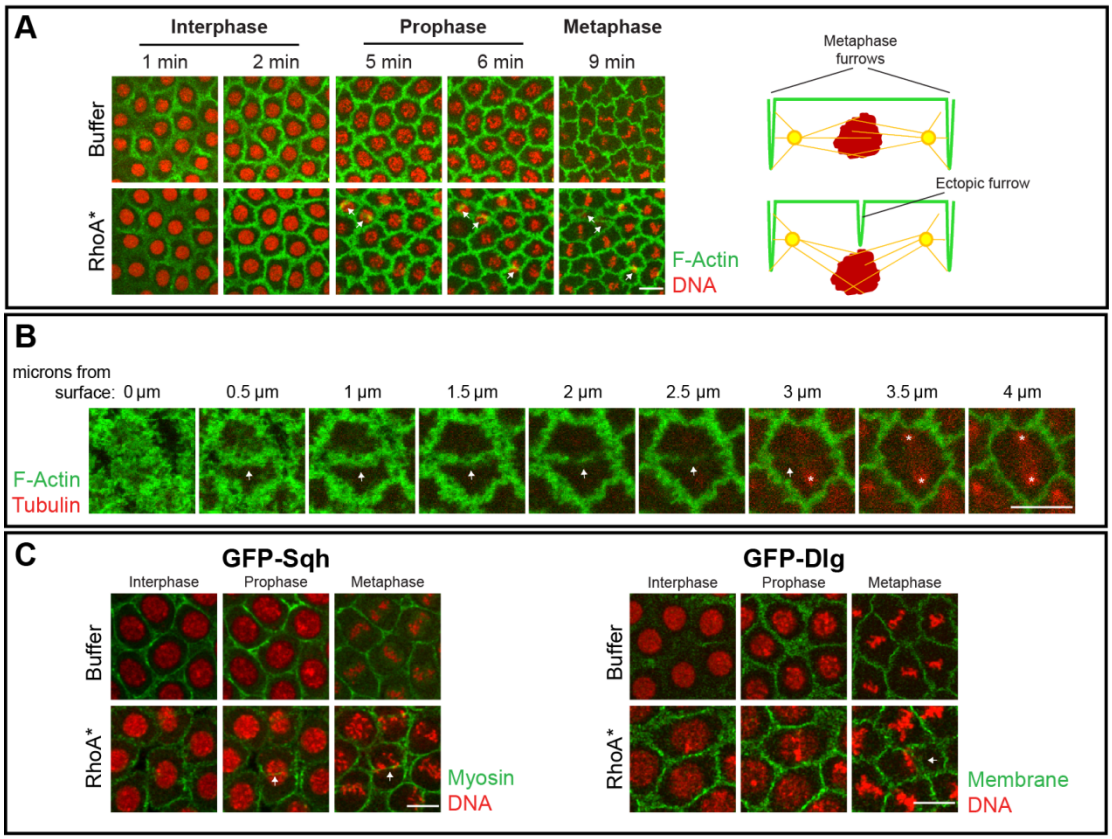

Figure 3.4. **Ectopic furrows induced by activated–RhoA* injection are similar to cytokinetic furrows.** (A) Living embryos injected during interphase of cycle 12 with either buffer or activated RhoA (RhoA*). GFP-Moe (green) labels F-actin and injected Cy5-Histone (red) labels DNA. Time following injection is indicated above each panel. Actin is shown at a depth of 3-4µm below the cortex. Note that arrows indicate the formation of ectopic furrows above nuclei, which have been superimposed from a lower z-plane in order to show nuclear orientation and morphology. To the right of each treatment is a schematic of a cross section through one nucleus at prophase. Note that the ectopic furrows in RhoA*-injected embryos basally displace nuclei from the cortex (see schematic). (B) Actin labeling Moe-GFP (green) embryos were injected with RhoA* and rhodamine-labeled tubulin (red) at the beginning of interphase. Images are of one prophase nucleus from the actin cortex (0µm) to the bipolar spindle (4µm). Arrow indicates the ectopic furrow forming above the nucleus. Asterisks label the tubulin rich centrosomes of the spindle. (C) GFP-Sqh (green) embryos labeling non-muscle myosin and Cy5-labelled histones (red) were injected with buffer or RhoA*. Dlg-GFP (green) embryos labeling membrane were treated similarly. Both membrane and myosin are observed in the ectopic furrows. Scale bars equal 10µm.

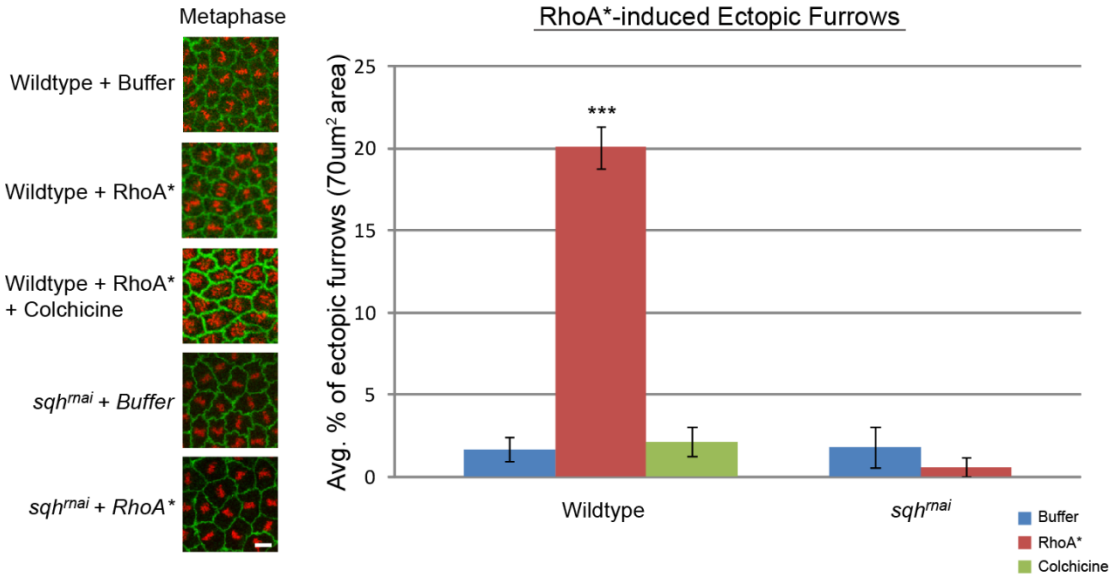

Figure 3.5. **Ectopic furrows require microtubules and myosin.** Pharmacological and genetic methods were used to disrupt spindle microtubules (colchicine) and myosin (sqh^{rnai}) in embryos injected with buffer or RhoA*at the beginning of interphase of nuclear cycle 12. The embryos were imaged throughout the following metaphase and the percent of ectopic furrows was quantified in a region of 5000µm^2 (graph). Colchicine embryos were labeled with GFP-Moesin and RFP-Histone. Colchicine was injected immediately after RhoA*. Note the lack of organization of the condensed chromosomes at metaphase indicative of spindle defects. Sqh^{rnai} embryos were injected with rhodamine actin (green) and Cy5-histones (red) prior to cycle 12. Bars in graph represent the averages of at least 5 embryos. (***) indicates a significant difference (p>.001) from the associated buffer control. Scale bar equals 5µm.

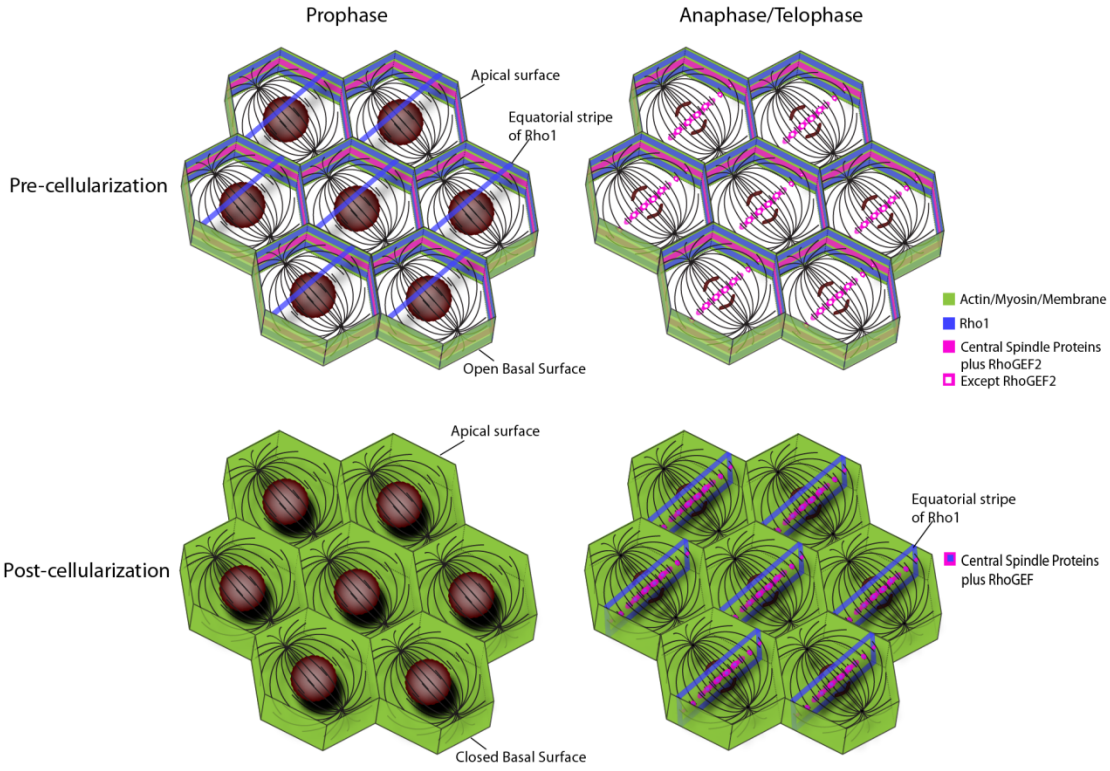

Figure 3.6. **Schematic of spatio-temporal differences of furrow determinants in the syncytial and cellularized embryos.** Apical surfaces have been removed. During the syncytial divisions, central spindle proteins are localized to the metaphase furrows as early as interphase, and have midzone localization at telophase with exception of RhoGEF2. Note the premature equatorial stripe of Rho1 and the absence of a stripe during anaphase/telophase. The cellularized epithelium has a basal cortex and shows localization of the central spindle components, including RhoGEF at the midzone during anaphase/telophase, which coincides with an equatorial stripe of Rho1.

Chapter 4: Vesicle-mediated furrow formation is regulated Polo-dependent phosphorylation of Nuf.

Introduction

Cytokinesis is the final step in cell division, which physically divides the two daughter cells from one another. This process is driven in large part by the formation of an acto-myosin based contractile ring that forms at the equatorial cortex and invaginates the membrane down the midzone during anaphase and telophase. Although much is known about the steps of initiation, progression and abscission of cleavage furrows, many questions still remain. One unresolved issue is how all of the furrow-associated components are recruited to the site of cytokinesis. It is known that microtubules play a pivotal role in furrow formation (Rappaport, 1961). The current model proposes that overlapping microtubules serve as accumulation sites for a majority of these components. Some of these components, such as the centralspindlin complex, have associated microtubule motors (mKLP1) which are thought to transport them along these microtubule arrays (Mishima et al., 2002; Yuce et al., 2005). However, the mechanisms by which the other central spindle components (i.e. PRC1, RhoGEF) or cortical components (i.e. Rho1) are not as well understood. Recent work describing the role of membrane trafficking in cytokinesis may reveal the solution to some of these questions (Cao et al., 2008).

Previously it was thought that cytokinesis in animal cells was solely achieved through actin-myosin contraction as opposed to plant cells which, due to the rigidity of the cell wall, primarily rely on membrane trafficking to the midzone which forms the new cell periphery (Jurgens, 2005). However, many studies now suggest a new model of animal cytokinesis which incorporates an essential role of vesicle trafficking to the furrow (Albertson et al., 2008; Otegui et al., 2005; Strickland and Burgess, 2004). These vesicles have been implicated in both trafficking of furrow components as well as simply membrane addition. In the *Drosophila* embryo, the ER and golgi have been identified as playing a role in furrow formation (Rothwell et al., 1999; Sisson et al., 2000). Maternal effect mutant screens in the early syncytial embryo have been used to identify genes that affect the formation of metaphase furrows, which are cytokinetic furrow analogs, that form during the 11-14th divisions prior to cellularization (Sullivan and Theurkauf, 1995). These structures form outside of the spindle rather than bisecting it and occur from interphase to metaphase rather than anaphase/telophase. Despite this, they have been shown to be a powerful genetic tool to understand cleavage furrows in general. To this end our lab has identified the gene Nuclear Fallout (Nuf) as a critical component for metaphase furrows (Riggs et al., 2003; Rothwell et al., 1999).

Nuclear Fallout (Nuf) was identified as a homologue of the mammalian Rab11 effector FIP3 (Rothwell et al., 1998). In mammalian cells, FIP3 has been shown to be required for both furrow ingression and abscission events (Hickson et al., 2003). Similarly, in *Drosophila* embryos, Nuf has been shown to be required for

furrow integrity (Riggs et al., 2003; Rothwell et al., 1999). These results lend support to the growing model of membrane trafficking in cytokinesis. The specific role that Nuf plays seems to be in the activation of recycling endosome (RE) trafficking, specifically, by way of its interaction with Rab11, an RE associated GTPase. Rab11 is a key activator of RE vesicle trafficking and relies on its association with effector proteins, such as FIP3, for targeted vesicle delivery. Loss of this interaction results in weak localization of actin and actin remodelers, such as RhoGEF2 and Rho1, to the site of furrow formation (Cao et al., 2008; Riggs et al., 2007). The regulation of these events within the cell cycle is less clear.

Previous work found that Nuf does not always associate with the RE during the cell cycle. In fact, Nuf accumulates at the RE throughout interphase and until metaphase when it rapidly becomes diffuse (Riggs et al., 2007). This timing correlates with the formation of metaphase furrows which form throughout interphase and fall apart during anaphase and telophase. Furthermore, it has been shown that Nuf is highly phosphorylated during prophase which coincides with its diffusion from the RE (Riggs et al., 2007). Whether this phosphorylation and localization of Nuf are related to one another or merely correlative has yet to be shown.

Here we show that Nuf localization to the recycling endosome is affected by Polo kinase. Perturbing Polo activity and protein levels in the embryo results in changes of Nuf localization to the RE. Using in vitro assays we also find that Polo is sufficient to phosphorylate Nuf at two residues. Specific staining of these phosphorylated residues shows that these phosphor-isoforms do not localize to the

RE. Therefore, we propose a model in which regulation of vesicle trafficking related to furrow formation is directly through Polo. This suggests a model in which vesicle trafficking may play in important role in timing the formation or destruction of a furrow.

Materials and Methods

Fly strains

Stocks were raised as described in chapter 1. *Nuf*^{1}*/TM3, Sb* (Rothwell et al., 1999), *polo*^{10}*/TM6C, Tb, Sb* (Bloomington), *UASp-Polo** (Bloomington), *GFP-Nuf/ CyO (Riggs et al., 2003), alphaTub-Gal4:VP16* (Bloomington).*Sqh-GFP* ((Royou et al., 2004), *Moesin-GFP* (Cao et al., 2008).

Embryo Fixation and Immunostaining

Collection and fixation of embryos were described in chapter 2. The primary antibodies used include: Rb anti-Nuf (1:250; (Rothwell et al., 1999), Rb anti-pNuf S225 (1:30; (Otani et al., 2011)). Secondary Alexa 488-conjugated antibodies were used at 1:300 (Molecular Probes).

Confocal microscopy and FRAP

Confocal microscopy was performed as described in chapter 2. FRAP techniques was performed as described in chapter 2 with the exception that a 5μm^2 area was used for bleaching which was sufficient to cover the entire Nuf accumulation around the centrosome. For quantification, the unbleached centrosome pair was used for comparison.

Embryo western immunoblots

Immunoblots of staged embryos were prepared as previously described (Riggs et al., 2007). Collected embryos were dechorionated in 50% bleach for 2 min, extensively rinsed, permeabilized in heptane, and transferred into a mixture with equal volume of heptane and methanol (containing 1 mM Na3VO4) for fixation. Embryos were rinsed three times in ice-cold 99% methanol with 1 mM Na3VO4 and rehydrated with embryo buffer (EB) containing 10 mM of NaF. The embryos were then stained with EB containing 4 μg/ml Hoechst 33258 for 3–4 min, rinsed twice in EB, and transferred to 40%EB/60% glycerol. Embryos were staged visually using the DAPI channel of a fluorescent microscope. Handpicked cycle 13 embryos (4 per sample) were dissolved in 2× SDS sample buffer and run on SDS-PAGE and immunoblotting using standard procedures.

Kinase assay

Full length Polo kinase cDNA was cloned into a Gateway Baculovirus expression construct (Invitrogen) with a 6x Histidine tag. Sf9 cells were infected and then harvested on a nickel column at a concentration of 0.5mg/ml. GST tagged Nuf (Rothwell et al., 1999), was purified using glutathione sepharose beads to a concentration of 1mg/ml. Dephosphorylated Casein (sigma) was dissolved in water to 1mg/ml. Kinase reactions were assembled using 5μg of substrate (Casein or GST-Nuf), 0.05mM ATP, 0.05μg Polo-6His, 5μCi ATP^{32}, and kinase buffer (Tavares et al., 1996). Extracts from Sf9 cells infected with empty virus were used as control

kinases at 0.5mg/ml. 25µl reactions were carried out at 30°C for 20minutes then boiled in 2x sample buffer and run on SDS-PAGE.

Nuf Pulldowns and co-immunoprecipitation

Immunoprecipitation experiments were carried out on extracts of *Drosophila* embryos aged 0–4 h. Homogenization, incubation, and wash steps were in 50 mM HEPES, pH 7.4, 150 mM KCl, 0.9 M glycerol, 0.5 mM dithiothreitol (DTT), and 0.1% Triton X-100 supplemented with protease inhibitors, plus 2 mM phenylmethylsulfonyl fluoride (PMSF). Rb-anti Nuf antibodies and M-IgG antibodies (Santa Cruz Biotech) were allowed to bind to Protein A Sepharose beads (Sigma) and then incubated with equal amounts of embryo extract (~0.6mg of total protein in 300µl) overnight at 4°C. Beads were washed three times, the last two without TritonX-100. Each pellet was boiled in 20µL of 2x SDS buffer and run on SDS-PAGE. Antibody to *Drosophila* Arp1 (Gridlock) was used to probe (Haghnia et al., 2007).

Results

Nuf is turning over at the recycling endosome

Previously, our lab has shown that Nuf accumulates pericentrosomally at the recycling endosome from interphase to metaphase. At metaphase, Nuf rapidly dissociates and becomes diffuse in the cytoplasm (Riggs et al., 2007; Rothwell et al., 1999). In order to further understand the nature of this accumulation, we first asked whether Nuf is stably associating with the recycling endosome or whether it is turning over. To answer this question we assayed GFP-Nuf embryos using Fluorescence Recovery After Photobleaching (FRAP). GFP-Nuf embryos were allowed to develop until early interphase of cycle 13. Pairs of centrosomes were selected for analysis where one was bleached over ~9s in an area that diminished Nuf fluorescence to zero and which encompassed the entire centrosome and pericentrosomal region. This area was allowed to recover and was standardized to the complimentary, unbleached centrosome. We found that Nuf recovered to near 100% after 102s±7.8s. The recovery of 50% fluorescence was reached after 11s±1.3s (N= 9) (Fig 4.1). Furthermore, following recovery, the amount of Nuf at the centrosome was not significantly reduced compared to the unbleached centrosome. Thus, during interphase, Nuf does not seem to be stably associated with the recycling endosome and is in fact turning over relatively quickly. Therefore, Nuf must be constantly recruited to the RE from interphase to prophase.

A dosage-sensitive interaction between Nuf and Polo

Previously, we have shown that Nuf is phosphorylated from interphase to prometaphase (Riggs et al., 2007). The highest level of phosphorylation observed is in prometaphase coinciding with nuclear envelope breakdown (NEB). Taking this into account we used a previously published genetic screen (Cao et al., 2008) to genetically identify mitotic kinases that interact with Nuf and may in fact phosphorylate it. The strategy of the screen was to reduce Nuf protein levels by half in the early embryo by using nuf^{1} heterozygous mothers. All of these embryos were fixed and stained to assay metaphase furrow morphology. In contrast to the *nuf* homozygous embryos, heterozygotes displayed normal furrow morphology (Fig. 4.2). Next, candidate mitotic kinases (Cdk1, Polo, Mei41, etc.) were crossed into this heterozygous background. By themselves, the heterozygous kinases did not produce furrow defects (Fig. 4.2), however, $polo^{10}/nuf^{1}$ embryos showed a synthetic furrow phenotype exhibited by weakly defined actin furrows (Fig. 4.2) and breaks in the furrows. None of the other kinases tested, six in all, produced phenotypes. Thus, Polo, or a downstream target of Polo, interacts with Nuf and is required for proper furrow integrity.

Misexpression of Polo alters Nuf phosphorylation and localization

To test whether Polo could affect the phosphorylation and the localization of Nuf we live imaged *GFP-nuf/+*:$polo^{10}$/+ and compared to *GFP-nuf/+* embryos. $polo^{10}$/+ embryos had significantly more Nuf localized during the interphase to

prophase duration (Fig. 4.3A). Furthermore, when Nuf is no longer visible at the centrosomes from metaphase to telophase in *GFP-nuf/+* embryos, $polo^{10}/+$ embryos had reduced, but significant amounts maintained at the centrosome region throughout mitosis (Fig. 4.3A).

Next we tested whether increasing Polo activity also affects Nuf localization. Using a constitutively active UAS-driven polo*, we overexpressed this isoform in embryos and fixed and stained for Nuf localization (Fig.3B). At prophase, Nuf is normally at the centrosome in wildtype embryos. Upon expression of active polo we saw almost no accumulation of Nuf to the centrosome during prophase. Therefore, reducing polo results in an increase of Nuf localization to the centrosome while increasing polo results in its premature removal from the centrosome.

Given these results we asked what the phosphorylation state of Nuf is in these genetic perturbations. Embryos from *Tubulin-Gal4; UAS polo** mothers were fixed and staged and run on SDS-PAGE. Compared to wildtype, Cycle 13 *UAS polo** embryos show an increase in the higher isoforms of Nuf (Fig. 4.3C). Conversely, reducing Polo levels with either a heterozygous null allele ($polo^{10}/+$) resulted in a reduction of the higher isoforms of Nuf (Fig. 4.3C). Thus, Polo levels can either directly or indirectly affect the state of Nuf phosphorylation, which may be responsible for its dynamic localization.

Taken together, these data indicate a significant link between the phosphorylation of Nuf and its removal from the centrosome by the end of prophase. Furthermore, this link is likely mediated by Polo kinase.

In vitro purified Nuf can bind to *in vitro* purified Polo

In order to determine whether Nuf and Polo directly interact we performed pulldown assays using bacterial purified GST-Nuf. This was bound to glutathione covered sepharose beads and incubated with bacterial purified MBP-tagged Polo. These beads were then washed, boiled and run on an SDS-PAGE. Western blotting using an MBP antibody detected Polo in this fraction and not significantly in GST bound beads (Figure 4.4A). This indicates that Nuf and Polo directly interact with one another.

Polo can directly phosphorylate Nuf *in vitro*

In order to test whether Polo was sufficient to phosphorylate Nuf we performed an in vitro kinase assay using baculovirus purified Polo and bacterial purified GST-Nuf. Figure 4.4B, an autoradiograph of the assays, shows the positive control, Casein, was strongly phosphorylated by Polo. Similar levels of phosphorylation were also observed in GST-Nuf reactions. Negative controls used extract from Sf9 cells that were infected by baculovirus not containing the Polo insert. Only faint bands can be seen for GST-Nuf in these lanes which may be due to background kinases or endogenous levels of Polo. From these gels, the slowest moving bands (~100kDa) were excised and liquid chromatography tandem mass spectrometry (LC MS/MS) was used to identify two phosphorylated residues, S225

and T227 (Fig. 4.4B). Interestingly, a genome-wide phosphorylation study previously found that Nuf is phosphorylated at these sites as well (Zhai et al., 2008).

Nuf phosphorylated at S225 does not localize to RE

A recent study found that Nuf is phosphorylated by IKK□ in follicle producing cells (Otani et al., 2011). Interestingly, they mapped this phosphorylation site to S225 as well. Using the S225 specific antibody they generated we tested whether in the syncytial embryo if pS225 Nuf would be able to accumulate at the RE. Cycle 13 embryos labeled with pNuf antibody showed no accumulation of pNuf at the centrosome (Fig. 4.4C). Therefore, phosphorylation of Nuf at S225 by Polo is sufficient to prevent Nuf from localizing to the RE.

Nuf binds the central component of the Dynactin complex Arp1

In order to identify binding partners for Nuf, we purified GST-labeled Nuf and bound it to Glutathione Sepharose beads. Wildtype embryo extract from 0-3hr AED embryos was flowed through both GST and GST-Nuf columns. Bound proteins were eluted under high salt conditions and run on SDS-PAGE. Coomassie stains were used to identify unique protein bands in the GST-Nuf eluate. Bands were excised and underwent Tandem-mass spectrometry. A band at the 40-70kDa range was identified as Arp1 (gridlock). Arp1 is a major component of the Dynactin complex that specifically binds to the cargo being transported by Dynein. A Co-IP of wildtype extract was then performed using Protein-A beads coupled to Nuf antibody. Bound

proteins were eluted under denaturing conditions and subjected to SDS-PAGE. Western Blotting using an antibody to Arp1 showed a 74kDA band, which corresponds to Arp1 and a 36kDa band, which most likely corresponds to actin since it has been reported that this antibody cross reacts with actin (Haghnia et al., 2007). Therefore, we propose that Nuf interacts with Dynein and specifically the Dynactin complex to translocate to the RE. This is supported by evidence that Nuf interacts with dynein, however since dynactin serves as linker between dynein and its cargo, our result may be more direct binding (Riggs et al., 2007).

Discussion

Nuf localization to the recycling endosome is regulated through phosphorylation by Polo

Our data show that Polo kinase directly phosphorylates Nuf at two specific residues. Furthermore, perturbations of Polo activity *in vivo* results in both changes in localization and phosphorylation of Nuf. We propose a model where unphosphorylated Nuf can bind dynein/dynactin motor complexes on astral microtubules and accumulates at the recycling endosome (RE) located pericentrosomally (Fig. 4.6). Previously, we have shown that dynein co-immunoprecipitates with Nuf and inhibition of dynein results in the gradual loss of Nuf at the RE (Riggs et al., 2007). One potential mechanism for phosphorylation regulating Nuf is that it affects either its dynein interaction or Rab11 interaction. The latter is less likely due to the phosphor-sites not being in the Rab11 binding domain. The interaction with dynein is a model we favor since similar proteins have been shown to be regulated this way. The protein Nlp, for example, localizes to the centrosome via its dynein interaction. Phosphorylation by Polo causes Nlp to lose its binding to dynein and accumulation is rapidly lost (Casenghi et al., 2005). Interestingly, a recent report found that in hair follicle producing cells in *Drosophila*, Nuf trafficking of RE vesicles was found to be directly regulated by IKK□ kinase which phosphorylates Nuf and affects its association with dynein (Otani et al., 2011). Moreover, they found that phosphorylation was at S225, one of the sites found in our

study. This lends support to our model that Polo phosphorylation at these sites does in fact alter Nuf/dynein interactions. A third possibility might be interaction with an as yet unknown kinesin that removes Nuf from the RE. It is still not clear whether this is the case however since inhibition of dynein does not result in rapid removal of Nuf from the RE, but rather a more passive diffusion-like removal (Riggs et al., 2007). Another, outstanding issue is the identification of the phosphatase that dephosphorylates Nuf, presumably allowing it to translocate to the RE again. One large-scale screen of interacting proteins showed an interaction between Nuf and the phosphatase Csw, but more direct evidence will need to be pursued.

Nuf phosphorylation is a timing mechanism for furrow formation and destruction

The proper timing of furrow formation is important in syncytial divisions as it is in somatic divisions. Ill timed furrow ingression can result in the inappropriate separation of DNA or cell determinates or simply a failure of cytokinesis all together. Our model suggests that in our cell type, Nuf regulated vesicle trafficking is used to specifically time when a furrow is started, maintained and deconstructed. This timing is cleverly achieved through the activation of Polo, which likely serves as an inhibitory signal to furrow formation at prometaphase. Following mitosis, Polo is inactive through the next interphase, which allows Nuf to accumulate and build a furrow by trafficking of RhoGEF2 (Cao et al., 2008). Given the unique cell cycle timing of metaphase furrows; this may be a syncytial specific method of regulating

furrow formation. Although it may be that Nuf/Polo interactions are utilized in somatic divisions for previously undescribed furrow initiation events that set up the components required for cytokinesis upon entry into mitosis. In terms of the conserved mammalian homologue of Nuf, FIP3, recent evidence has suggested that it too is extensively phosphorylated during the cell cycle (Collins et al., 2012).They find that Cdk1-CycB directly phosphorylates FIP3 and alters its subcellular localization and function. However, the described phosphor-sites are not conserved in Nuf . Therefore, *Drosophila* may simply use Polo as its major regulator rather than Cdk1.

Figures

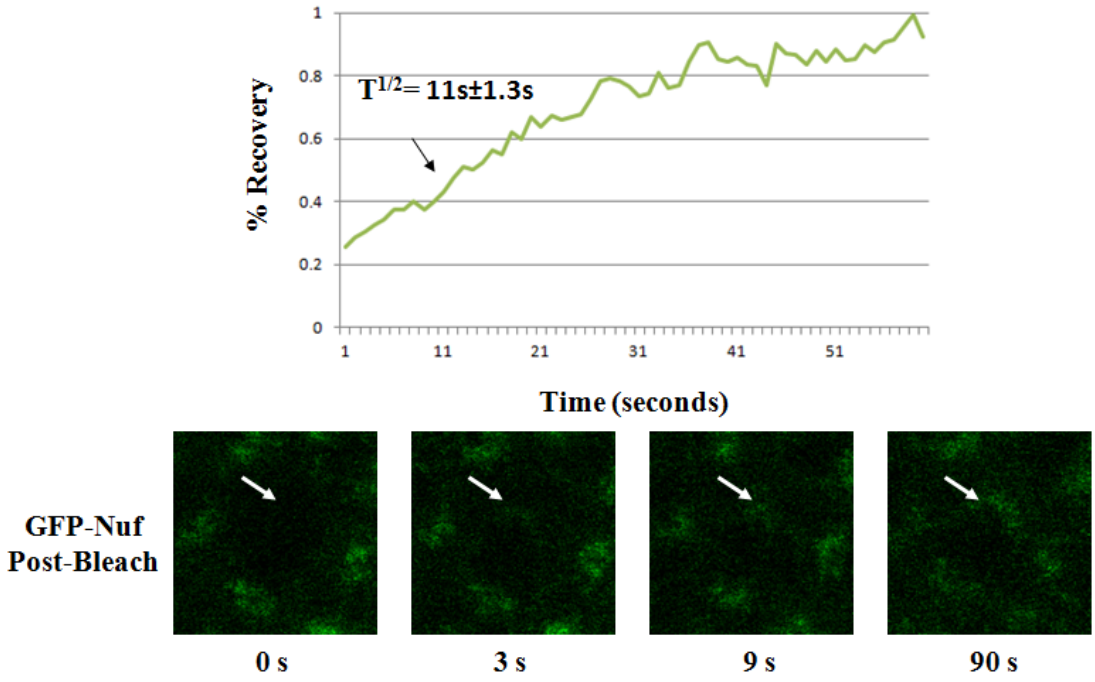

Figure 4.1. **Nuf turns over at the recycling endosome throughout interphase.** GFP-Nuf embryos were live imaged during interphase of cycle 13. Pairs of centrosomes were either bleached (arrow) or unbleached and their fluorescence recovery was measured over time. Bleached GFP recovery was standardized and compared to the unbleached centrosome pair. $T^{1/2}$ indicates 50% recovery.

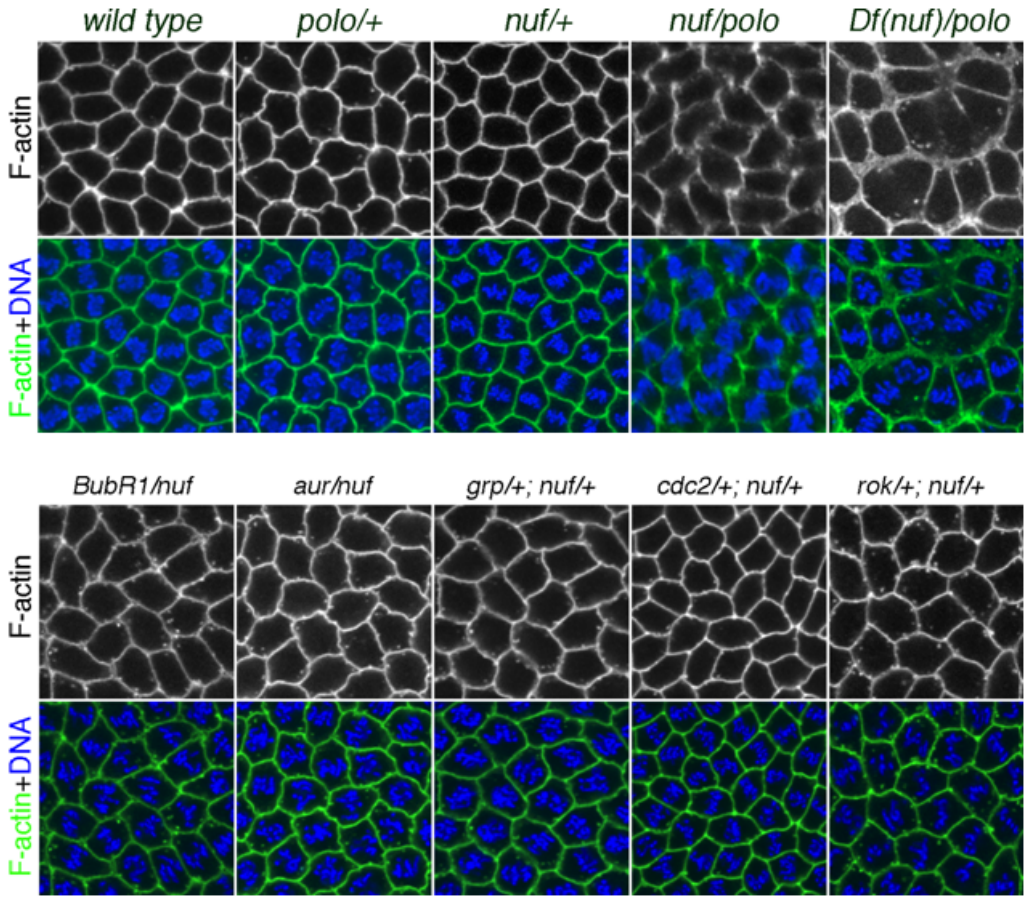

Figure 4.2. **Polo kinase genetically interacts with Nuf.** A genetic loss of function screen for kinases that interact with nuf. Heterozygous mutants of kinases and nuf were found to have normal furrow formation based on actin staining (green). Polo, a positive interactor, is shown in the top row crossed to both the *nuf*^{1} allele and a deficiency that uncovers the *nuf* locus. Negative interactors are seen in the bottom panels.

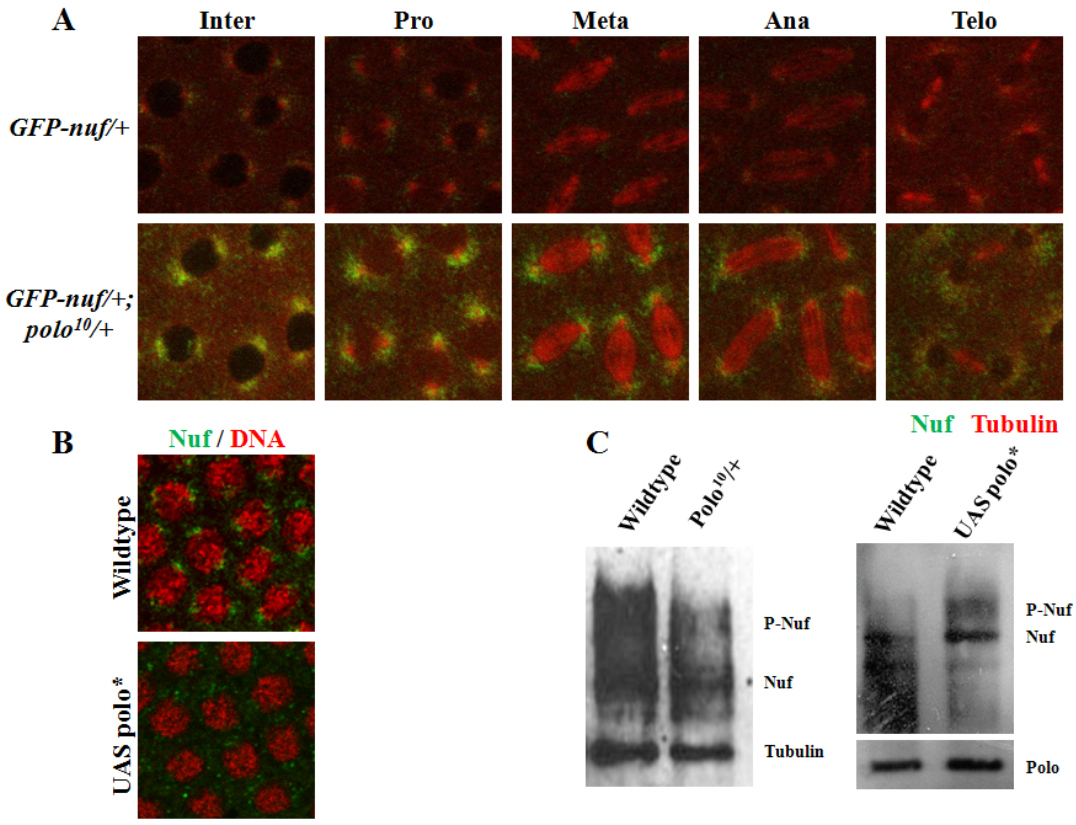

Figure 4.3. **Polo kinase affects both localization and phosphorylation of Nuf.** (A) Stills of live imaging GFP-Nuf/+ and GFP-Nuf/+;polo10/+. Nuf (green) accumulates around the tubulin rich (red) centrosomes. (B) Fixed prophase cycle 13 embryos. Nuclei are stained in red an either Nuf or P-S225 Nuf are stained in green. UAS polo* embryos show a lack of accumulated Nuf compared to wildtype (C) Western blots of methanol fixed embryo with either normal levels of Polo (wildtype), reduced levels (*polo*^{10}/+) or excess constitutively active Polo (*UAS polo**). Phosphorylated isoforms (p-Nuf) of Nuf are reduced in *polo*^{10}/+ and increased in *UAS polo**.

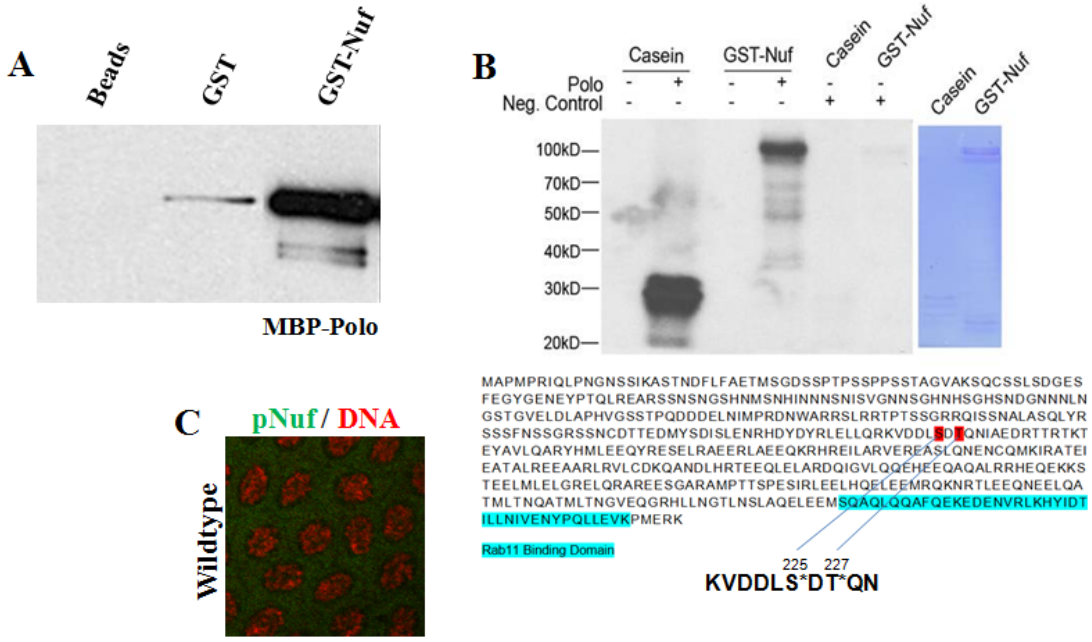

Figure 4.4. **Polo binds and phosphorylates Nuf at two sites *in vitro*.** (A) Sepharose beads were bound to bacterial purified GST or GST-Nuf. Beads were incubated with purified MBP-Polo. Beads were washed and bound protein was eluted and run on SDS-PAGE then probed for MBP. (B) *in vitro* kinase assay was performed using baculovirus purified Polo and bacterial purified GST-Nuf. Casein was used as a positive control. Extracts from negative Polo cells were used as negative controls. Coomassie gel of Casein and GST-Nuf are shown in blue. Phosphorylated GST-Nuf was analyzed by LC MS/MS for phosphorylated residues. Ser-225 and Thr-227 were the only identified as being phosphorylated. (C) pNuf antibody (Otani et al., 2011) staining against phosphorylated S225 (green) and DNA (red) of prophase cycle 13 embryo.

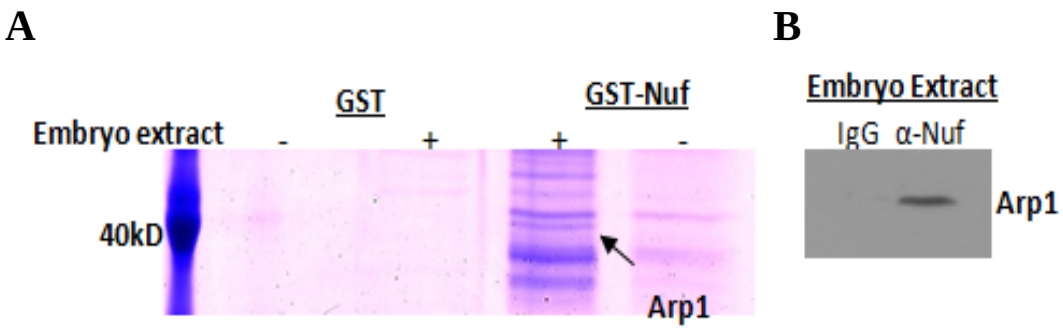

Figure 4.5. **GST pulldown and Immunoprecipitation identify Arp1 as a Nuf interacting protein.** (A) Sepharose beads bound to GST or GST-Nuf were incubated with wildtype embryo extract. Coomassie gel band of the proteins bound to GST-Nuf were identified by mass spectrometry identifying Arp1, a component of the dynactin complex. (B) Immunoprecipitation of Nuf using a polyclonal antibody to Nuf incubated in wildtype embryo extract. Arp1 antibody was used to identify co-precipitated Arp1. IgG was used as a negative control.

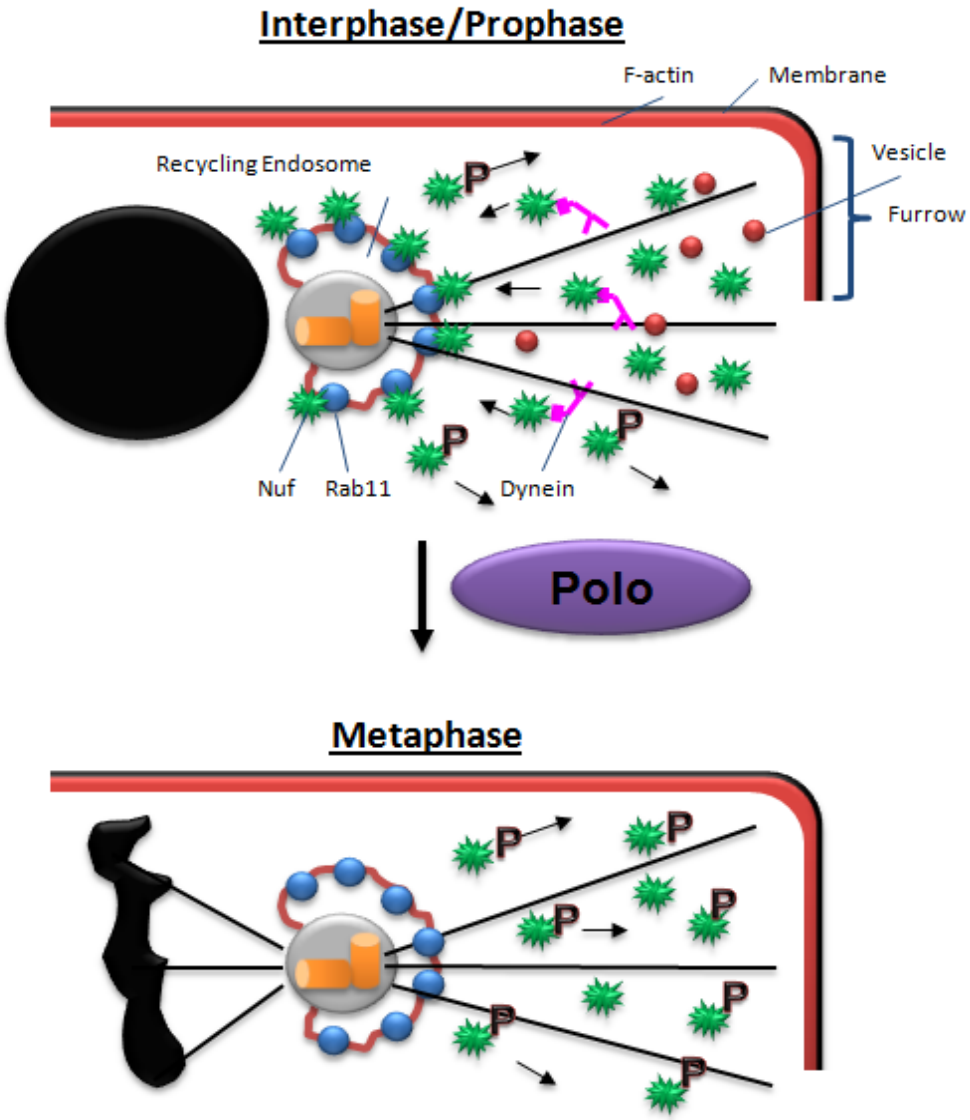

Figure 4.6. **Schematic model of Nuf-regulated vesicle trafficking to metaphase furrows.**

Chapter 5: Folic acid metabolism is required for proper cleavage furrow regulation in the early *Drosophila* embryo.

Introduction

Drosophila cellularization is a specific developmental stage that requires dramatic cytoskeleton as well as nuclear morphogenesis and coincides with the timing of maternal-zygotic transition. Cellularization occurs after 13 rapid, synchronous nuclear divisions that occur in a syncytium. These 13 divisions are controlled primarily by mRNA or protein provided by the mother during oogenesis. Cycles 11-13 occur near the cortex of the embryo and feature dramatic rearrangements of cortical actin into invaginating furrows that encompass each nucleus (Sisson et al., 1999; Sullivan and Theurkauf, 1995). At cellularization in cycle 14, these "metaphase furrows" surround each nucleus and fuse to form a cellular epithelium (Mazumdar and Mazumdar, 2002). This process requires many of the components of cytokinetic furrows (anillin, septins, membrane, etc.) as well as a specific array of microtubules (Miller and Kiehart, 1995; Stevenson et al., 2002). Lastly, it requires the contractile force of actin and myosin to fuse together that is synonymous with cytokinesis (Miller and Kiehart, 1995; Warn et al., 1980). Identifying the major upstream regulators of these processes is an area that still requires attention as no major kinases have been implicated despite the work shown in the previous chapter.

In order to identify new regulators of cellularization in the early embryo, we employed a strategy of EMS-and P-element based screens that have identified maternal-effect mutations that disrupt cellularization (Castrillon et al., 1993; Poodry et al., 1973; Sullivan et al., 1993). The fruitfulness of these screens is evidenced by the identification of many novel genes involved in cell-cycle regulation (*grapes, mei-41 and dwee1*), actin remodeling (*scrambled, RhoGEF2* and *diaphanous*), and membrane trafficking (*nuf, rab11 and dynamitin*). However, by their very nature, these screens rely on female sterility, which overlooks genes required for zygotic as well as maternal development due to the lethality of the homozygote animal. An alternative method for examining the maternal-effect of zygotic lethals is to employ temperature-sensitive alleles. After rearing at the permissive temperature, females homozygous for the temperature-sensitive allele can be placed at the restrictive temperature and their embryos examined. Additionally, zygotic phenotypes can be examined by raising homozygous animals at restrictive temperature following embryogenesis. Therefore, we performed an EMS screen that identified maternal effect lethal mutations that were also temperature sensitive alleles. These lines were specifically screened for phenotypes related to actin organization at the cortex during the late syncytial and early cellularized epithelia. One of these genes, *push pop (pops)*, is reported here.

The following study presents the cloning and characterization of *push pop*. Our results show that Pops is a homologue of the mammalian Folypolyglutamate synthase (FPGS), which is required for add glutamate to folic acid as it enters the cell.

The folic acid pathway is a series of enzymatic steps that converts reduced folic acid into substrates for *de novo* purine synthesis or S-adenyl methionine (SAM) which is used by methyl transferases for general substrate methylation (Loenen, 2006). Folic acid deficiencies in mammals has been linked to failures in neural tube closure, a morphogenetic event that requires a high degree of cytoskeletal remodeling (Rolo et al., 2009). We propose a novel role of folic acid metabolism in regulating the cytoskeletal changes required for cellularization which may give valuable insight into the regulation of actin and microtubules during embryonic development.

Materials and Methods

Screen for temperature-sensitive zygotic lethal mutations

X-linked lethal mutations were generated and identified by mutagenizing *yw* males with ethylmethylsulfonate (EMS). These mutagenized males were mated to females homozygous for FM7A. Single virgin females from the F1 were crossed to FM7A male siblings at 29°C. Lines failing to produce non-FM7 males were scored as lethal mutations. This yielded 4090 lethal lines out of 9312 EMS-treated chromosomes. Assuming a random distribution of the lethals on the X chromosome, each EMS-treated chromosome carried on the average 0.57 lethal mutations. A Poisson distribution of the 4090 lethal lines indicates that 3026 (74%) carry one lethal mutation, 885 (22%) carry 2 lethal mutations and 179 (4%) carry 3 or more lethal mutations. Of the 4090 lines, only 231 were homozygous viable at the permissive temperature (18-21°C), therefore only these viable lines were kept as balanced stocks and classified as temperature sensitive zygotic lethals (ts zygotic lethals). After retesting these stocks, only 213 were found to be workable temperature sensitives.

Embryo Fixation and Immunostaining

Collection and fixation of embryos was previously described in chapter 2. The primary antibodies used include: anti-Dah (1:300, Ref), anti-alpha tubulin DM1A (1:250, Sigma). Secondary Alexa 488-conjugated antibodies were used at 1:300 (Molecular Probes).

Fixed and live imaging

All confocal microscope images were captured on an inverted photoscope (DMIRB; Leitz) equipped with a laser confocal imaging system (TCS SP2; Leica) using an HCX PL APO 1.4 NA 63x oil objective (Leica). Wide-field images For live imaging, embryos were collected for 1hr on grape juice agar and allowed to age for ~45' at 29°. They were then hand dechorionated and desiccated for 4-6min at room temperature. Desiccated embryos were covered in Halocarbon oil and placed on a temperature-controlled stage set to 29°. Rhodamine-labeled actin or tubulin injections were performed at this point according to (Cao et al., 2008).

Synthesis and injection of dsRNA

Genomic DNA from Oregon-R flies was used to PCR fragments of *CG2543, GFP*. A 576bp fragment of the first exon of CG2543 was amplified using the following primers: TAATACGACTCACTATAGGGAGACCACATCTTGGGAT TTCATGTTTTCG and TAATACGACTCACTATAGGGAGACCACCATGCTTTC CAGAGTGTGAGC. A 300bp fragment of the 3 exon of *GFP* was amplified using the following primers: TAATACGACTCACTATAGGGAGACCACGCCATCACG AGATTTCGATT and TAATACGACTCACTATAGGGAGACCACGCTGAAGC CAGTTACCTTCG. The first 27 nucleotides of each primer encode for T7 polymerase promoter sites. To ensure that no errors were introduced into the sequence a high fidelity polymerase, Pfu Turbo (Stratagene), was used for the PCR. These DNA templates were *in vitro* transcribed using a T7 RiboMax Express RNAi

System (Promega) and the sense and antisense strands were allowed to anneal. RNA was dissolved in injection buffer (Spradling 1986) to a final concentration of 2.5μM and injected into dechorionated embryos (cycles 8-10) at an approximate volume of 85pL. Injected embryos were allowed to develop at 25°C until reaching cycle 14, at which point the halocarbon oil was washed away with heptane and the embryos transferred to a 1:1 heptane/PBS mixture for 45 seconds before adding an volume of 16.5% formaldehyde + 18% paraformaldehyde (EM Sciences). The embryos were fixed for 22-25 minutes at 25˚C and devitellinized by hand with a needle under a dissecting microscope.

Results

Identification of temperature-sensitive maternal-effect lethal lines

Our EMS screen identified 213 temperature sensitive zygotic lethal lines. To determine which of these mutations had a maternal effect, we tested homozygous mutant females from 81 lines by mating them to wild-type males. These crosses were maintained at 29°C for three days, after which egg hatching rates were determined. We performed an initial screen of 43 lines to determine zygotic lethality of homozygotes at restrictive and permissive temperatures (Table 5.1). This primary screen found 21 temperature sensitive lines that yielded viable homozygotes at permissive temperature, but few to none at restrictive temperature. The viable homozygote females of these 21 lines at permissive temperature enabled us to perform a secondary screen for maternal effect sterility. Of the 21 lines, 13 had reduced hatching rates (<55%) when mothers were kept at 28C for 3 days. The embryos from these lines were checked for normal egg morphology and classified as maternal-effect lethals. These maternal-effect lines were tested for specific defects in metaphase furrow formation and cellularization. Several genes of interest came out of this initial screen as well as a second screen of the original 81 lines, which included the gene which we report here, *push pop (pops)*, due to its severe defects in cellularizing and metaphase furrow formation.

Maternal and zygotic affects of *pops* embryos

Raising *pops* animals at 29°C from late embryogenesis (24hrs after egg

deposition) develop normally through larval instars with brains and imaginal discs of appropriate size and morphology by late third instar. Despite this, nearly all of the animals undergo abnormally long pupariations followed by a failure to fully eclose from their pupal cases (Fig. 5.2B). Head eclosion is achieved in all animals, however full eclosion from the pupal case occurs in less than 2% of animals. Dissecting these animals from the pupal cases we observe a depression running laterally across the mesonotum and a majority of them missing the two most caudal bands of hairs on the dorsal aspect of the abdomen (data not shown).These phenotypes were not seen in *pops*^{ts} animals raised at 29°C after third instar indicating that FPGS may be required for developmental patterning in the larval instars, but not pupal development.

Temperature induced defects are not immediately rescued by reducing temperature

The temperature sensitive allele of *pops*, *pops*^{ts}, was initially characterized by hatching rates of homozygous mothers kept at permissive (22°C) or restrictive (29°C) temperatures for 3 days. This results in hatching rates of less than 5%. We initially wanted to evaluate the kinetic nature of the ts-phenotype. Therefore, we performed a temperature profiling assay on the early embryo using hatching rates. Figure 5.3 shows a hatching rate profile of two sets of homozygous *pops*^{ts} mothers with hatching rates taken every 24 hours. Embryos from these mothers were collected over 3 hours at their respective temperature, which would give a range of embryos from cycle 1 to cellularization, at which time they would be down shifted to 22°C until hatching.

Presumably this would tell us whether the observed lethality prior to cellularization could be rescued or whether the perdurance of the maternally loaded abnormal protein is unaffected by an acute temperature shift. For this analysis, the permissive control was kept at 22°C for the duration while the experimental group was shifted from restrictive to permissive. On day one, hatching rates of both were taken at 22°C to establish the relative fecundity of the two groups. Next the experimental group was shifted to 29°C. On day two, eggs were collected and allowed to develop at 22°C. This was repeated on each day. By day 4 the hatching rate of the experimental mothers was less than 5%. At this point the experimental mothers were downshifted to permissive temperature to follow the recovery. After 4 days at permissive temperature, hatching rate returned to within 10% of the control flies. Since the embryos did not recover to control levels after being shifted to permissive following egg collection, we assume that the changes in the Pops protein with respect to temperature are not quickly recovered or the downstream affects of its initial mutant state are not nullified by shifting to 22°C during the syncytial divisions. Interestingly, when the experimental mothers were shifted back to permissive temperatures, the hatching rates did not recover fully until 3-4 days. This may indicate a more pleiotropic downstream affect of having the mutant form of Pops expressed in the maternal germline for so long.

Next we performed a temperature shift profile looking at the zygotic expression of Pops and its associated pupal lethality (Fig. 5.4) In addition to the early maternal phenotypes of *pops*^{ts}, which result from shifting to restrictive temperature

during oogenesis, we also observe that if the shift occurs at progressively later stages of development that embryos do hatch and viable larvae are produced. If the upshift is performed during embryogenesis up until mid-3rd instar, animals develop until adult pupae, however, nearly all fail to completely eclose from the pupal case. If the upshift is performed from late-3rd instar to late pupae, however, then a majority of the animals eclose into viable adults (Fig. 5.4).This indicates that a critical developmental time for Pops is during early embryogenesis and larval development, but not pupal or adult stages.

pops^{ts} is an allele of a novel gene *CG2543*

In order to identify the gene mutated in our *pops^{ts}* allele, meiotic recombination with the multiple marker *y w f v c v* and deficiency mapping were used in combination with the restrictive temperature lethality. Based on this analysis, *pop^{ts}* was isolated to the cytologic interval 11B1-11B7. Further meiotic mapping with two P-element insertions carrying the mini white (w+) gene narrowed *pops^{ts}* down to an interval of 11B2-11B5. *PG44*, a P-element insertion into *CG2543*. failed to compliment both zygotic and maternal lethal phenotypes of *pops^{ts}*.

Immuno-cytology analysis of *pops^{ts}* during cellularization showed a lack of actin furrow formation, which resulted in nuclear abnormalities and fallout from the cortex (Fig. 5.5). The P-element of CG2543 (PG44) was then crossed to dpop mutants to get embryos from *pops^{ts}/CG2543^{PG44}* mothers at 29°C. These embryos showed similar furrow abnormalities and more extreme nuclear fallout phenotypes. Similar

results were seen with dsRNAi injection of CG2543 into wildtype embryos (Fig. 5.5)

CG2543 is a homolog of a widely conserved protein folylpolyglutamate synthase (FPGS, Fig. 5.6B). FPGS is a cytoplasmic and mitochondrial enzyme, which catalyzes the addition of glutamate to folic acid upon entering the cell or mitochondria (Moran, 1999). Glutamated folic acid results in a cascade of one-carbon transfers that are involved in two separate biochemical pathways: *de novo* purine and thymidine synthesis, and methylation of DNA, proteins, catechols and lipids (Moran, 1999). Sequencing of CG2543 in the $pops^{ts}$ line revealed one nucleotide substitution at nucleotide 1363. This substitution changed the codon from threonine to isoleucine (Fig. 5.6A). Interestingly, this amino acid residue resides in the putative P-Loop domain of CG2543, which along with the Ω-loop, makes up the ATP-nucleotide binding pocket (Saraste et al., 1990).

$pops^{ts}$ exhibits cytoskeletal and nuclear defects at cellularization

Cellularization is a critical step in early embryogenesis, which surrounds each nucleus with membrane and actin to form a cellularized epithelium. From fixed analysis, about 50% of $pops^{ts}$ embryos at 29°C develop to cycle 14 interphase. However, ~80% of these embryos exhibit severe defects: very little F-actin and membrane recruited to the ingressing furrow (Fig. 5.7A). Additionally, microtubules fail to form the “inverted baskets”, which guide cellularization. Furthermore, the furrow canals, which normally accumulate Dah , one of the prerequisite proteins required for stable formation of membrane and septins to the furrow, fail to

accumulate Dah in *pops*^{ts} embryos (Fig. 5.7B; (Zhang et al., 1996)).

Live imaging of *pops*^{ts} reveals an interphase arrest and deregulation of actin furrows

Live analysis of *pops*^{ts} embryos carrying Histone-GFP fail to develop past cycle 12 or 13 in 3 out of 9 cases. Of the 6 embryos which failed to develop to cycle 14, 4 arrested in cycle 12 and 2 arrested in cycle 13. Furthermore, all of these embryos arrested during interphase. *His-GFP/+* embryos at 29°C display a 15min ± 1.8min (N=10) interphase duration in cycle 12 and 25min ± 2.6min interphase duration in cycle 13 (N=10) (Fig. 5.8) .

pops^{ts} embryos at 29°C in cycle 12 arrest after 16min±3.5min (N=5) interphase which is evidenced by a lack of chromosome condensation indicative of prophase and the loss of nuclei from the cortex. The actin furrows were observed to form normally during interphase, but retract rapidly in concert with the nuclear fall in (Fig. 5.8). Since FPGS is known to affect purine synthesis, we asked whether the phenotypes observed were due solely to replication stalls from lack of nucleotides. In order to artificially stall replication, we injected wildtype embryos at 29°C with aphidicolin (Fig. 5.8). These embryos exhibited a similar interphase arrest, which lasted on average 58min±8.6min (N=3). Following this arrest, nuclei would fall away from the cortex, however, actin furrows remained intact throughout the arrest and fallout suggesting that the *pops*^{ts} phenotype is distinctly different from a replication

stall. Interestingly, *pops*^{ts} embryos appear to lack the ability to arrest the cytoskeleton when the nucleus is arrested.

Discussion

Push Pop may regulate the level of cytoskeletal methylation

Push Pop (*pops*^{ts}), a mutant in the folic acid pathway, has revealed a previously undescribed requirement of Folic acid derivatives during cytokinesis. Folic acid plays to fundamentally important roles in the cell: *de* novo purine synthesis and methylation of proteins and lipids (Moran, 1999). Embryos deficient in *pops* exhibit nuclear arrests corresponding to a lack of nucleotide synthesis. The purine synthesis aspect of the folic acid pathway may account for these nuclear phenotypes simply though a stall in replication, however additional cytoskeletal defects are also observed that cannot be explained by replication stalls.

One possible explanation for this comes from evidence that actin and tubulin subunits are methylated at their binding regions, which affects their polymerization dynamics (Moephuli et al., 1997). In eukaryotes, evolutionary conserved residues in Actin, His73, and Tubulin, Lys394, have been shown to be methylated. However, assigning function to these modifications has been difficult since mutations in these residues do not alter a variety of functions *in vivo or in vitro* (Solomon and Rubenstein, 1987; Szasz et al., 1993). However, these studies do not preclude the involvement of methylated residues in cytokinetic events. Therefore, we favor a hypothesis that reduced methylation of actin in the blastoderm divisions of the early embryo alter the dynamic nature of the ingressing furrow, which requires precise timing and positioning to function properly. Given this, it would also be of interest to

study cycles 4-7 which occur in the middle of the embryo and are characterized by a series of microfilament-dependent axial expansions (Baker et al., 1993).

Methylation of the cytoskeleton may account for folic acid-related morphogenetic movements

At restrictive temperature, a small percentage of embryos can cellularize and develop to gastrulation. Given that the dramatic morphogenetic movements that are associated with gastrulation are in large part driven by cytoskeletal contractions and redistributions, it would be interesting to study the effects of Push Pop in this system. Ventral furrowing occurs early in gastrulation and forms a tube-like valley of epithelial cells. Testing Push Pop embryos during this event may provide novel insight into these cell movements. By comparison, several human diseases involving closure of the neural tube show a direct correlation with folic acid metabolism. Spina bifida has been shown to be greatly reduced by supplementation of folic acid (MRC, 2003). The connection between closure defects and folic acid, however, are still unclear. Evidence in rat embryos suggests that hypomethylation of actin and tubulin result in the loss proper apical basal distribution and a lack of columnar cell morphology in the cells of the presumptive neural tube (Moephuli et al., 1997). Since the bulk of neural tube defect literature has focused on the methylation of DNA and gene regulation as the culprit it would be interesting to study the methylation of the cytoskeleton, especially in such a genetically malleable organism such as *Drosophila*. Another explanation might be in the methylation required generally for cell cycle

regulation. For example, the activity of the mitotic initiating phosphatase, PP2A, has been shown to be regulated through its direct methylation (Tolstykh et al., 2000). PP2A has many cell cycle targets and knocking it down in the *Drosophila* embryo results in a host of effects on the cytoskeleton (Kotadia et al., 2008). Furthermore, the effect on DNA methylation also cannot be ignored. Very little transcription is occurring during cycles 12 and 13, but at cellularization there is a burst of zygotic transcription. Any phenotypes observed during or after this time could be greatly affected by changes in gene expression.

Figures

	Zygotic Lethality							Maternal Sterility							
	Temp : 28			Temp : 20				ts/ts viable?	Temp : 28			wildtype	% hatch	% hatch	Mat. Effect ?
Line	ts/ts	total	%	ts/ts	total	%	diff. in % ts	(Yes/No)	hatched	total	%	control	rate	ratio	(Yes/No)
280	0	38	0	19	72	26.4	26.4	Y	1	33	3	OR-R	67	4	Y
319	32	82	39	17	38	44.7	5.7	Y	10	185	5	OR-R	67	7	Y
316	0	52	0	3	43	7	7	Y	10	142	7	OR-R	67	10	Y
299	0	49	18	41	43.9	43.9	43.9	Y	74	334	22	OR-R	67	33	Y
211	2	35	5.7	16	99	16.2	10.5	Y	79	274	28.8	OR-R	88.3	33	Y
226	0	79	0	8	48	16.7	17	Y	20	80	25	OR-R	67	37	Y
242	0	52	0	13	48	27.1	27.1	Y	72	268	27	OR-R	67	40	Y
310	0	45	0	6	57	10.5	10.5	Y	221	611	36.2	OR-R	88.3	41	Y
208	0	35	0	22	141	15.6	15.6	Y	174	524	33	OR-R	67	49	Y
178	0	50	0	4	123	3.3	3.3	Y	38	120	31.7	OR-R	63	50	Y
185	9	56	16	37	110	33.6	17.6	Y	112	333	34	OR-R	67	51	Y
182	1	58	1.7	2	95	2.1	0.4	Y	150	335	44.8	OR-R	88.3	51	Y
286	0	114	0	21	48	43.8	43.8	Y	417	879	47.4	OR-R	88.3	54	Y
271	21	31	67.7	23	34	67.6	-0.1	Y	766	1355	56.5	OR-R	88.3	64	N
174	8	71	11.3	15	97	15.5	4.2	Y	360	614	58.6	OR-R	88.3	66	N
258	20	108	18.5	17	58	29.3	10.8	Y	652	1092	59.7	OR-R	88.3	68	N
216	0	49	0	28	61	45.9	45.9	Y	330	719	46	OR-R	67	69	N
209	0	75	0	29	132	22	22	Y	1649	2558	64.5	OR-R	88.3	73	N
221	0	77	0	6	48	12.5	12.5	Y	9	16	56	OR-R	67	84	N
255	0	75	0	1	67	1.5	1.5	Y	507	678	74.8	OR-R	88.3	85	N
102	0	28	0	23	116	19.8	19.8	Y	1274	1597	80	OR-R	88.3	91	N
6	0	29	0	0	118	0	0	N	-	-	-	-	-	-	-
42	0	70	0	0	108	0	0	N	-	-	-	-	-	-	-
193	0	59	0	0	135	0	0	N	-	-	-	-	-	-	-
200	0	38	0	0	168	0	0	N	-	-	-	-	-	-	-
205	0	67	0	0	89	0	0	N	-	-	-	-	-	-	-
206	0	56	0	0	86	0	0	N	-	-	-	-	-	-	-
207	3	67	4.4	3	113	2.7	-1.7	N	-	-	-	-	-	-	-
214	0	53	0	0	109	0	0	N	-	-	-	-	-	-	-
234	0	55	0	0	56	0	0	N	-	-	-	-	-	-	-
236	0	53	0	0	45	0	0	N	-	-	-	-	-	-	-
241	0	81	0	0	52	0	0	N	-	-	-	-	-	-	-
263	0	73	0	0	42	0	0	N	-	-	-	-	-	-	-
265	0	90	0	3	36	8.3	8.3	N	-	-	-	-	-	-	-
274	0	47	0	0	41	0	0	N	-	-	-	-	-	-	-
277	3	64	4.7	1	47	2.1	-2.6	N	-	-	-	-	-	-	-
284	0	81	0	3	58	5.2	5.2	N	-	-	-	-	-	-	-
287	0	52	0	0	35	0	0	N	-	-	-	-	-	-	-
296	0	35	0	0	32	0	0	N	-	-	-	-	-	-	-
308	0	47	0	0	36	0	0	N	-	-	-	-	-	-	-
322	0	57	0	0	26	0	0	N	-	-	-	-	-	-	-
177	5	55	9.1	0	65	0	-9.1	N	-	-	-	-	-	-	-
257	0	107	0	0	107	0	0	N	-	-	-	-	-	-	-

Table 5.1**. EMS screen identified 43 temperature sensitive maternal effect lethal mutations.** Homozygous EMS lines were raised during larval development at 28C and 20C and scored for zygotic lethality. Lines that showed >15% reduction of viability at higher temperature were considered for further study. Maternal sterility was tested in lines that produced viable homozygotes. These mothers were raised at 28C for 3 days then eggs were collected and scored for hatching. Hatching rates below 60% were considered maternal effect temperature sensitive alleles.

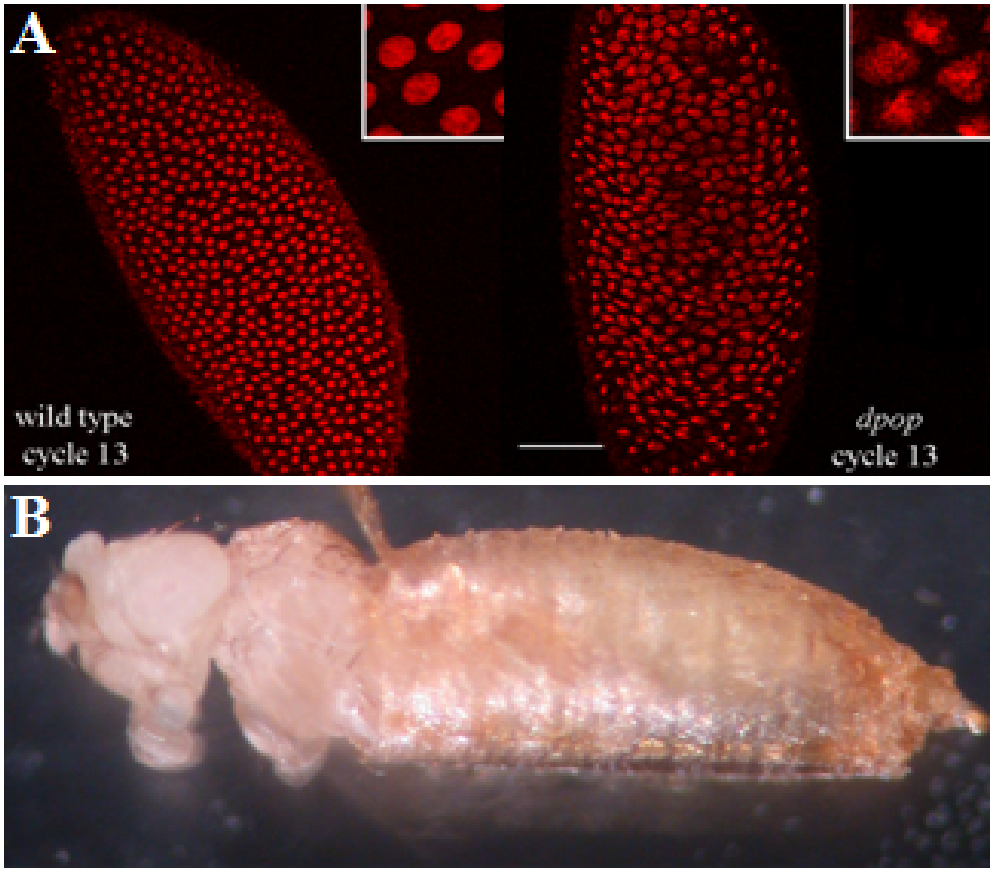

Figure 5.2. ***pops^{ts}*** **exhibits embryonic lethal phenotype at cycle 13 and zygotic lethal phenotype at pupal eclosion.** (A) Fixed embryos from *pops^{ts}*-homozygous mothers raised at restrictive temperature displayed abnormal nuclear morphology at cycle 13. Nuclei (red) have abnormal shape and spacing at cellularization indicative of metaphase furrow defects. (B) Zygotic lethal phenotype of *pops^{ts}*-homozygous animals raised at restrictive temperature during larval stages die while attempting to eclose from the pupal case. Scale bar equals 50microns.

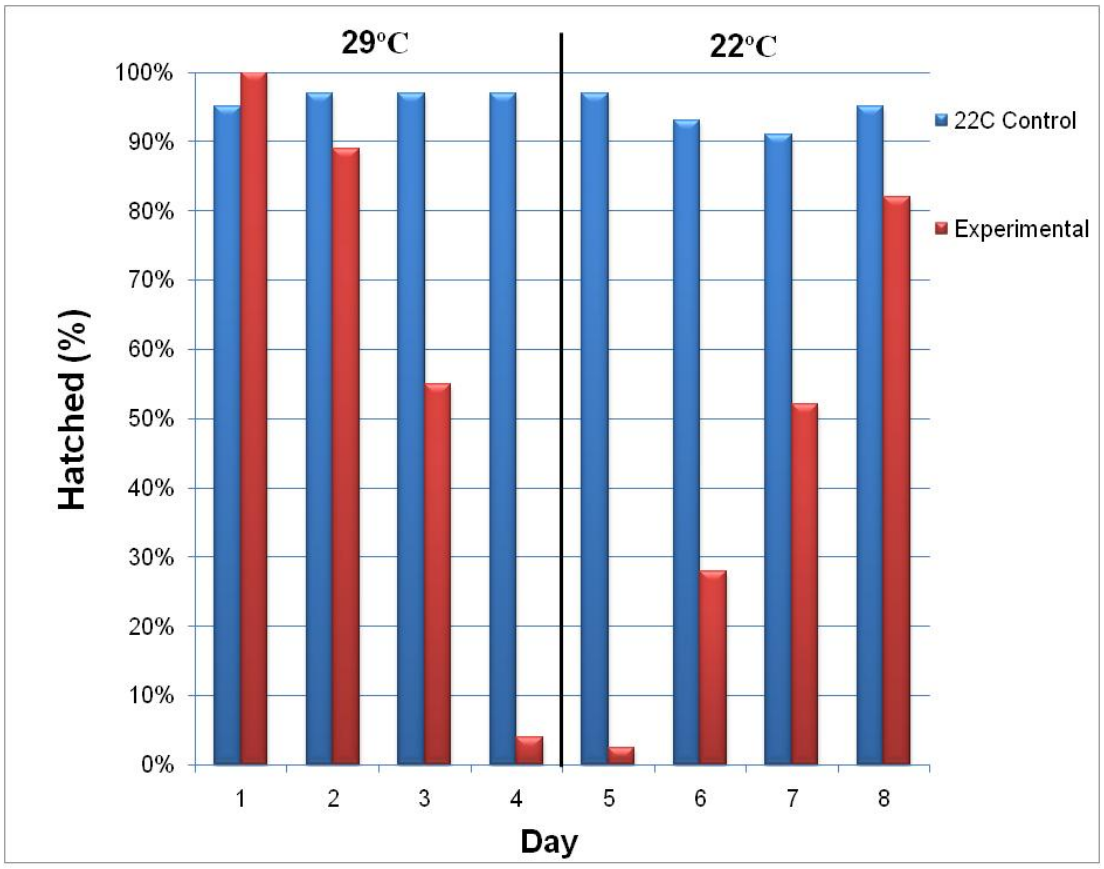

Figure 5.3. **Perdurance of mutant *pops^{ts}* at restrictive and permissive temperatures.** At day 0, females homozygous for *pops* were placed at either 22°C (control) or 29°C (experimental). After each 24hr period, embryos were collected and allowed to develop at 22°C until hatching (36hrs). After 4 days, the experimental line was placed at 22°C to recover and collections were again made every day. For both control and experimental, N>120 embryos per day.

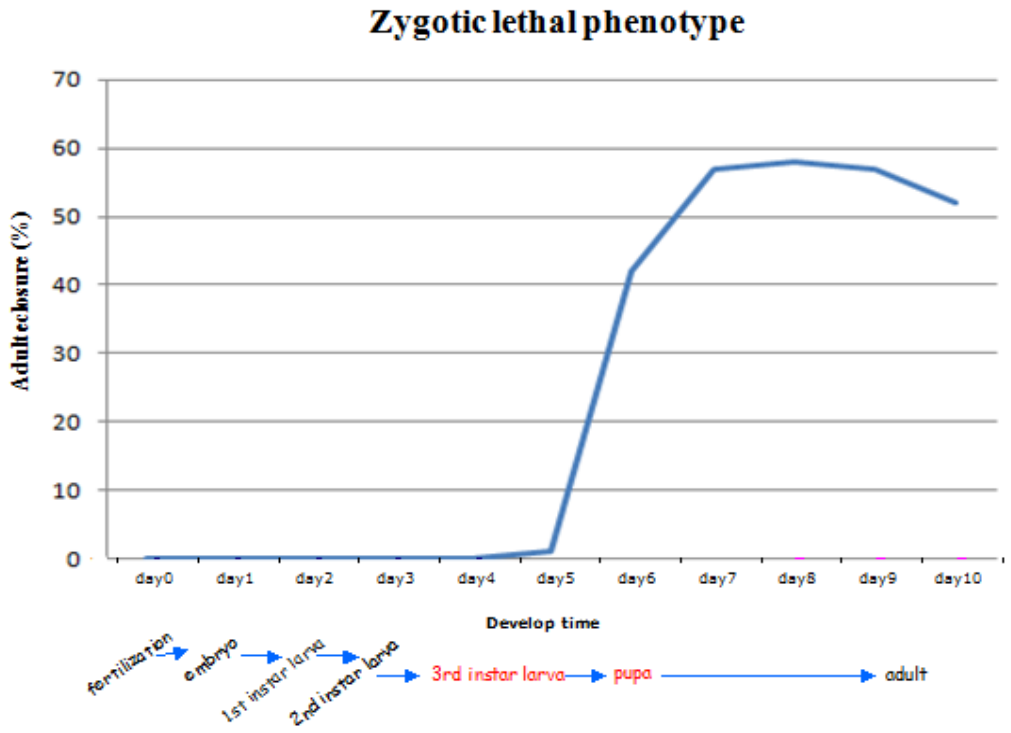

Figure 5.4. **Temperature shift profile of zygotic lethal *pops*^{ts} phenotype.** Homozygous *pops* animals were raised at permissive temperature and upshifted to 29°C at 24hr intervals. Animals shifted during embryogenesis failed to hatch. Shifting after larval development increased survival rate dramatically. Percentage of adults eclosed was scored.

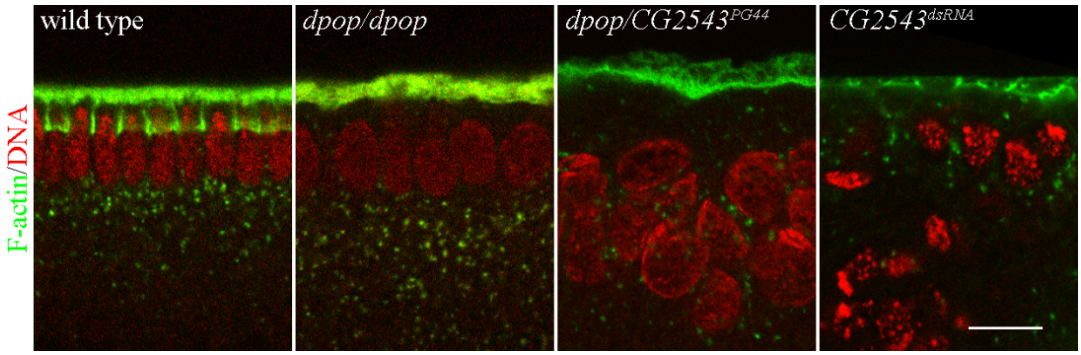

Figure 5.5. **CG2543^{PG44} and RNAi phenocopy *pops^{ts}* homozygotes.** Embryos fixed at during cellularization with F-actin (green) and DNA (red). *pops^{ts}* homozygotes at restrictive temperature show no actin rich furrows and have unorganized nuclei at the cortex. Transheterozygous *pops^{ts}* and CG2543PG44 (a p-element insertion into CG2543) and injected dsRNA of CG2543 both showed similar, yet more severe phenotypes. Scale bar equals 10 microns.

A)

MAACLLRYLVRQSRKPRSLVVSRESSHCSRMSTYSTVTNLSTVKMQRIQHLA
AFRSGVSLAERVLNPPQQSINGNHVSGNIQCSSDNNNKDTNAAFELAIKQLNS
LQSNDAAIRNSMSNSRVDTKADTIKYLERSGLPLETVEQLSFIHVAGIKGKGS
TCALTESLLRHQGFRTGFFSSPHILFTNERIRIDGQLLSKDKFTEQFWKVYNRL
WDLREHDHDMPAYFKFLTILGFHVFVAENVDVVVLEVGIGGEHDCTNIVRN
VRTVGITSLGLEHTELLGRTLPEIAWQKAGIIKTGSHVFTHVTQPECLEVIRQR
TKEHSATLYEVPPTEDYFRSKAYAPIWQTFSNLIRLNGSLAIQLAQDWLSQSG
KQQHTPNEVKMDPQLLDGLISTHWPGRCQLIEWHGMRLHLDGAHTLESMEV
CTDWFEKNVRDSVNPKILIFNRTGESGFAPLLKLLNRTCDFDMVCFVPNLATS
TPNAPSQVMVRFSPEMQLNRARIIASAWSDLCATEQKKDVGQVYNTLTDAF
TAIRQRFPQATDNEGQLEVLVTGSIHLLGAAISALDLIDDPKSRTDK

Ω-Loop
P-Loop
Thr to Iso mutation

B)

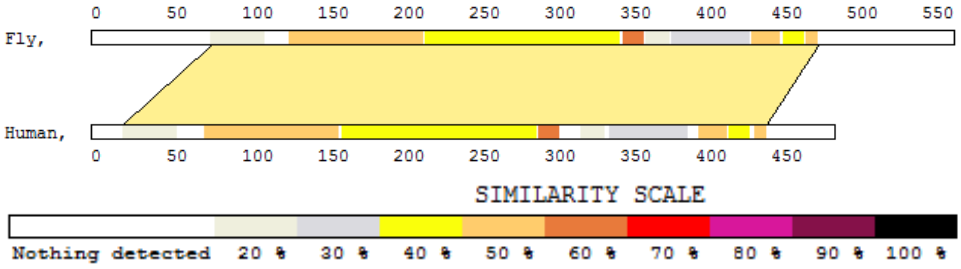

Figure 5.6**. Pops is a homologue mammalian FPGS.** (A) *pops*^{ts} allele amino acid sequence. Sequences which make up the ATP-binding pocket, P-loop (underline) and Ω-Loop (red), are highlighted. Note the T to I mutation in the P-Loop domain. (B) Protein sequence similarity alignment of Pops and Human FPGS isoform A.

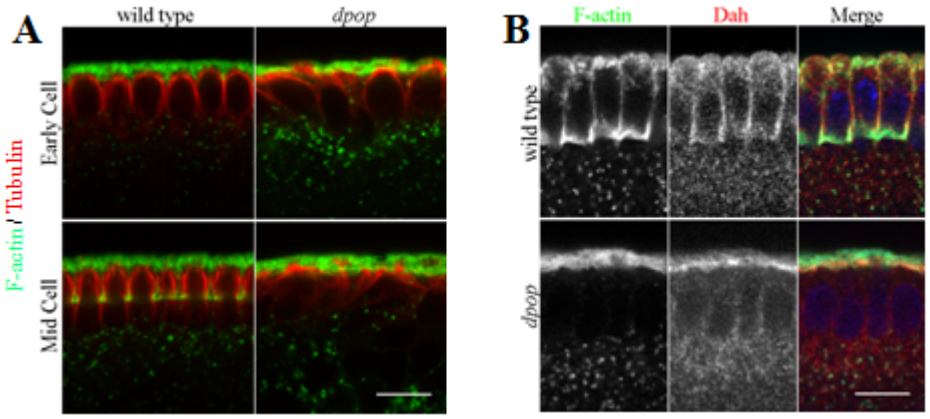

Figure 5.7. ***pops^{ts}*** **fails to organize actin and Dah during cellularization.** (A) ts161 embryos fail to form the inverted "baskets" of microtubules (red) necessary for cellularization furrows (green) to form. Excess actin puncta are also observed basal to the nuclei. (B) Dah, a protein required for furrow invagination and the recruitment of septins, is not properly localized in *pops^{ts}* embryos at cellularization. Scale bar equals 10microns.

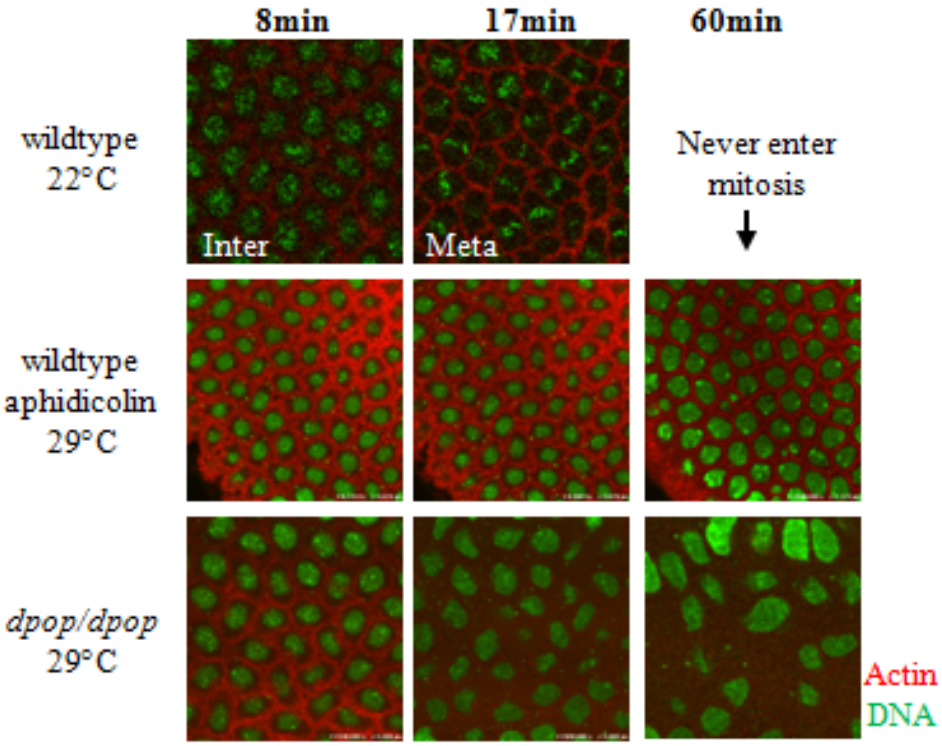

Figure 5.8. **Interphase arrest of *pops*^{ts} embryos is different from aphidicolin arrested embryos.** Cycle 13 embryos of wildtype (22°C), aphidicolin-injected (29°C) and *pops*^{ts}/*pops*^{ts} (29°C). Both aphidicolin treated and pops embryos exhibit a failure to entire mitosis. *pops*^{ts} embryos show a premature loss of nuclear integrity at the cortex due to the retraction of the actin furrows at 17min. Furrows persist throughout for aphidicolin treated embryos.

Bibliography

Adams, R.R., H. Maiato, W.C. Earnshaw, and M. Carmena. 2001. Essential roles of Drosophila inner centromere protein (INCENP) and aurora B in histone H3 phosphorylation, metaphase chromosome alignment, kinetochore disjunction, and chromosome segregation. *J Cell Biol*. 153:865-80.

Afshar, K., B. Stuart, and S.A. Wasserman. 2000. Functional analysis of the Drosophila diaphanous FH protein in early embryonic development. *Development*. 127:1887-97.

Albertson, R., J. Cao, T.S. Hsieh, and W. Sullivan. 2008. Vesicles and actin are targeted to the cleavage furrow via furrow microtubules and the central spindle. *J Cell Biol*. 181:777-90.

Amano, M., M. Ito, K. Kimura, Y. Fukata, K. Chihara, T. Nakano, Y. Matsuura, and K. Kaibuchi. 1996. Phosphorylation and activation of myosin by Rho-associated kinase (Rho-kinase). *J Biol Chem*. 271:20246-9.

Asnes, C.F., and T.E. Schroeder. 1979. Cell cleavage. Ultrastructural evidence against equatorial stimulation by aster microtubules. *Exp Cell Res*. 122:327-38.

Baker, J., W.E. Theurkauf, and G. Schubiger. 1993. Dynamic changes in microtubule configuration correlate with nuclear migration in the preblastoderm Drosophila embryo. *J Cell Biol*. 122:113-21.

Balasubramanian, M.K., D.M. Helfman, and S.M. Hemmingsen. 1992. A new tropomyosin essential for cytokinesis in the fission yeast S. pombe. *Nature*. 360:84-7.

Barr, F.A., and U. Gruneberg. 2007. Cytokinesis: placing and making the final cut. *Cell*. 131:847-60.

Bement, W.M., H.A. Benink, and G. von Dassow. 2005. A microtubule-dependent zone of active RhoA during cleavage plane specification. *J Cell Biol*. 170:91-101.

Bi, E., P. Maddox, D.J. Lew, E.D. Salmon, J.N. McMillan, E. Yeh, and J.R. Pringle. 1998. Involvement of an actomyosin contractile ring in Saccharomyces cerevisiae cytokinesis. *J Cell Biol*. 142:1301-12.

Boveri, T. 2008. Concerning the origin of malignant tumours by Theodor Boveri. Translated and annotated by Henry Harris. *J Cell Sci*. 121 Suppl 1:1-84.

Bringmann, H., and A.A. Hyman. 2005. A cytokinesis furrow is positioned by two consecutive signals. *Nature*. 436:731-4.

Buttrick, G.J., L.M. Beaumont, J. Leitch, C. Yau, J.R. Hughes, and J.G. Wakefield. 2008. Akt regulates centrosome migration and spindle orientation in the early Drosophila melanogaster embryo. *J Cell Biol*. 180:537-48.

Canman, J.C., L.A. Cameron, P.S. Maddox, A. Straight, J.S. Tirnauer, T.J. Mitchison, G. Fang, T.M. Kapoor, and E.D. Salmon. 2003. Determining the position of the cell division plane. *Nature*. 424:1074-8.

Cao, J., R. Albertson, B. Riggs, C.M. Field, and W. Sullivan. 2008. Nuf, a Rab11 effector, maintains cytokinetic furrow integrity by promoting local actin polymerization. *J Cell Biol*. 182:301-13.

Carmena, M. 2008. Cytokinesis: the final stop for the chromosomal passengers. *Biochem Soc Trans*. 36:367-70.

Casenghi, M., F.A. Barr, and E.A. Nigg. 2005. Phosphorylation of Nlp by Plk1 negatively regulates its dynein-dynactin-dependent targeting to the centrosome. *J Cell Sci*. 118:5101-8.

Castrillon, D.H., P. Gonczy, S. Alexander, R. Rawson, C.G. Eberhart, S. Viswanathan, S. DiNardo, and S.A. Wasserman. 1993. Toward a molecular genetic analysis of spermatogenesis in Drosophila melanogaster: characterization of male-sterile mutants generated by single P element mutagenesis. *Genetics*. 135:489-505.

Chou, T.B., and N. Perrimon. 1996. The autosomal FLP-DFS technique for generating germline mosaics in Drosophila melanogaster. *Genetics*. 144:1673-9.

Collins, L.L., G. Simon, J. Matheson, C. Wu, M.C. Miller, T. Otani, X. Yu, S. Hayashi, R. Prekeris, and G.W. Gould. 2012. Rab11-FIP3 is a cell cycle-regulated phosphoprotein. *BMC Cell Biol*. 13:4.

Cytrynbaum, E.N., P. Sommi, I. Brust-Mascher, J.M. Scholey, and A. Mogilner. 2005. Early spindle assembly in Drosophila embryos: role of a force balance

involving cytoskeletal dynamics and nuclear mechanics. *Mol Biol Cell*. 16:4967-81.

D'Avino, P.P., and D.M. Glover. 2009. Cytokinesis: mind the GAP. *Nat Cell Biol*. 11:112-4.

D'Avino, P.P., M.S. Savoian, and D.M. Glover. 2005. Cleavage furrow formation and ingression during animal cytokinesis: a microtubule legacy. *J Cell Sci*. 118:1549-58.

Dechant, R., and M. Glotzer. 2003. Centrosome separation and central spindle assembly act in redundant pathways that regulate microtubule density and trigger cleavage furrow formation. *Dev Cell*. 4:333-44.

Devore, J.J., G.W. Conrad, and R. Rappaport. 1989. A model for astral stimulation of cytokinesis in animal cells. *J Cell Biol*. 109:2225-32.

Ebrahimi, S., H. Fraval, M. Murray, R. Saint, and S.L. Gregory. 2010. Polo kinase interacts with RacGAP50C and is required to localize the cytokinesis initiation complex. *J Biol Chem*. 285:28667-73.

Echard, A., G.R. Hickson, E. Foley, and P.H. O'Farrell. 2004. Terminal cytokinesis events uncovered after an RNAi screen. *Curr Biol*. 14:1685-93.

Edgar, B.A., C.P. Kiehle, and G. Schubiger. 1986. Cell cycle control by the nucleo-cytoplasmic ratio in early Drosophila development. *Cell*. 44:365-72.

Edgar, B.A., and P.H. O'Farrell. 1989. Genetic control of cell division patterns in the Drosophila embryo. *Cell*. 57:177-87.

Edwards, K.A., M. Demsky, R.A. Montague, N. Weymouth, and D.P. Kiehart. 1997. GFP-moesin illuminates actin cytoskeleton dynamics in living tissue and demonstrates cell shape changes during morphogenesis in Drosophila. *Dev Biol*. 191:103-17.

Eggert, U.S., T.J. Mitchison, and C.M. Field. 2006. Animal cytokinesis: from parts list to mechanisms. *Annu Rev Biochem*. 75:543-66.

Finger, F.P., and J.G. White. 2002. Fusion and fission: membrane trafficking in animal cytokinesis. *Cell*. 108:727-30.

Flemming, W. 1965. Contributions to the Knowledge of the Cell and Its Vital Processes. *J Cell Biol*. 25:3-69.

Foe, V.E., and B.M. Alberts. 1983. Studies of nuclear and cytoplasmic behaviour during the five mitotic cycles that precede gastrulation in Drosophila embryogenesis. *J Cell Sci*. 61:31-70.

Fujiwara, K., and T.D. Pollard. 1976. Fluorescent antibody localization of myosin in the cytoplasm, cleavage furrow, and mitotic spindle of human cells. *J Cell Biol*. 71:848-75.

Gatti, M., M.G. Giansanti, and S. Bonaccorsi. 2000. Relationships between the central spindle and the contractile ring during cytokinesis in animal cells. *Microsc Res Tech*. 49:202-8.

Glotzer, M. 2005. The molecular requirements for cytokinesis. *Science*. 307:1735-9.

Glotzer, M. 2009. The 3Ms of central spindle assembly: microtubules, motors and MAPs. *Nat Rev Mol Cell Biol*. 10:9-20.

Gregory, S.L., N. Lorensuhewa, and R. Saint. 2010. Signalling through the RhoGEF Pebble in Drosophila. *IUBMB Life*. 62:290-5.

Grieder, N.C., M. de Cuevas, and A.C. Spradling. 2000. The fusome organizes the microtubule network during oocyte differentiation in Drosophila. *Development*. 127:4253-64.

Haghnia, M., V. Cavalli, S.B. Shah, K. Schimmelpfeng, R. Brusch, G. Yang, C. Herrera, A. Pilling, and L.S. Goldstein. 2007. Dynactin is required for coordinated bidirectional motility, but not for dynein membrane attachment. *Mol Biol Cell*. 18:2081-9.

Hickson, G.R., J. Matheson, B. Riggs, V.H. Maier, A.B. Fielding, R. Prekeris, W. Sullivan, F.A. Barr, and G.W. Gould. 2003. Arfophilins are dual Arf/Rab 11 binding proteins that regulate recycling endosome distribution and are related to Drosophila nuclear fallout. *Mol Biol Cell*. 14:2908-20.

Hime, G., and R. Saint. 1992. Zygotic expression of the pebble locus is required for cytokinesis during the postblastoderm mitoses of Drosophila. *Development*. 114:165-71.

Hu, C.K., M. Coughlin, C.M. Field, and T.J. Mitchison. 2008. Cell polarization during monopolar cytokinesis. *J Cell Biol*. 181:195-202.

Jurgens, G. 2005. Plant cytokinesis: fission by fusion. *Trends Cell Biol*. 15:277-83.

Karr, T.L., and B.M. Alberts. 1986. Organization of the cytoskeleton in early Drosophila embryos. *J Cell Biol*. 102:1494-509.

Kawamura, K. 1977. Microdissection studies on the dividing neuroblast of the grasshopper, with special reference to the mechanism of unequal cytokinesis. *Exp Cell Res*. 106:127-37.

Kotadia, S., L.R. Kao, S.A. Comerford, R.T. Jones, R.E. Hammer, and T.L. Megraw. 2008. PP2A-dependent disruption of centrosome replication and cytoskeleton organization in Drosophila by SV40 small tumor antigen. *Oncogene*. 27:6334-46.

Lecuit, T., R. Samanta, and E. Wieschaus. 2002. slam encodes a developmental regulator of polarized membrane growth during cleavage of the Drosophila embryo. *Dev Cell*. 2:425-36.

Lecuit, T., and E. Wieschaus. 2000. Polarized insertion of new membrane from a cytoplasmic reservoir during cleavage of the Drosophila embryo. *J Cell Biol*. 150:849-60.

Lehner, C.F. 1992. The pebble gene is required for cytokinesis in Drosophila. *J Cell Sci*. 103 (Pt 4):1021-30.

Loenen, W.A. 2006. S-adenosylmethionine: jack of all trades and master of everything? *Biochem Soc Trans*. 34:330-3.

Mabuchi, I., and M. Okuno. 1977. The effect of myosin antibody on the division of starfish blastomeres. *J Cell Biol*. 74:251-63.

Mazumdar, A., and M. Mazumdar. 2002. How one becomes many: blastoderm cellularization in Drosophila melanogaster. *Bioessays*. 24:1012-22.

McCartney, B.M., D.G. McEwen, E. Grevengoed, P. Maddox, A. Bejsovec, and M. Peifer. 2001. Drosophila APC2 and Armadillo participate in tethering mitotic spindles to cortical actin. *Nat Cell Biol*. 3:933-8.

Miller, K.G. 1995. Role of the actin cytoskeleton in early Drosophila development. *Curr Top Dev Biol*. 31:167-96.

Miller, K.G., and D.P. Kiehart. 1995. Fly division. *J Cell Biol*. 131:1-5.

Minestrini, G., A.S. Harley, and D.M. Glover. 2003. Localization of Pavarotti-KLP in living Drosophila embryos suggests roles in reorganizing the cortical cytoskeleton during the mitotic cycle. *Mol Biol Cell*. 14:4028-38.

Mishima, M., S. Kaitna, and M. Glotzer. 2002. Central spindle assembly and cytokinesis require a kinesin-like protein/RhoGAP complex with microtubule bundling activity. *Dev Cell*. 2:41-54.

Moephuli, S.R., N.W. Klein, M.T. Baldwin, and H.M. Krider. 1997. Effects of methionine on the cytoplasmic distribution of actin and tubulin during neural tube closure in rat embryos. *Proc Natl Acad Sci U S A*. 94:543-8.

Mollinari, C., J.P. Kleman, W. Jiang, G. Schoehn, T. Hunter, and R.L. Margolis. 2002. PRC1 is a microtubule binding and bundling protein essential to maintain the mitotic spindle midzone. *J Cell Biol*. 157:1175-86.

Moran, R.G. 1999. Roles of folylpoly-gamma-glutamate synthetase in therapeutics with tetrahydrofolate antimetabolites: an overview. *Semin Oncol*. 26:24-32.

MRC, V.S.R.G. 2003. Prevention of neural tube defects: Results of the Medical Research Council Vitamin Study. *The Lancet*. 338:131-137.

Neef, R., U. Gruneberg, R. Kopajtich, X. Li, E.A. Nigg, H. Sillje, and F.A. Barr. 2007. Choice of Plk1 docking partners during mitosis and cytokinesis is controlled by the activation state of Cdk1. *Nat Cell Biol*. 9:436-44.

Nishimura, Y., and S. Yonemura. 2006. Centralspindlin regulates ECT2 and RhoA accumulation at the equatorial cortex during cytokinesis. *J Cell Sci*. 119:104-14.

O'Keefe, L., W.G. Somers, A. Harley, and R. Saint. 2001. The pebble GTP exchange factor and the control of cytokinesis. *Cell Struct Funct*. 26:619-26.

Oegema, K., and T.J. Mitchison. 1997. Rappaport rules: cleavage furrow induction in animal cells. *Proc Natl Acad Sci U S A*. 94:4817-20.

Oliferenko, S., T.G. Chew, and M.K. Balasubramanian. 2009. Positioning cytokinesis. *Genes Dev*. 23:660-74.

Otani, T., K. Oshima, S. Onishi, M. Takeda, K. Shinmyozu, S. Yonemura, and S. Hayashi. 2011. IKKepsilon regulates cell elongation through recycling endosome shuttling. *Dev Cell*. 20:219-32.

Otegui, M.S., K.J. Verbrugghe, and A.R. Skop. 2005. Midbodies and phragmoplasts: analogous structures involved in cytokinesis. *Trends Cell Biol*. 15:404-13.

Padash Barmchi, M., S. Rogers, and U. Hacker. 2005. DRhoGEF2 regulates actin organization and contractility in the Drosophila blastoderm embryo. *J Cell Biol*. 168:575-85.

Pandey, R., S. Heidmann, and C.F. Lehner. 2005. Epithelial re-organization and dynamics of progression through mitosis in Drosophila separase complex mutants. *J Cell Sci*. 118:733-42.

Petronczki, M., M. Glotzer, N. Kraut, and J.M. Peters. 2007. Polo-like kinase 1 triggers the initiation of cytokinesis in human cells by promoting recruitment of the RhoGEF Ect2 to the central spindle. *Dev Cell*. 12:713-25.

Piekny, A., M. Werner, and M. Glotzer. 2005. Cytokinesis: welcome to the Rho zone. *Trends Cell Biol*. 15:651-8.

Poodry, C.A., L. Hall, and D.T. Suzuki. 1973. Developmental properties of Shibire: a pleiotropic mutation affecting larval and adult locomotion and development. *Dev Biol*. 32:373-86.

Postner, M.A., K.G. Miller, and E.F. Wieschaus. 1992. Maternal effect mutations of the sponge locus affect actin cytoskeletal rearrangements in Drosophila melanogaster embryos. *J Cell Biol*. 119:1205-18.

Quinones-Coello, A.T., L.N. Petrella, K. Ayers, A. Melillo, S. Mazzalupo, A.M. Hudson, S. Wang, C. Castiblanco, M. Buszczak, R.A. Hoskins, and L. Cooley. 2007. Exploring strategies for protein trapping in Drosophila. *Genetics*. 175:1089-104.

Rape, M. 2007. Cell cycle: on-time delivery of Plk1 during cytokinesis. *Curr Biol*. 17:R506-8.

Rappaport, R. 1961. Experiments concerning the cleavage stimulus in sand dollar eggs. *J Exp Zool*. 148:81-9.

Rappaport, R. 1971. Cytokinesis in animal cells. *Int Rev Cytol*. 31:169-213.

Riggs, B., B. Fasulo, A. Royou, S. Mische, J. Cao, T.S. Hays, and W. Sullivan. 2007. The concentration of Nuf, a Rab11 effector, at the microtubule-organizing center is cell cycle regulated, dynein-dependent, and coincides with furrow formation. *Mol Biol Cell*. 18:3313-22.

Riggs, B., W. Rothwell, S. Mische, G.R. Hickson, J. Matheson, T.S. Hays, G.W. Gould, and W. Sullivan. 2003. Actin cytoskeleton remodeling during early Drosophila furrow formation requires recycling endosomal components Nuclear-fallout and Rab11. *J Cell Biol*. 163:143-54.

Ris, H. 1949. The anaphase movement of chromosomes in the spermatocytes of the grasshopper. *Biol Bull*. 96:90-106.

Robinson, J.T., E.J. Wojcik, M.A. Sanders, M. McGrail, and T.S. Hays. 1999. Cytoplasmic dynein is required for the nuclear attachment and migration of centrosomes during mitosis in Drosophila. *J Cell Biol*. 146:597-608.

Rogers, S.L., U. Wiedemann, U. Hacker, C. Turck, and R.D. Vale. 2004. Drosophila RhoGEF2 associates with microtubule plus ends in an EB1-dependent manner. *Curr Biol*. 14:1827-33.

Rolo, A., P. Skoglund, and R. Keller. 2009. Morphogenetic movements driving neural tube closure in Xenopus require myosin IIB. *Dev Biol*. 327:327-38.

Rosenblatt, J. 2005. Spindle assembly: asters part their separate ways. *Nat Cell Biol*. 7:219-22.

Rosenblatt, J., L.P. Cramer, B. Baum, and K.M. McGee. 2004. Myosin II-dependent cortical movement is required for centrosome separation and positioning during mitotic spindle assembly. *Cell*. 117:361-72.

Rothwell, W.F., P. Fogarty, C.M. Field, and W. Sullivan. 1998. Nuclear-fallout, a Drosophila protein that cycles from the cytoplasm to the centrosomes, regulates cortical microfilament organization. *Development*. 125:1295-303.

Rothwell, W.F., C.X. Zhang, C. Zelano, T.S. Hsieh, and W. Sullivan. 1999. The Drosophila centrosomal protein Nuf is required for recruiting Dah, a membrane associated protein, to furrows in the early embryo. *J Cell Sci*. 112 (Pt 17):2885-93.

Royou, A., C. Field, J.C. Sisson, W. Sullivan, and R. Karess. 2004. Reassessing the role and dynamics of nonmuscle myosin II during furrow formation in early Drosophila embryos. *Mol Biol Cell*. 15:838-50.

Saraste, M., P.R. Sibbald, and A. Wittinghofer. 1990. The P-loop--a common motif in ATP- and GTP-binding proteins. *Trends Biochem Sci*. 15:430-4.

Schroeder, T.E. 1968. Cytokinesis: filaments in the cleavage furrow. *Exp Cell Res*. 53:272-6.

Schweitzer, J.K., and C. D'Souza-Schorey. 2004. Finishing the job: cytoskeletal and membrane events bring cytokinesis to an end. *Exp Cell Res*. 295:1-8.

Severson, A.F., D.R. Hamill, J.C. Carter, J. Schumacher, and B. Bowerman. 2000. The aurora-related kinase AIR-2 recruits ZEN-4/CeMKLP1 to the mitotic spindle at metaphase and is required for cytokinesis. *Curr Biol*. 10:1162-71.

Sharp, D.J., H.M. Brown, M. Kwon, G.C. Rogers, G. Holland, and J.M. Scholey. 2000. Functional coordination of three mitotic motors in Drosophila embryos. *Mol Biol Cell*. 11:241-53.

Sharp, D.J., K.R. Yu, J.C. Sisson, W. Sullivan, and J.M. Scholey. 1999. Antagonistic microtubule-sliding motors position mitotic centrosomes in Drosophila early embryos. *Nat Cell Biol*. 1:51-4.

Sisson, J.C., C. Field, R. Ventura, A. Royou, and W. Sullivan. 2000. Lava lamp, a novel peripheral golgi protein, is required for Drosophila melanogaster cellularization. *J Cell Biol*. 151:905-18.

Sisson, J.C., W.F. Rothwell, and W. Sullivan. 1999. Cytokinesis: lessons from rappaport and the Drosophila blastoderm embryo. *Cell Biol Int*. 23:871-6.

Solomon, L.R., and P.A. Rubenstein. 1987. Studies on the role of actin's N tau-methylhistidine using oligodeoxynucleotide-directed site-specific mutagenesis. *J Biol Chem*. 262:11382-8.

Somers, W.G., and R. Saint. 2003. A RhoGEF and Rho family GTPase-activating protein complex links the contractile ring to cortical microtubules at the onset of cytokinesis. *Dev Cell*. 4:29-39.

Stein, J.A., H.T. Broihier, L.A. Moore, and R. Lehmann. 2002. Slow as molasses is required for polarized membrane growth and germ cell migration in Drosophila. *Development*. 129:3925-34.

Stevenson, V., A. Hudson, L. Cooley, and W.E. Theurkauf. 2002. Arp2/3-dependent pseudocleavage [correction of psuedocleavage] furrow assembly in syncytial Drosophila embryos. *Curr Biol*. 12:705-11.

Stevenson, V.A., J. Kramer, J. Kuhn, and W.E. Theurkauf. 2001. Centrosomes and the Scrambled protein coordinate microtubule-independent actin reorganization. *Nat Cell Biol*. 3:68-75.

Strickland, L.I., and D.R. Burgess. 2004. Pathways for membrane trafficking during cytokinesis. *Trends Cell Biol*. 14:115-8.

Sullivan, W., P. Fogarty, and W. Theurkauf. 1993. Mutations affecting the cytoskeletal organization of syncytial Drosophila embryos. *Development*. 118:1245-54.

Sullivan, W., and W.E. Theurkauf. 1995. The cytoskeleton and morphogenesis of the early Drosophila embryo. *Curr Opin Cell Biol*. 7:18-22.

Szasz, J., M.B. Yaffe, and H. Sternlicht. 1993. Site-directed mutagenesis of alpha-tubulin. Reductive methylation studies of the Lys 394 region. *Biophys J*. 64:792-802.

Szollosi, D., P. Calarco, and R.P. Donahue. 1972. Absence of centrioles in the first and second meiotic spindles of mouse oocytes. *J Cell Sci*. 11:521-41.

Tavares, A.A., D.M. Glover, and C.E. Sunkel. 1996. The conserved mitotic kinase polo is regulated by phosphorylation and has preferred microtubule-associated substrates in Drosophila embryo extracts. *EMBO J*. 15:4873-83.

Tolstykh, T., J. Lee, S. Vafai, and J.B. Stock. 2000. Carboxyl methylation regulates phosphoprotein phosphatase 2A by controlling the association of regulatory B subunits. *EMBO J*. 19:5682-91.

Tram, U., B. Riggs, C. Koyama, A. Debec, and W. Sullivan. 2001. Methods for the study of centrosomes in Drosophila during embryogenesis. *Methods Cell Biol*. 67:113-23.

Uzbekov, R., I. Kireyev, and C. Prigent. 2002. Centrosome separation: respective role of microtubules and actin filaments. *Biol Cell*. 94:275-88.

Vaisberg, E.A., M.P. Koonce, and J.R. McIntosh. 1993. Cytoplasmic dynein plays a role in mammalian mitotic spindle formation. *J Cell Biol*. 123:849-58.

Verni, F., M.P. Somma, K.C. Gunsalus, S. Bonaccorsi, G. Belloni, M.L. Goldberg, and M. Gatti. 2004. Feo, the Drosophila homolog of PRC1, is required for central-spindle formation and cytokinesis. *Curr Biol*. 14:1569-75.

von Dassow, G. 2009. Concurrent cues for cytokinetic furrow induction in animal cells. *Trends Cell Biol*. 19:165-73.

Wang, W., L. Chen, Y. Ding, J. Jin, and K. Liao. 2008. Centrosome separation driven by actin-microfilaments during mitosis is mediated by centrosome-associated tyrosine-phosphorylated cortactin. *J Cell Sci*. 121:1334-43.

Warn, R.M., B. Bullard, and R. Magrath. 1980. Changes in the distribution of cortical myosin during the cellularization of the Drosophila embryo. *J Embryol Exp Morphol*. 57:167-76.

Watanabe, N., P. Madaule, T. Reid, T. Ishizaki, G. Watanabe, A. Kakizuka, Y. Saito, K. Nakao, B.M. Jockusch, and S. Narumiya. 1997. p140mDia, a mammalian homolog of Drosophila diaphanous, is a target protein for Rho small GTPase and is a ligand for profilin. *EMBO J*. 16:3044-56.

Webb, R.L., M.N. Zhou, and B.M. McCartney. 2009. A novel role for an APC2-Diaphanous complex in regulating actin organization in Drosophila. *Development*. 136:1283-93.

Wenzl, C., S. Yan, P. Laupsien, and J. Grosshans. 2010. Localization of RhoGEF2 during Drosophila cellularization is developmentally controlled by Slam. *Mech Dev*. 127:371-84.

Wheatley, S.P., and Y. Wang. 1996. Midzone microtubule bundles are continuously required for cytokinesis in cultured epithelial cells. *J Cell Biol*. 135:981-9.

White, J.G., and G.G. Borisy. 1983. On the mechanisms of cytokinesis in animal cells. *J Theor Biol*. 101:289-316.

Whitehead, C.M., R.J. Winkfein, and J.B. Rattner. 1996. The relationship of HsEg5 and the actin cytoskeleton to centrosome separation. *Cell Motil Cytoskeleton*. 35:298-308.

Yonemura, S., K. Hirao-Minakuchi, and Y. Nishimura. 2004. Rho localization in cells and tissues. *Exp Cell Res*. 295:300-14.

Yoshigaki, T. 2003. Theoretical evidence that more microtubules reach the cortex at the pole than at the equator during anaphase in sea urchin eggs. *Acta Biotheor*. 51:43-53.

Yuce, O., A. Piekny, and M. Glotzer. 2005. An ECT2-centralspindlin complex regulates the localization and function of RhoA. *J Cell Biol*. 170:571-82.

Zalokar, M.a.E., I. 1976. Division and migration of nuclei during early embryogenesis of Drosophila melanogaster. *Journal of Microbial Cell*. 25:97-106.

Zhai, B., J. Villen, S.A. Beausoleil, J. Mintseris, and S.P. Gygi. 2008. Phosphoproteome analysis of Drosophila melanogaster embryos. *J Proteome Res*. 7:1675-82.

Zhang, C.X., M.P. Lee, A.D. Chen, S.D. Brown, and T. Hsieh. 1996. Isolation and characterization of a Drosophila gene essential for early embryonic development and formation of cortical cleavage furrows. *J Cell Biol*. 134:923-34.